

**STOCHASTIC OPTIMIZATION OF HYDRAULIC FRACTURE AND
HORIZONTAL WELL PARAMETERS IN SHALE GAS RESERVOIRS**

BY

MUZAMMIL HUSSAIN RAMMAY

A Thesis Presented to the
DEANSHIP OF GRADUATE STUDIES

KING FAHD UNIVERSITY OF PETROLEUM & MINERALS

DHAHRAN, SAUDI ARABIA

In Partial Fulfillment of the
Requirements for the Degree of

MASTER OF SCIENCE

In

PETROLEUM ENGINEERING

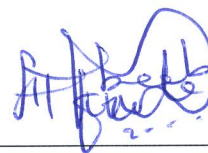
DECEMBER 2015

KING FAHD UNIVERSITY OF PETROLEUM & MINERALS

DHAHRAN- 31261, SAUDI ARABIA

DEANSHIP OF GRADUATE STUDIES

This thesis, written by **MUZAMMIL HUSSAIN RAMMAY** under the direction his thesis advisor and approved by his thesis committee, has been presented and accepted by the Dean of Graduate Studies, in partial fulfillment of the requirements for the degree of **MASTER OF SCIENCE IN PETROLEUM ENGINEERING.**



Dr. Abee A. Awotunde
(Advisor)



Dr. Abdullah Saad Sultan
Department Chairman



Dr. Hasan Al-Yousef
(Member)



Dr. Salam A. Zummo
Dean of Graduate Studies



Dr. Abdullah A. Alshuhail
(Member)

29/12/15

Date

© Muzammil Hussain Ramma

2015

*I dedicate this work to my beloved mother and father for their limitless love, prayers
and moral support.*

ACKNOWLEDGMENTS

First of all I thank Allah Almighty for His limitless mercy and blessings. My academic journey in King Fahd University of Petroleum and Minerals is one of His numerous blessings.

I would like to extend my gratitude to KFUPM and the Petroleum Engineering Department for providing me this wonderful opportunity and for all of their help, resources and support throughout my MS program. I learned a lot from KFUPM that I ever imagine. The knowledge and skills that I have gained here will really play a great role on my future endeavors.

I deeply acknowledge and thanks to my Thesis Advisor Dr. Abee Awotunde for his continuous guidance and support throughout my research work. All of my interactions with my Advisor have been very beneficial. I learned a lot from his guidance and complex problem solving abilities. I would also like to acknowledge and thanks my thesis committee members Dr. Hasan Al-Yousef and Dr. Abdullah A. Alshuhail for their guidance.

I am grateful to my friend Rizwan Ahmed Khan for in depth technical support related to optimization algorithms and resolving the issues I faced during my research. I would love to thank all my friends, classmates and university mates. My immense gratitude goes to my family members; their continuous love, support and prayers contribute greatly for solving and completing this research work.

TABLE OF CONTENTS

ACKNOWLEDGMENTS	I
TABLE OF CONTENTS	II
LIST OF FIGURES	V
LIST OF TABLES	X
ABSTRACT	XI
ملخص الرسالة	XIII
CHAPTER 1 INTRODUCTION	1
1.1 INTRODUCTION TO SHALE GAS RESOURCE	1
1.2 ECONOMIC AND ENVIRONMENTAL IMPACTS	3
CHAPTER 2 LITERATURE REVIEW	5
2.1 MULTISTAGE HYDRAULIC FRACTURING IN HORIZONTAL WELLS	5
2.2 SHALE GAS SIMULATION MODELING APPROACHES	8
2.3 PREVIOUS HYDRAULIC FRACTURING OPTIMIZATION APPROACHES IN SHALE GAS	12
2.4 STOCHASTIC OPTIMIZATION ALGORITHMS	24
2.4.1 <i>Differential Evolution</i>	24
CHAPTER 3 PROBLEM STATEMENT AND RESEARCH OBJECTIVES	28
3.1 PROBLEM STATEMENT	28
3.2 RESEARCH OBJECTIVES	29

CHAPTER 4 SHALE GAS SIMULATION MODELING AND	
 OPTIMIZATION METHODOLOGY	30
4.1 SHALE GAS RESERVOIR SIMULATION MODEL	30
4.1.1 <i>Langmuir Isotherm for Desorbed/Adsorbed Gas in Shale Gas</i>	
<i>Simulation Modeling.....</i>	<i>31</i>
4.1.2 <i>Geo-mechanical effects of Hydraulic Fractures in Shale</i>	
<i>gas simulation modeling.....</i>	<i>32</i>
4.1.3 <i>Shale gas reservoir simulation model calibration/History matching</i>	
<i>to real Field data.....</i>	<i>34</i>
4.2 ECONOMIC MODEL, OBJECTIVE AND COST FUNCTIONS	37
4.3 OPTIMIZATION METHODOLOGY	46
4.3.1 <i>Case 1</i>	<i>46</i>
4.3.2 <i>Case 2</i>	<i>49</i>
4.3.3 <i>Case 3</i>	<i>52</i>
CHAPTER 5 RESULTS AND DISCUSSIONS	55
5.1 SENSITIVITY STUDY OF FRACTURE SPACING AND FRACTURE CONDUCTIVITY	55
5.2 CASE 1 - OPTIMIZATION OF FRACTURE LENGTHS AND FRACTURE CONDUCTIVITIES	69
5.3 CASE 2 - OPTIMIZATION OF FRACTURE LENGTHS, CONDUCTIVITIES, SPACINGS	
AND NUMBER OF STAGES	75
5.4 CASE 3 - OPTIMIZATION OF FRACTURE LENGTHS, CONDUCTIVITIES,	
SPACINGS, NUMBER OF FRACTURE STAGES AND WELL LENGTH	81
5.5 COMPARISON OF CASES.....	87

CHAPTER 6 CONCLUSIONS AND RECOMMENDATIONS	95
NOMENCLATURE.....	97
APPENDIX: SHALE GAS SIMULATION MODEL PARAMETERS	100
REFERENCES.....	101
VITAE.....	109

LIST OF FIGURES

Figure 1.1: Global shale gas potential, adapted from EIA, (2011) www.eia.gov	2
Figure 1.2: US natural gas production (past and future projections) from 1990-2035,..... adapted from “US EIA, Annual Energy Outlook 2012 Early Release”	4
Figure 2.1: Influence of all Shale gas reservoir parameters on cumulative gas production	12
Figure 2.2: Influence of all Shale gas reservoir parameters on cumulative gas production	13
Figure 2.3: Flow Chart for Differential Evolution algorithm	27
Figure 4.1: Langmuir isotherm curve for Barnett Shale.....	33
Figure 4.2: Fracture Conductivity multiplier versus Pore Pressure for Barnett Shale.....	33
Figure 4.3: Top view of Shale gas reservoir model with hydraulic fractures of different.... lengths	36
Figure 4.4: History Matched Results of Shale gas reservoir simulation model with Real Field Data	36
Figure 4.5: Relationship of Fracture conductivity (1000-10000 md-ft) to Proppant concentration	40
Figure 4.6: Relationship of Fracture conductivity (1-100 md-ft) to Proppant concentration.....	41
Figure 4.7: Mathematical Relationship of Fracture conductivity (0-1000 md-ft) to Proppant concentration	42
Figure 4.8: Mathematical Relationship of Fracture conductivity (1000-10000 md-ft)..... to Proppant concentration	42

Figure 4.9: Relationship between length of horizontal well and cost of horizontal well .	45
Figure 4.10: Flow Chart for Differential Evolution Algorithm for Case 1.....	48
Figure 4.11: Flow Chart for Differential Evolution Algorithm for Case 2.....	51
Figure 4.12: Flow Chart for Differential Evolution Algorithm for Case 3.....	54
Figure 5.1a: Total Cumulative Gas Production versus Fracture Spacing at Fracture.....	
Conductivity 1 to 5 md-ft.....	56
Figure 5.1b: NPV versus Fracture Spacing at Fracture Conductivity 1 to 5 md-ft	57
Figure 5.2a: Total Cumulative Gas Production versus Fracture Spacing at Fracture.....	
Conductivity 6 to 10 md-ft.....	57
Figure 5.2b: NPV versus Fracture Spacing at Fracture Conductivity 6 to 10 md-ft	58
Figure 5.3a: Total Cumulative Gas Production versus Fracture Spacing at Fracture.....	
Conductivity 20 to 60 md-ft.....	59
Figure 5.3b: NPV versus Fracture Spacing at Fracture Conductivity 20 to 60 md-ft	59
Figure 5.4a: Total Cumulative Gas Production versus Fracture Spacing at Fracture.....	
Conductivity 70 to 200 md-ft.....	60
Figure 5.4b: NPV versus Fracture Spacing at Fracture Conductivity 70 to 200 md-ft	60
Figure 5.5a: Total Cumulative Gas Production versus Fracture Spacing at Fracture.....	
Conductivity 300 to 700 md-ft.....	62
Figure 5.5b: NPV versus Fracture Spacing at Fracture Conductivity 300 to 700 md-ft ..	62
Figure 5.6a: Total Cumulative Gas Production versus Fracture Spacing at Fracture.....	
Conductivity 800 to 3000 md-ft.....	63
Figure 5.6b: NPV versus Fracture Spacing at Fracture Conductivity 800 to 3000 md-ft	63

Figure 5.7a: Total Cumulative Gas Production versus Fracture Spacing at Fracture.....	
Conductivity 4000 to 8000 md-ft.....	64
Figure 5.7b: NPV versus Fracture Spacing at Fracture Conductivity	
4000 to 8000 md-ft.....	64
Figure 5.8a: Total Cumulative Gas Production versus Fracture Spacing at Fracture.....	
Conductivity 9000 to 10000 md-ft.....	65
Figure 5.8b: NPV versus Fracture Spacing at Fracture Conductivity	
9000 to 10000 md-ft.....	65
Figure 5.9a: Total Cumulative Gas Production versus Fracture Conductivity at	
Fracture Spacing 50 to 200 ft.....	67
Figure 5.9b: NPV versus Fracture Conductivity at Fracture Spacing 50 to 200 ft.....	67
Figure 5.10a: Total Cumulative Gas Production versus Fracture Conductivity at	
Fracture Spacing 250 to 400 ft.....	68
Figure 5.10b: NPV versus Fracture Conductivity at Fracture Spacing 250 to 400 ft.....	68
Figure 5.11: Comparison of Net Present Value versus Realization Number.....	
for all three cases	70
Figure 5.12: Optimal Fracture Lengths and Fracture Conductivities for Case 1	
best NPV realization	71
Figure 5.13: Optimal Fracture Conductivities for Case 1 best NPV realization	71
Figure 5.14: Optimal Fracture Lengths and Fracture Conductivities	
for Case 1 median NPV realization	73
Figure 5.15: Optimal Fracture Conductivities for Case 1 median NPV realization.....	73

Figure 5.16: Optimal Fracture Lengths and Fracture Conductivities	
for Case 1 lowest NPV realization.....	74
Figure 5.17: Optimal Fracture Conductivities for Case 1 lowest NPV realization	74
Figure 5.18: Optimal Fracture Lengths, Conductivities, Spacings and	
Number of Fracture Stages for Case 2 best NPV realization.....	78
Figure 5.19: Optimal Fracture Conductivities for Case 2 best NPV realization	78
Figure 5.20: Optimal Fracture Lengths, Conductivities, Spacings and	
Number of Fracture Stages for Case 2 median NPV realization	79
Figure 5.21: Optimal Fracture Conductivities for Case 2 median NPV realization	79
Figure 5.22: Optimal Fracture Lengths, Conductivities, Spacings and	
Number of Fracture Stages for Case 2 lowest NPV realization.....	80
Figure 5.23: Optimal Fracture Conductivities for Case 2 lowest NPV realization	80
Figure 5.24: Optimal Fracture Lengths, Conductivities, Spacings, Number of Fracture.....	
Stages and Well Length for Case 3 best NPV realization	84
Figure 5.25: Optimal Fracture Conductivities for Case 3 best NPV realization	84
Figure 5.26: Optimal Fracture Lengths, Conductivities, Spacings, Number of Fracture.....	
Stages and Well Length for Case 3 median NPV realization	85
Figure 5.27: Optimal Fracture Conductivities for Case 3 median NPV realization	85
Figure 5.28: Optimal Fracture Lengths, Conductivities, Spacings, Number of Fracture.....	
Stages and Well Length for Case 3 lowest NPV realization	86
Figure 5.29: Optimal Fracture Conductivities for Case 3 lowest NPV realization	86
Figure 5.30: Comparison of three Cases best Net present value results	
versus Iterations of DE.....	89

Figure 5.31: Comparison of three Cases median Net present value	
results versus Iterations of DE	90
Figure 5.32: Comparison of three Cases worst Net present value	
results versus Iterations of DE	90
Figure 5.33: Comparison of three Cases of best realizations.....	92
Figure 5.34: Comparison of three Cases with Base Case for best	
Net present value results	92
Figure 5.35: Comparison of Case 1 original optimal, 100 md-ft cut off,	
200 md-ft cut off	93
Figure 5.36: Comparison of Case 2 original optimal, 100 md-ft cut off,	
200 md-ft cut off	93
Figure 5.37: Comparison of Case 3 original optimal, 100 md-ft cut off,	
200 md-ft cut off	94
Figure 5.38: Comparison of Cases original optimal, 100 md-ft cut off,	
200 md-ft cut off	94

LIST OF TABLES

Table 1.1: Assessment results of shale gas Total Recoverable Reserves (TRR)	
worldwide, in Tcf Zhenzhen Dong et al, (2014).....	3
Table 4.1: Basic Shale Gas Reservoir Information.....	35
Table 4.2: Economic parameters related to Hydraulic Fracturing.....	39
Table 4.3: Economic parameters related to Horizontal Well	
(Wei Yu and Kamy Sepehrnoori, 2013b).....	43
Table A-1: Variables used in the relative permeability and capillary pressure	
curves construction. Based on experimental values on very tight	
sandstones by Maas (2011).....	100

Abstract

Full Name : Muzammil Hussain Rammay
Thesis Title : Stochastic Optimization of Hydraulic Fractures and Horizontal Well Parameters in Shale Gas Reservoirs
Major Field : Petroleum Engineering
Date of Degree : December 2015

Multistage hydraulic fracturing has become one of the most important techniques in the successful exploitation and development of shale or unconventional reservoirs. Most of the unconventional reservoirs like coal bed methane, shale gas, shale oil, tight gas and tight oil reservoirs rely heavily on the multistage hydraulic fracturing technique for commercial success, feasibility and viability.

The ultimate goal in unconventional or shale gas reservoir is to contact as much as possible with a hydraulic fracture or a hydraulic fracture network of optimal fracture conductivity. This ultimate goal is accomplished by horizontal well drilling of appropriate length with creation of traverse multi fracture stages by hydraulic fracturing process. Shale gas reservoir contact with the horizontal well bore is optimized by defining the optimal length of horizontal well, optimal fracturing fluid volume with optimal mass of proppant, number of multi frac stages to be placed in horizontal lateral of well and fracture spacings or isolation between fracture stages. Optimal fracturing fluid volume and mass of proppant depend on the optimal fracture lengths and optimal fracture conductivities of each fracturing stage.

Multistage fracturing and long length horizontal wells increase the cost of shale gas field development as compared to conventional field development. The economics of shale gas field development can be improved significantly by using global optimization

algorithms to find the maximum Net Present value. In shale gas reservoirs the parameters of hydraulic fracturing like fracture half length, amount of proppant with desired fracture conductivity, fracture Patterns, number of fracturing stages and fracture spacing should be optimized in order to maximize the profit or Net Present Value.

In this work, stochastic optimization is implemented in order to maximize the profit in terms of Net Present Value by optimizing hydraulic fracturing parameters and horizontal well length. In the optimizations considered here, global optimization algorithm, Differential Evolution is applied and seek to determine the optimal fracture lengths, fracture spacings, number of fracture stages, fracture conductivities and horizontal well length.

Stochastic optimization successfully implemented in more realistic LGR based gas shale reservoir simulation model by coupling with global optimization algorithm. Net present value is maximized for three different cases by finding global optimum solution for the multistage hydraulic fractures parameters and horizontal well using Differential Evolution algorithm. The comparison of the automated optimization results with base case indicates that the significant profit increase observed by using coupled Differential Evolution algorithm. This work can be significant valued addition for oil and gas industry, because by using these computational algorithms, workflows and framework, they can maximize Profits in terms of Net Present value from shale gas reservoirs.

ملخص الرسالة

الاسم الكامل	:	مزمل حسين رامي
عنوان الرسالة	:	الاستمثال العشوائي لعناصر الصدوع الهيدوليية والأبار الأفقية في مكانم الغاز الصخري
التخصص	:	هندسة البترول
تاريخ التخرج	:	ديسمبر 2015م

أصبحت عملية التصديع الهيدولي ذو المراحل المتعددة واحدة من التقنيات المهمة في نجاح عملية استثمار وتطوير المكانم غير الإعتيادية، معظم هذه المكانم غير الإعتيادية كمكانم ميثان سرير الفحم، مكانم الغاز الصخري، مكانم النفط الصخري، مكانم الغاز الحبيس ومكانم النفط الحبيس تستجيب بصورة عميقة لتقنيات التصديع الهيدولي المتعدد المراحل لنجاحها الإقتصادي ولجودتها ولقدرتها على البقاء.

يكن الهدف الأسمى في عمل إرتباط بأكبر صورة ممكنة بين مكانم الغاز الصخري أو المكانم غير الإعتيادية مع شبكة التصديع الهيدولي لتحقيق إرتباط تصديعي أمثل. يحقق هذا الهدف الأسمى بواسطة حفر الأبار الأفقية بطول مناسب بخلق تصديعات متعددة بواسطة عملية التصديع الهيدولي. يتم استمثال ربط مكانم الغاز الصخري بالأبار الأفقية عن طريق تعريف الطول الأمثل للبئر، الحجم الأمثل لمانع التصديع الهيدولي بالكتلة المثلى لمادة السيراميك، عدد مراحل التصديع التي يتم وضعها في الطول الأفقي للبئر والفاصل البعدي بين هذه التصديعات. يعتمد عملية استمثال حجم مانع التصديع وكتلة السيراميك على الأطوال والتوصيلات المثلى لكل مراحل التصديع. تتطلب عملية التصديع الهيدولي وحفر الأبار الأفقية الطويلة تكلفه أعلى في تطوير حقول الغاز الصخري مقارنة مع تطوير الحقول الإعتيادية. يمكن تحسينه الجانب الإقتصادي من تطوير حقول الغاز الصخري بصورة واضحة عن طريق استخدام خوارزميات الاستمثال الشامل لإيجاد أقصى قيمة لصادفي القيمة الحالية (NPV). في مكانم الغاز الصخري، لابد أن يتم استمثال كل عناصر عملية التصديع الهيدولي كطول الصدع، كمية السيراميك لتحقيق التوصيلية المرغوبة للصدوع، مسارات الصدوع، عدد مراحل التصديع والفاصل البعدي للتصديعات لتحقيق أقصى ربح وقيمة عالية.

في هذا العمل، طبقت عملية الاستمثال العشوائي لتحقيق أعلى ربح من حيث صافي القيمة الحالية باستمثال عناصر عملية التصديع الهيدولي وطول الأبار الأفقية. في عمليات الاستمثال هذه، طبقت خوارزميات الاستمثال الشامل وعملية التطوير التفاضلي لإيجاد أمثل قيم لعناصر التصديع الهيدولي كطول الصدوع، الفواصل البعيدة للصدوع، عدد مراحل التصديعات، توصيلات التصدعات وطول الأبار الأفقية.

طبقت عملية الاستمثال العشوائي في نمذجة مكنن غاز صخري حقيقي بدمجها مع خوارزمية الاستمثال الشامل. رفعت قيم صافي القيمة الحالية لأعلى قيم لها في ثلاث حالات باستخدام حل استمثال شامل لعناصر التصديع الهيدولي متعدد المراحل والبئر الأفقية باستخدام خوارزمية التطوير التفاضلي. أشارت المقارنة في نتائج عمليات الاستمثال الآلي إلى أن هنالك زيادة واضحة في الربح بواسطة استخدام خوارزمية التطوير التفاضلي. هذا العمل يعطي صورة إيجابية في صناعة النفط والغاز، لأن استخدام هذه الخوارزميات الحاسوبية وهيكلة النظام يؤدي إلى إزدياد الربح من حيث قيم صافي القيمة الحالية لمكامن الغاز الصخري.

Chapter 1 INTRODUCTION

1.1 Introduction to Shale Gas Resource

Two decades ago, gas in shale reservoirs was considered technically and economically unrecoverable. The development of Barnett shale is considered a watershed in the shale gas industry. The two most important factors for this extraordinary success are horizontal drilling and advancement in fracturing technology. This has been significantly assisted by high brittleness of Barnett shale (Wang and Reed, 2009). The development of other shale plays in US is assumed to follow relatively similar trends.

There is also considerable potential for shale gas exploitation globally. According to EIA (EIA, 2011) the total gas resources of the world are estimated to be about 22,600 TCF of which 40% is now contributed by shale plays. Also, at the current global consumption rate of 160 TCF/year, the total gas reserves of the world will last about 140 years. Figure 1.1 shows the global shale gas resource outlook.

In 2000, shale gas was 1% of domestic gas production in the United States. In 2013, it had risen to 32% and it is expected to account for half of total US domestic gas supply in two decades from now. The US who is the second largest energy consumer in the world after China has seen a decline in its net import of energy since 2007. In Europe, a recent report in the UK suggests that Shale gas in Northern England could meet Britain's gas need for 40 years (A.A. Oyekunle, 2014).

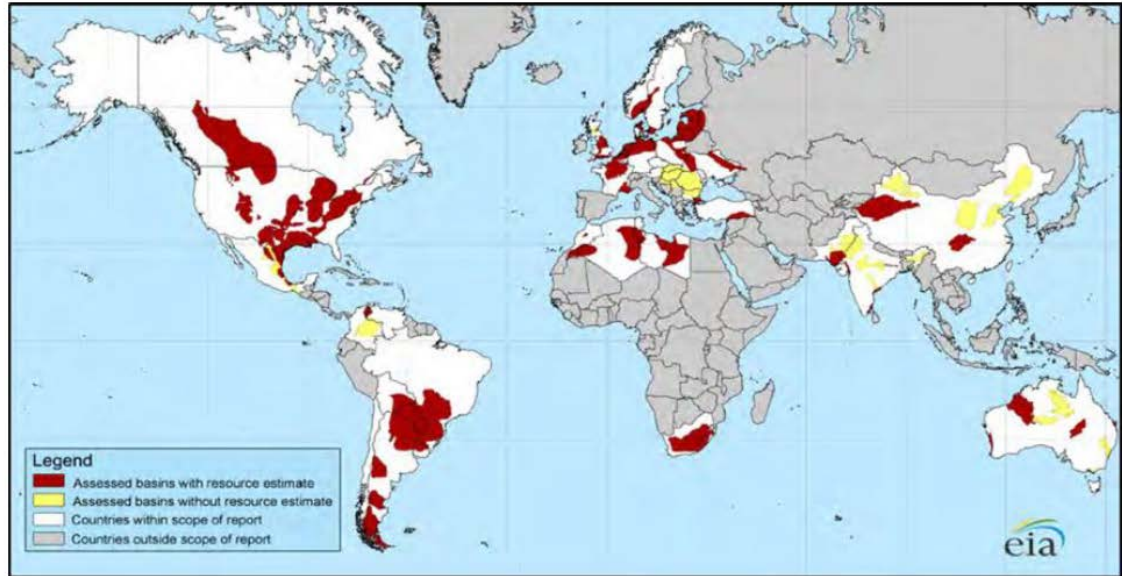


Figure 1.1: Global shale gas potential, adapted from EIA, (2011) www.eia.gov.

Zhenzhen Dong et al, (2014) did Probabilistic Assessment of World Recoverable Shale Gas resources and conducted a world assessment of shale gas resources, quantified the uncertainty in the resources estimates, and reached the following conclusion. The amount of shale-gas OGIP worldwide is 34,000 (P90) to 73,000 (P10) Tcf, with total recoverable reserves (TRR) of 4,000 (P90) to 24,000 (P10) Tcf. Significant technically recoverable shale gas resources exist in the CIS region and Middle East. Table 1.1 lists the P90, P50, and P10 shale gas total recoverable reserves (TRR) estimated for the seven world regions and worldwide by their study.

**Table 1.1: Assessment results of shale gas Total Recoverable Reserves (TRR) worldwide, in Tcf
Zhenzhen Dong et al, (2014)**

Region	TRR estimated in this study		
	P90	P50	P10
MET	1,354	3,415	7,974
CIS	1,136	3,520	7,541
NAM	466	1,395	2,975
AFR	341	862	1,991
LAM	342	836	1,921
AAO	218	582	1,184
EUP	188	504	1,068
World	4,418	11,032	23,657

Middle East (MET), Commonwealth of Independent State (CIS), North America (NAM)* (*Includes United States and Canada), Africa (AFR), Latin America (LAM), Austral-Asia (AAO), Europe (EUP).

1.2 Economic and Environmental Impacts

In the last five years shale gas developments have revolutionized the energy outlook of the US and it will continue to play its favorable economic role in the coming decades all over the globe. According to US EIA Annual Energy Outlook (early release) 2012, the gas production in 2012 from shales will increase from 5.0 TCF (23% of total US dry gas production) to 13.6 TCF in 2035 (49% of total US dry gas production). Figure 1.2 shows past and estimated future gas production from various gas resources of US.

Although shale gas development has been rewarding commercially, it has also caused some environmental concerns. This has instigated many recent studies to evaluate the

exact environmental impact of shale gas development. Hydraulic fracturing is considered a requisite for wells completed in shales. In this process, a complex mixture of clays, silica, gels and proppants is injected into the reservoir at high pressures. If the well is not completed properly or if fluid injection process is designed or carried out incorrectly, near-by aquifers may be contaminated. Also, due to the low drainage of shale gas wells, additional development wells have to be drilled to properly exploit this resource. This may disrupt some natural habitats and cause additional conservational concerns. Therefore, shale gas development poses a massive environmental challenge for operating and service providing companies. It will be interesting to observe how industry develops the right balance between financial gains and potential environmental hazards connected with its development.

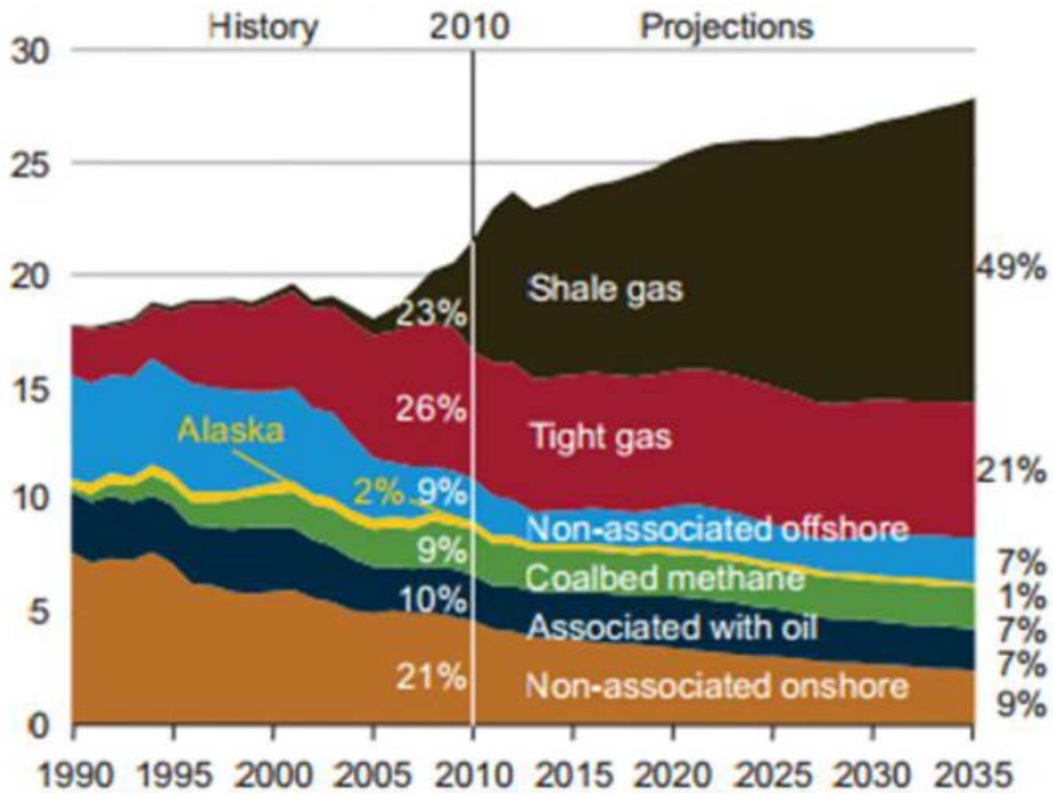


Figure 1.2: US natural gas production (past and future projections) from 1990-2035, adapted from "US EIA, Annual Energy Outlook 2012 Early Release"

Chapter 2 LITERATURE REVIEW

2.1 Multistage Hydraulic Fracturing in Horizontal Wells

Hydraulic fracturing is one of the most important reservoir stimulation techniques for improving oil and gas well productivity. This is done by,

- Creating a conductive hydraulic fracture through near well bore, for increasing permeability.
- Creating the significant length of fracture into the reservoir to increase production of Oil/Gas.
- Placing the hydraulic fracture such that oil or gas flow in the reservoir is increased.

Now-a-days horizontally wells are drilled, which can contact thousands of feet of prospective producing reservoir. The placement of the hydraulic fracture treatment in these instances is often accomplished by pumping multiple fracture treatments in stages. The perspective reservoir is divided into discrete sections and hydraulically fractured in sequential stages to place the desired treatment in the most productive intervals and lessen the potential to fracture nonproductive reservoir rock.

Michael J. Economides and Tony Martin (2007) discussed the multistage treatment and execution in horizontal wells in their book 'Modern Fracturing (Enhanced Natural Gas Production)'. They stated that, "The direction in which a wellbore is drilled controls whether an induced hydraulic fracture is created longitudinally along the horizontal lateral or whether multiple induced fractures can be created transverse to the drilled lateral (Edgeman and Walser, 2003; and Soliman, et al., 2006). The planning process for hydraulic fracturing of a horizontal well must begin before the actual drilling of horizontal well.

The length of horizontal well should be chosen based on the number of multi-fracture stages that can be practically placed or completed in a given horizontal well length. Many times excessive horizontal sections (4000 ft or greater) are drilled to “expose more reservoir,” when in actuality the entire horizontally exposed reservoir does not, or cannot, contribute to the productivity of the well due to the inability (usually based on economics) to properly stimulate enough of the horizontal reservoir. As with vertical wells, horizontal wells are more effectively completed through hydraulic fracture stimulation.

Staging processes for horizontally drilled laterals have evolved to optimize the hydraulic fracture stimulation process but for the most part continue to include variations of vertical techniques. Some of the horizontal well technologies include tractors to convey perforating guns and plugs through a horizontal wellbore; pump-down guns and plugs; and sliding-sleeve assemblies, which in some cases require pumping the fracture treatment through the annulus of the casing or liner and a tubing string which is subsequently needed to engage the sleeve assemblies and prepare the well for the subsequent stage. Most of these methods have merit but cannot be applied in all situations.

L. E. East Jr et al, (2004) showed that successful application of multistage hydraulic fractures on horizontal wells drilled in shale reservoir, which has relatively very high thickness. Multistage hydraulic fracturing has become one of the most important techniques in the successful exploitation and development of shale or unconventional reservoirs. Most of the unconventional reservoirs like coal bed methane, shale gas, shale oil, tight gas and tight oil reservoirs rely heavily on the multistage hydraulic fracturing

technique for commercial success, feasibility and viability. The ultimate goal in unconventional or shale gas reservoir is to contact as much as possible with a hydraulic fracture or a hydraulic fracture network of optimal fracture conductivity. This ultimate goal is accomplished by horizontal well drilling of appropriate length with creation of traverse multi fracture stages by hydraulic fracturing process along with the horizontal well lateral. Unconventional reservoir contact with the horizontal well bore is optimized by defining the optimal length of horizontal well, optimal fracturing fluid volume with optimal mass of Proppant, number of multi frac stages to be placed in horizontal lateral of well and fracture spacings or isolation between fracture stages. Optimal fracturing fluid volume and mass of Proppant depend on the optimal fracture lengths and optimal fracture conductivities of each fracturing stage.

In recent years, especially, under the impetus of the multistage fracturing technique of horizontal well [B. Mille et al, (2008), C. L. Cipolla, (2009)] and a great success has been achieved in developing unconventional natural gas of low permeability shale reservoirs in USA, and its annual production in 2011 reached $1720 \times 10^8 \text{ m}^3$, far more than 2011 natural gas total production in China $1025.3 \times 10^8 \text{ m}^3$.

2.2 Shale Gas Simulation Modeling Approaches

Shale gas reservoir simulation modeling is different from the conventional reservoir simulation approaches due to the Gas desorption effect and presence of natural fractures in Shales. Moreover shale gas cannot be produced economically without any Stimulation i.e. Hydraulic Fracturing treatment. Therefore Multistage Hydraulic fracturing usually is the common practice in shale gas reservoirs. In order to properly the production profiles the engineers should incorporate multistage hydraulic fracture in Shale Gas Simulation model. Furthermore the Geomechanics effect around Hydraulic Fracture should also be taken into account because Fracture conductivity decreases with pore pressure reduction or increase in stress in the Hydraulic Fractures. Many authors tried to incorporate these effects in order to realistically simulate the Shale Gas Production. The authors works, related to Shale Gas Simulation modeling in Literature, are given below.

X Zhang *et al* (2009) performed shale gas simulation modeling. They performed upscaling of properties from the Discrete Fracture Network model to dual porosity system in order to incorporate natural fractures effects in Shale Gas reservoirs. They also considered the decrease of fracture conductivity with the decrease of pore pressure and stress around the hydraulic fracture. But they did not considered the Gas desorption effect in Shale Gas Reservoir.

C.L. Cipolla *et al*, (2010), proposed the Reservoir Simulation modeling technique in Shale Gas Reservoir. In this paper Shale Gas was modeled using Dual Permeability grid and Langmuir Isotherm was used in order to incorporate the gas desorption in Shale Reservoirs. This paper extended previous shale gas reservoir simulation modeling work (Mayerhofer *et al*. 2006, 2010; Warpinski *et al*. 2008; Cipolla *et al*. 2008a, 2009b), which

discussed the impact of stress-sensitive fracture conductivity and gas adsorption or desorption effect on well performance.

Barry Rubin (2010), discussed more about Dual Permeability Grid and Non Darcy Flow incorporation in to the Shale Gas Reservoir Simulation models. In this work, he compared the solutions from simulation models, (which have different number of simplified grids and only take total simulation time in minutes) to the results of the reference solutions (which take many hours of simulation time). He compared multiple interacting continua (MINC) models and dual permeability models with the reference solutions. He investigated dual permeability models to simulate shale gas reservoir and models the hydraulic fracture network explicitly using local grid refinement (LGR), within the Stimulated Reservoir Volume. The result of this study is a shale gas simulation technique, which uses small logarithmically spaced Local refined grids in global dual permeability (DK) grid within the Stimulated Reservoir Volume coupled to standard dual permeability (DK) grids outside of the Stimulated Reservoir Volume. The hydraulic fractures modeled explicitly in the Local Refined Grids, these hydraulic fractures are represented accurately by 2.0 ft. wide cells (local refined cells in global cells) using a procedure which scales both the fracture width, fracture permeability using equivalent fracture conductivity.

R.S. Taylor, (2010), used combination of fracturing modeling simulation and shale gas reservoir simulation. The required input data for this purpose were got through integration of advanced well log and special core analyses, rate transient analysis (RTA), diagnostic fracture injection testing (DFIT), and characterization of fracture geometry and different fracture lengths using micro-seismic measurements.

Wei Yu and Kamy Sepehrnoori, (2013a) employed numerical reservoir simulation techniques to Shale Gas Reservoirs same as C.L. Cipolla et al, (2010), and Barry Rubin (2010). They validated their model with real field production data from Barnett Shale, to model natural fractures and multi stage hydraulic fractures. They also consider effects of stress sensitive or pore pressure fracture conductivity. They classified shale formation into three categories: soft, medium and stiff. This classification is based on published laboratory data of stress or pore pressure dependent fracture conductivity due to proppant crushing and embedding in various shale samples. The effects of stress-dependent propped fracture conductivity on ultimate gas recovery were investigated for these soft, medium and stiff shale formations. Sensitivity studies were performed on the initial fracture conductivity, permeability, and bottom- hole pressure to understand critical parameters that control this process more significantly.

Wei Yu and Kamy Sepehrnoori, (2013c), performed shale gas simulation modeling with the consideration of gas desorption and geomechanics effects. They modeled the Shale Reservoir with the same approach as discussed by the C.L. Cipolla et al, (2010), and Barry Rubin (2010). History matching or simulation model calibration was performed based on two field production data from Marcellus Shale and Barnett Shale. They evaluated geomechanics and gas desorption or adsorption effects for Marcellus Shale and Barnett Shale. They numerically studied the effect of gas desorption or adsorption effect on ultimate gas recovery. They done this by use of available laboratory data of Langmuir isotherm for gas desorption or adsorption from five different shale formations including New Albany Shale, Marcellus Shale, Eagleford Shale, Barnett Shale and Haynesville Shale. They presented the comparison of gas adsorption or desorption effect of different

shale formations. They investigated the increment in gas production due to gas adsorption or desorption effect. Moreover they investigated the decrease in gas production due to geomechanics effect due to decrease in fracture conductivity with the increase in effective stress or decrease in pore pressure.

Wei Yu and Kamy Sepehrnoori, (2014a), proposed reservoir simulation approach to optimize and design shale gas production. In this paper, they presented a framework to obtain the best gas-production scenario with respect to profit by optimizing the input parameters by integrating commercial simulators, an economic model, design of experiment (DoE), and response-surface methodology (RSM). They used factorial design to screen insignificant factors and find the most significant input parameters and design. They used RSM to design over those most significant input parameters to fit a response surface using net present value (NPV) as the objective function.

2.3 Previous Hydraulic fracturing optimization approaches in Shale Gas

There are various types of approaches have been used for the purpose of Hydraulic Fracturing modeling and optimization in Shale Gas Reservoir. Some authors used sensitivity studies for optimization of Hydraulic properties parameters. Some authors used optimization algorithms for the optimization of Hydraulic properties parameters.

X Zhang *et al* (2009) performed shale gas simulation modeling and did Sensitivity study of hydraulic fractures parameters on Cumulative Gas Production. They performed upscaling of properties from the Discrete Fracture Network model to dual porosity system. In terms of Shale Gas reservoir parameters, they found that stimulated fracture network permeability as most influence on Shale Gas Cumulative Production as shown in figure 2.1.

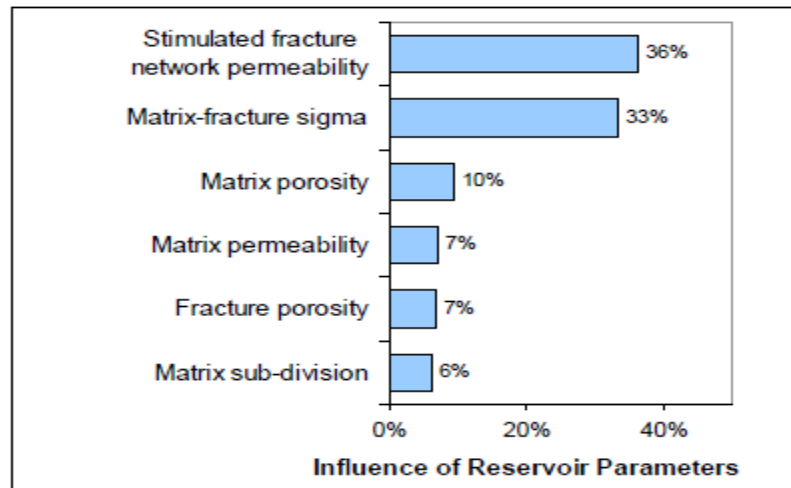


Figure 2.1: Influence of all Shale gas reservoir parameters on cumulative gas production

They found out the fracture half length as the most influence of hydraulic fracture parameters on Shale Gas Cumulative Production as shown in figure 2.2.

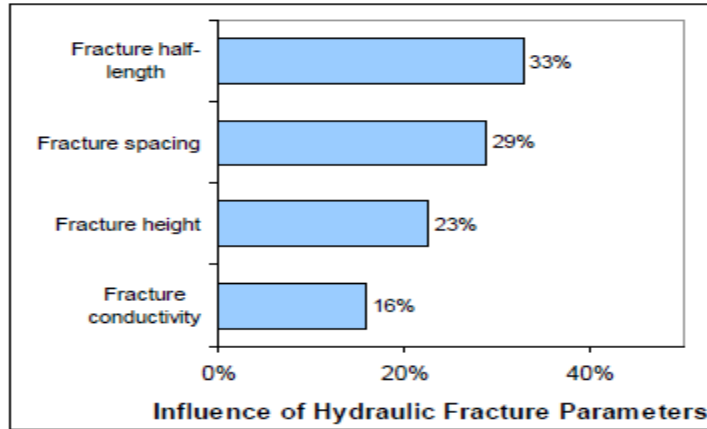


Figure 2.2: Influence of all Shale gas reservoir parameters on cumulative gas production

C. Cipolla et al (2011) discussed the primary challenges for optimizing hydraulic fracture treatment in shale gas or tight gas reservoirs. These challenges include the lack of hydraulic fracture models that properly simulate complex hydraulic fracture propagation during fracturing in many shale gas reservoir, efficient methods to create discrete reservoir simulation grids to rigorously model the hydrocarbon production from complex multi stage hydraulic fractures, automated hydraulic fracture treatment staging algorithms (which can place optimal hydraulic fracture stages automatically through optimization algorithms), and the ability to efficiently integrate geological, geophysical data with micro-seismic measurements of fracture lengths or extent of fracture propagation.

Anish Singh et al (2011) did the Sensitivity study of shale oil production for different hydraulic fracture parameters like fracture spacings between different multi-fracture stages, fracture half length of each hydraulic fracture stage and fracture conductivity each hydraulic fracture stage. Based on this study, they made following conclusions.

1. The transient flow of oil in the multistage hydraulic fracture or stimulated reservoir volume from shale oil reservoirs can be captured by logarithmically spaced locally refined grids.
2. Initial shale gas production is higher than shale oil production because of lower viscosity of gas in comparison to oil.
3. They investigated that closer fracture spacing between multi fracture stages gives higher initial oil production rates as well as higher ultimate oil recovery factor.
4. Higher hydraulic fractures length means bigger Stimulated Reservoir Volume or more reservoir contact to horizontal well and they investigated that this leads to higher cumulative oil production or ultimate oil recovery factor per well.

Sam Holt (2011) found the optimal placement of hydraulic fracture stages along a horizontal well bore by using gradient based optimization algorithms. He used three gradient-based optimization algorithms (Ensemble based Optimization: EnOpt (Chen, 2008), Simultaneous Perturbation Stochastic Approximation: SPSA (Spall, 1998) and finite difference gradient estimation) that work with continuous variables, in order to find the optimal placement of hydraulic fracturing stages. Two cases were investigated with three horizontal wells, all in the y-direction, both with fixed positions for the hydraulic fracture stages and fixed well lengths of 40 grid blocks. He recommended PSO or genetic algorithm would be interesting for optimization, both in terms of computational efficiency and objective function value.

P. Saldungaray and T. Palisch, (2013) presented a framework to assess the realistic fracture conductivity shale reservoir in-situ conditions. They also presented economic

implications and sensitivity on proppant selection in optimization of multi-stage hydraulic fracturing in shale gas reservoirs. They found that the proppant pack conductivity for particular proppant is a function of many parameters including proppant strength, proppant particle size, fracturing fluid damage, proppant grain shape (roundness and sphericity), effective stress on proppant, embedment into the frac faces, fines migration, and fluid flow effects (non-Darcy and multi-phase flow). Due to the effects of these parameters, proppant pack conductivity can be reduced by more than two orders of magnitude. During selection process of proppants, these factors for conductivity reductions should be considered so that the optimal fracture conductivity during multi stage hydraulic fracturing can be employed. They stated that the process for selecting proppant should consist of following steps.

1. Calculation of conductivity of the hydraulic fracture should be done at realistic conditions.
2. Predict the oil or gas production performance achieved with each proppant.
3. Evaluate the cost vs. profit and select the proppant that maximizes the multi stage hydraulic fracturing economics.

Mei Yang and Michael J. Economides (2012) stated that commonly accepted notion is that manmade proppants (such as ceramics) should be applied at higher closure stress environment, invariably deeper reservoirs. In this study, they showed that there is an optimum Proppant Number corresponding to maximum NPV for various reservoir permeabilities. Based on that notion, they proposed a systematic way of choosing proppant type and mass to maximize NPV in eagle ford shale reservoirs. They considered

Different Proppant Types and its associated Cost, fracturing fluid cost and pumping charges and applied Unified Fracturing Design optimization technique for determination of optimum Mass of Proppant, which gives highest NPV.

C.J. Jin et al, (2013), This paper uses a numerical reservoir simulation study to develop simple correlations that quantify the required fracture spacing necessary to optimize recovery factors in unconventional shale oil reservoirs and how various hydraulic fracture parameters and non-ideal reservoir behavior affect the horizontal well completion design. The detailed hydraulic fracture parameters discussed in this paper are spatial distribution of fracture conductivity, effective fracture height, effective fracture length, and fracture conductivity degradation. The non-ideal reservoir behaviors discussed include stress-sensitive reservoir permeability and overpressure.

Xiaodan Ma et al, (2013a) tried to solve the problem of optimal hydraulic fracture placement with the gradient-based discrete simultaneous perturbation stochastic approximation (DSPSA), finite difference method (FD), and genetic algorithm (GA). They conclude that their numerical study indicate higher efficiency of DSPSA and GA. They had three objectives in their study Horizontal Well Placement Optimization, Hydraulic Fracturing Stages Placement Optimization, Wellbore and Hydraulic Fracturing Stages Placement Stages Placement Hierarchal Optimization.

Wei Yu and Kamy Sepehrnoori, (2013b), employed response surface methodology in order to maximize Net Present Value (NPV) using simulation results integrated with economic analysis. They built shale reservoir simulation model and tried to optimize multiple horizontal well placement with multistage hydraulic fractures. This paper demonstrated the accuracy of numerical modeling of multistage hydraulic fractures by

considering the gas adsorption or desorption effect for actual Barnett Shale production data. There were six uncertain parameters considered in this study. These six parameters are fracture conductivity, fracture spacing, permeability, fracture half length, distance between two neighboring wells and porosity with a reasonable range based on Barnett Shale information. These parameters were used to fit a response surface of Net Present Value, which was used as the objective function. They identified the optimum multistage fracturing design under different gas prices scenarios based on NPV maximization. This integrated framework, approach and methodology contributed to obtaining the optimal drainage area of horizontal wells by optimizing horizontal well separation to other horizontal well and provide insight into hydraulic fracture interference between one horizontal well and neighboring horizontal wells.

Xiaodan Ma, (2013b) In this paper integrated horizontal well Placement and hydraulic fracture stages optimization in unconventional or shale gas reservoirs were performed using simultaneous perturbation stochastic approximation (SPSA) and Covariance Matrix Adaptation Evolution Strategy (CMA-ES) that is a stochastic, derivative-free numerical method. They proposed novel hierarchical optimization structure, which operates in the following way: it places a horizontal wellbore (or wellbores) on the upper level and then distributes HF stages along the fixed well trajectory (or trajectories) on the lower level. Both levels of the framework use gradient-based stochastic strategy, namely, the simultaneous perturbation stochastic approximation (SPSA). Application of this optimization technique permits to depart from the common practice of distributing HF stages evenly. They demonstrated the utility of this idea with highly heterogeneous geologic systems that require HF spacing with non-even intensity. To assess efficiency of

our approach, they compared the results obtained from SPSA optimization with those from CMA-ES.

Wei Yu and Kamy Sepehrnoori, (2013d), simulated proppant distribution effect on horizontal well performance in shale gas reservoirs. In this paper, shale gas reservoir simulation techniques, validated by field production data from Marcellus Shale, were employed to model the proppant distribution and geomechanics effect. A series of reservoir simulations was performed to quantify the impact of uneven proppant distribution between different clusters in the same stage on well performance. The fracture conductivity ratio of 1:1.5:2.5:4 for four clusters within one stage was investigated in this study. The simulations were performed by taking range of reservoir permeability from 0.00001 to 0.0001 md. Gas desorption effect was also taken into account. This work gives insights to develop an early understanding of the effects of proppant distribution shale gas well productivity, and provides operators into fracture conductivity requirements in shale gas reservoirs that can be used to improve hydraulic fracturing treatment design through improved proppant distribution.

Wei Yu et al, (2013e), presented the methodology to simulate production performance of shale gas reservoirs from multi-stage hydraulic fracture stages. Hydraulic fractures were divided into different groups based on different outer and inner fracture length patterns. The simulation results showed that more gas production was observed from outer fractures. Although hydraulic fractures improved gas production from shale gas wells, hydraulic fracturing is expensive. Long-laterals require greater volume of liquid sand proppants and contributing to higher cost. All of these studies suggest the importance of economic factors in optimizing multiple transverse hydraulic fractures. For example,

reduction in fracture spacing is expensive and may even cause interference and subsequent reduction in gas production. They also studied the effects of fracture spacing and fracture half-length on gas production published average reservoir data for the Barnett Shale in the new ark East field were used. They concluded the following main points from their study.

- Reduction of fracture spacing increases cumulative gas production, until the point at which fractures start to interfere.
- Increase in fracture half-length increases cumulative gas production.
- The contributions of outer fractures to cumulative gas production and gas flow rate are higher than the contributions of inner fractures.
- Depending on the characteristics of a shale reservoir, a scheme of outer and inner fracture scheme can be potentially designed to optimize gas production rate, cumulative gas production, and cost associated with the total induced half-length in a multistage fracturing job.

Luigi Saputelli et al, (2014) performed optimization of horizontal wells with multiple hydraulic fractures in the Bakken Shale. Economically attractive reserves recovery was modeled through multiple fracture placements in a 10,000-ft horizontal well. In this study Numerical simulation results showed that oil recovery increased between 8 to 15%, while net present value (NPV) increased 8 to 24%, as the number of fractures increased. Based on the critical assumptions in the study (permeability, natural fracture distribution, and stress orientation), an optimum number of fractures was identified. The results of the study hopefully can be used to improve the understanding of the role of fracture geometry, spacing, and open/cased-hole completion strategy to enhance an operator's

optimum completion design. There is an optimum value for the number of fractures per well, which is based on the critical assumptions of permeability and natural fracture distribution.

Wei Yu et al, (2014b), showed that in identification of fracture length patterns there was high uncertainty associated due to fracture interference in shale gas reservoirs. In this work, they used reservoir simulation to study five irregular and complex hydraulic fracture patterns. These fracture patterns have the fracture half-lengths. They compared well performance of these hydraulic fracture length patterns. They observed significant difference in ultimate gas recovery for different hydraulic fracture patterns. They also studied the effects of fracture conductivity, matrix permeability and cluster spacing on reservoir performance. The simulation results showed that there exists a big difference between these five fracture patterns in terms of recovery; the difference increases significantly with increasing matrix permeability, fracture conductivity, and to a lesser extent with increasing cluster spacing.

Atefeh Jahandideh, and Behnam Jafarpour, (2014), performed optimization of Hydraulic Fracturing Design under Spatially Variable Shale Fracability. The optimization of the hydraulic fracturing design was performed using the Simultaneous Perturbation Stochastic Approximation algorithm to maximize the net present value of the shale asset that includes the cost of fracturing and revenue from gas production. They used the SPSA algorithm to optimize fracture attributes such as location, length and number of stages in shale formations by considering the spatial variability in shale fracability. They optimized the location and number of fractures with a fixed length. To optimize the number of fractures, they considered a sequential optimization approach, where several optimization

subproblems were solved. In each subproblem, one or two fracture stages per each well were introduced and their optimal locations were identified by solving the fracture placement optimization problem.

Lan Ren et al (2014) studied hydraulic fracture propagation mechanism and its practical significance with theoretical aspect in shale reservoir. They showed that fracture propagation mechanism contributes significantly to improve efficiency of shale reservoir fracturing design. Reservoir geology, stronger rock elastic properties, magnitude of least principal stress, higher brittle mineral contents of rock and better developed natural fractures will be constructive to better extension and propagation of hydraulic fractures in shale reservoirs. Engineering aspects of fracturing operations, higher treating net pressure, lower fluid viscosity, and larger fracturing scale will be more helpful to form a fully propagated fracture network.

Wei Yu et al, (2014c), performed history matching with field data to determine fracture half-length and fracture conductivity, and then optimized fracture design using economic analysis for single horizontal well. Subsequently, they performed optimization for spacing of multiple horizontal wells using sensitivity analysis. They made the following conclusions.

- In the Middle Bakken, the fracture half-length is in the range of 210–345 ft with the geomechanics effect, and 170–260 ft without the geomechanics effect; the fracture conductivity is in the range of 1–2.5 md-ft with the geomechanics effect, and 0.5–1.5 md-ft without the geomechanics effect.

- The optimal fracture conductivities are 4 md-ft and 6 md-ft for the cases without and with the geomechanics effects respectively, regardless of the short-term and long-term period.
- The optimal horizontal well number is 6 for the cases without and with consideration of the geomechanics effect, regardless of considering short-term or long-term production periods.

F. Lalehrokh and J. Bouma, (2014) considered multiphase flow of gas and oil in shale reservoirs for the purpose of Well Spacing Optimization in Eagle Ford Shale. This study was based on the reservoir simulation modeling and economic analysis, well spacing of 330 ft and 400 ft maximizes the NPV of a black oil Eagle Ford reservoir by assuming 50 nD reservoir permeability and fracture half-length of 100 and 150 ft, respectively. Detailed results were also provided to illustrate the effect of fracture half-length, reservoir permeability as well as oil price variation. Reservoir permeability and fracture area were found to be the two most important factors regarding well spacing optimization in shale reservoirs.

Ming Gu et al, (2014), presented an approach to assess the optimum proppant amount injected by determining the post-frac conductivity. First, using three-dimensional finite difference reservoir simulations in a naturally fractured reservoir, which has both the hydraulic fracture and natural fractures modeled explicitly as discrete grid blocks, they found the cumulative production as a function of fracture conductivity. For a fixed propped length and production time, they observed a critical conductivity beyond which the production is insensitive to the conductivity. The numerical results showed that the critical conductivity increases with propped length and decreases with production time.

They also evaluated BHP flowing pressure on the critical conductivity and showed that critical conductivity is negatively correlated with flowing bottomhole pressure.

2.4 Stochastic optimization Algorithms

There are varieties of stochastic or global optimization algorithms, which can maximize or minimize any objective function. In this study, Differential Evolution is used as a stochastic or global optimization algorithm for optimization purpose, because it is one of best stochastic or global optimization algorithm.

2.4.1 Differential Evolution

Differential Evolution (DE) is a powerful global optimization algorithm and was introduced by Storn and Price (1995). DE grew out of Price's attempts to solve the Chebychev polynomial fitting problem that had been posed to him by Storn. Differential evolution algorithm is a parallel individual-based search algorithm, which uses Number of populations 'Np'. Each population is N-dimensional vector, (which are basically the Number of parameters to find or match) in each generation. For each population objective function is evaluated. Then it tries to evolve this population by simple arithmetic operations on these vectors to form new solutions to the problem. It includes five steps, which are discussed in the following sections.

Initialization:

The upper and lower limits or bounds for each parameter must be defined before the initial population can be generated. Two N-dimensional (Parameter dimension or Numbers of Parameters) initialization vectors, X_{MAX} and X_{MIN} , used to store these values, where subscripts MAX and MIN indicate maximum or minimum of the parameters respectively (Price et al., 2005). Once the initial maximum and minimum limits of the parameters have been specified, a random number generator assigns each parameter of every vector a value from within the given limits or range. In addition, each vector of

parameter is assigned a population index, i , which runs from 1 to total number of populations 'Np'.

The random number generator, $\text{rand}(0, 1)$, returns a uniformly distributed random number from within the range $[0, 1]$. The population vectors, of 'N' number of parameters up-to 'Np' numbers of populations, are generated by following equation.

$$x_{i,j} = \text{rand}_j [0,1] \cdot (x_{jmax} - x_{jmin}) + x_{jmin} \quad (2.4.1)$$

The index, $j= 1, 2 \dots N$, indicates the number of parameters of a vector, which are going to be optimized or estimated. The Index, $i, 1, 2 \dots Np$, indicates the number of populations of parameter vectors, which are generated by using equation (2.4.1).

Evaluation and Finding the Best Solution:

After initialization of total number of populations, the objective function value for each vector of population is calculated and then every vector of population is compared to each other in order to get the best solution, which has achieved the optimal objective. These values are stored externally and updated by comparison with all solutions in each iteration or generation.

Mutation:

The mutation operation is the first operation for generation of new solutions from the initial population parameters vectors. In mutation, for every solution (individual) in the population- i in generation- G : $x_i^{(G)}$, $i=1 \dots NP$, a Mutant vector $V_i^{(G+1)}$ is generated using one of the following formulas:

$$V_i^{(G+1)} = x_{r1}^{(G)} + F \left(x_{r2}^{(G)} - x_{r3}^{(G)} \right) \quad (2.4.2)$$

$$V_i^{(G+1)} = x_{best}^{(G)} + F \left(x_{r1}^{(G)} - x_{r2}^{(G)} \right) \quad (2.4.3)$$

$$V_i^{(G+1)} = x_i^{(G)} + F \left(x_{best}^{(G)} - x_i^{(G)} \right) + F \left(x_{r1}^{(G)} - x_{r2}^{(G)} \right) \quad (2.4.4)$$

$$V_i^{(G+1)} = x_{r1}^{(G)} + F \left(x_{r2}^{(G)} - x_{r3}^{(G)} \right) + F \left(x_{r4}^{(G)} - x_{r5}^{(G)} \right) \quad (2.4.5)$$

Where: $x_{r1}^{(G)}$, $x_{r2}^{(G)}$, $x_{r3}^{(G)}$, $x_{r4}^{(G)}$ and $x_{r5}^{(G)}$ are five randomly selected parameters solution vectors from the current generation (different from each other and the corresponding x_i) and $x_{best}^{(G)}$ is the parameter solution achieving best objective function value. 'F' is a mutation parameter or factor and it has the any value between 1 and 0. In this work mutation factor is taken as 0.85. The mutation factor or parameter 'F' plays significant role in controlling the optimization speed of convergence.

Crossover:

Crossover is used to enhance the capability and diversity of the Differential evolution algorithm. In differential evolution algorithm crossover operation is used to perturb the mutant vectors of parameter solutions. In this crossover operation the mutant vectors of parameter solutions and its corresponding vector i in the original population are copied to a trial solution according to a certain crossover factor 'CR'. In this work crossover factor is taken as 0.95. For each parameter, a random number is generated between the range of 0 to 1 and this random number is compared with crossover factor, and if random number value is less than or equal to crossover factor, the parameter value is taken from the mutant vector, otherwise it will be taken from the parent.

Selection:

Selection is done by comparing objective function values of parameter solutions of old or parent populations and objective function value of trial parameter solution obtained after mutation and crossover. If the trial solutions performed better than old or parent, then trial solution replace the parent solution, otherwise the old or parent solution is retained.

Stopping Criteria:

Once new generation is produced, the problem updates the global best and this process continues until the algorithm meets the stopping criteria or condition. In order to stop the optimization process there should be some criteria or condition, if this criteria or condition satisfies or meets the optimization algorithm stop to work. In most cases maximum number of iterations and maximum number of objective function evaluations are used as stopping criteria. In this study, maximum number of iterations criteria is used as stopping criteria.

Flow Chart for Differential Evolution algorithm is shown in the figure 2.3.

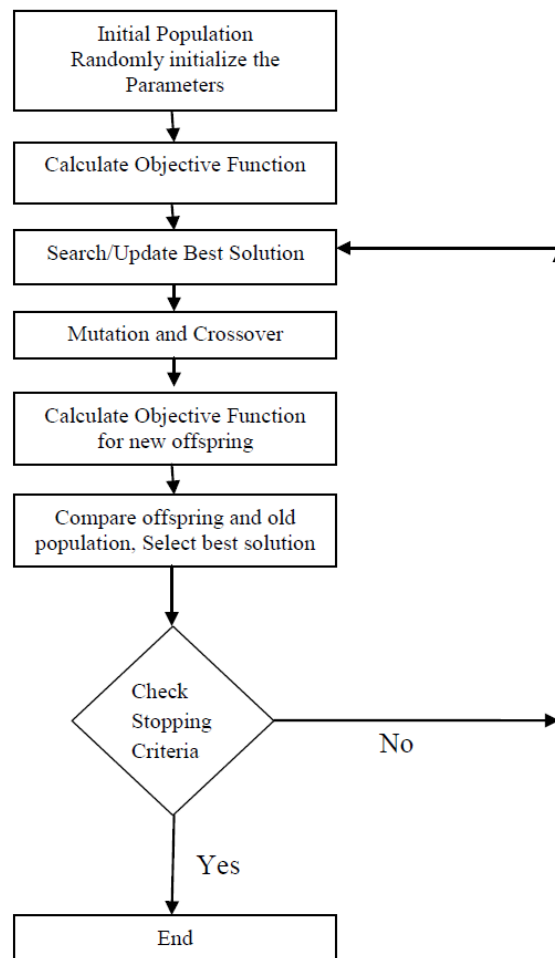


Figure 2.3: Flow Chart for Differential Evolution algorithm

Chapter 3 PROBLEM STATEMENT AND RESEARCH OBJECTIVES

3.1 PROBLEM STATEMENT

There is a challenge in the oil and gas industry to decide on the horizontal well length, number of fracture stages, fracture length patterns, fracture conductivity patterns and fracture spacings simultaneously. Current methods of optimization of Hydraulic Fracturing parameters in Shale Gas reservoir consists of gradient based optimization methods, which can stuck into local minimum solution and avoid global optimum solution. Current methods of optimization of hydraulic fracturing Parameters only cover few parameters like Number of Multistage Fracturing Stages and Multistage Fracturing Spacing. From the Literature review, it is clearly evident that the more parameters of Hydraulic Fracturing should also need to be optimized like Fracture Half Length, amount of Proppant with Fracture conductivity, Optimal Fracture Stages and Fracture Spacings simultaneously with horizontal well length, which give highest Net Present Value. Therefore research objectives of this thesis are optimization of mentioned Hydraulic Fracturing and Horizontal Well Parameters using Stochastic or Global optimization algorithms in Shale Gas Reservoirs.

3.2 RESEARCH OBJECTIVES

The Research objectives of this thesis with respect to optimization of hydraulic fracturing parameters using Stochastic or Global optimization algorithms are given below.

- i. Optimization of Fracture Lengths (Fracture Lengths Patterns).
- ii. Optimization of Fracture conductivity with amount of Proppant (Fracture Conductivities Patterns).
- iii. Optimization of Number of Fracturing Stages.
- iv. Optimization of Fracture Spacings.
- v. Optimization of Horizontal Well Length (Length of Horizontal Lateral).

Chapter 4 Shale Gas Simulation Modeling and Optimization Methodology

4.1 Shale Gas Reservoir Simulation Model

Reservoir simulation is the preferred method as compared to analytical models or decline curve analysis to predict and evaluate shale gas production, because they can include hydraulic fractures with interference of production between fractures, non darcy flow in hydraulic fractures, varying fracture lengths and fracture conductivities of multi stage hydraulic fractures and decrease in fracture conductivity due to increase in effective stress or decrease in pore pressure around hydraulic fractures.

In this study, reservoir simulator (Eclipse) is used to model multi hydraulic fracture stages and horizontal well in a shale gas reservoir for gas production forecasting and prediction. For realistic modeling of multi-fracture stages from horizontal well in shale gas reservoir for accurate gas production and pressure drop prediction and estimation, logarithmically spaced local grid refinement is used in grid cells (global cells) of simulation model. Logarithmically spaced local grid refinement is capable to accurately model multistage hydraulic fracture and long transient behavior of gas from shale matrix to hydraulic fracture. In global grid cells, the hydraulic fracture is explicitly modeled using logarithmically spaced local grid refinement and the hydraulic fracture local grid cells is 1 ft wide. Furthermore, rest of the logarithmically spaced local grids described the shale reservoir matrix. Shale matrix grid cells moving away logarithmically from the hydraulic fracture to properly simulate the large pressure drop between the shale matrix and the hydraulic fracture.

In addition, a dual porosity grid is used to allow simultaneous matrix to natural fracture flow. The turbulent gas flow due to high gas flow rate in propped hydraulic fractures is modeled as non-Darcy flow, which does not occur within the shale itself. The non-Darcy flow is modeled using the Forchheimer modification to Darcy's law given below:

$$-\nabla P = \frac{\mu}{k_f} v + \beta \rho v^2 \quad (4.1)$$

Where v is velocity, μ is viscosity, k_f is fracture permeability, ρ is phase density, β is the non-Darcy Beta factor used in the Forchheimer correction and is determined using a correlation proposed by Evans and Civan (1994) as given below:

$$\beta_{(f)} = \frac{1.485 * 10^9}{k_f^{1.021}} \quad (4.2)$$

Where the unit of k is md and unit of $\beta_{(f)}$ is ft^{-1} . The $\beta_{(f)}$ correlation was obtained using over 180 data points including those for propped fractures and was found to match the data very well with the correlation coefficient of 0.974. This equation is used to calculate $\beta_{(f)}$ and used into the numerical model accounting for non-Darcy flow in hydraulic fractures.

4.1.1 Langmuir Isotherm for Desorbed/Adsorbed Gas in Shale Gas Simulation Modeling

Langmuir isotherm is used to model gas desorption/adsorption phenomena in shale gas simulation model. It is one of the widely used method to include gas desorption/adsorption effect in shale gas reservoir. The amount of gas adsorbed on a solid surface is given by Langmuir equation below (Langmuir 1918), characterizing physical desorption processes as a function of pressure at constant temperature:

$$G_s = \frac{V_L P}{P + P_L} \quad (4.3)$$

where G_s is the gas content in scf/ton, V_L is the Langmuir volume in scf/ton, P_L is the Langmuir pressure in psi, and P is pressure in psi. The bulk density of shale (ρ_B) is needed to convert the typical gas content in scf/ft³ to scf/ton.

Langmuir pressure and Langmuir volume are two most important parameters for gas desorption or adsorption phenomena. Langmuir volume is defined as the gas volume adsorbed or desorbed at the infinite pressure. It also represents the maximum storage capacity of shale rock for gas. Langmuir pressure is defined as the pressure corresponding to one-half Langmuir volume. It is noted that higher Langmuir pressure releases more adsorbed gas at the same reservoir pressure. The Langmuir isotherm is often determined in laboratory using core samples. Eclipse 300 is used for shale gas simulation modeling, which has the capability to take Langmuir isotherm into consideration, if the reservoir is defined as Coal. In this work Barnett shale gas Langmuir isotherm data is used, which contains Langmuir pressure of 650 psi and Langmuir volume of 96 scf/ton (Mengal and Wattenbarger, 2011). Langmuir isotherm curve of the Barnett Shale is illustrated in Fig. 4.1.

4.1.2 Geo-mechanical effects of Hydraulic Fractures in Shale gas simulation modeling

The geomechanical effect in shales should not be ignored in order to model shale gas reservoir realistically. Effective stresses around the hydraulic fractures increase significantly with the decrease in pore pressure around the hydraulic fracture. This would result in the decrease in fracture conductivity or permeability of the hydraulic fractures.

Laboratory data showing the effect of closure stress, referred to as the difference between the minimum horizontal stress and the pressure inside the fracture, on propped fracture conductivity for different shale samples ranging from stiff to soft shales (Alramahi and Sundberg, 2012). Therefore Geomechanics of hydraulic fractures, i.e. stress or pore pressure dependent fracture conductivity, is also considered using a specific compaction table, accounting for the decreasing conductivities of propped fractures with an increase in closure stress or decrease in pressure, as shown in Fig. 4.2.

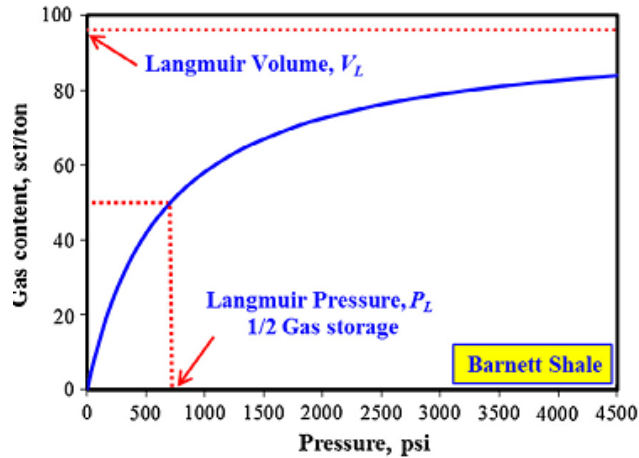


Figure 4.1: Langmuir isotherm curve for Barnett Shale

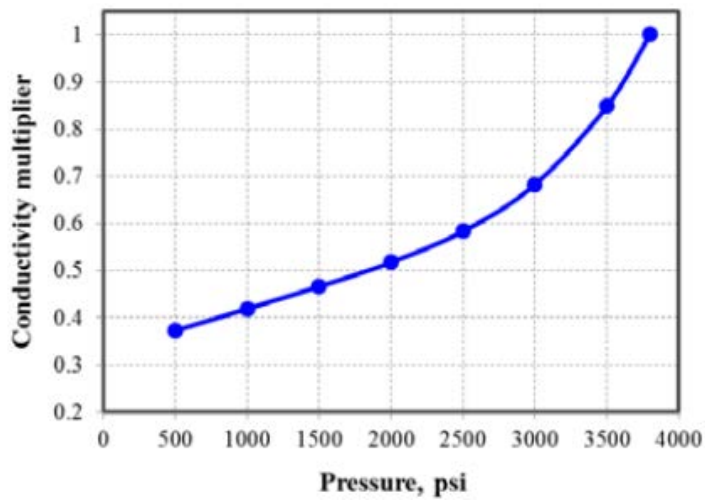


Figure 4.2: Fracture Conductivity multiplier versus Pore Pressure for Barnett Shale

4.1.3 Shale gas reservoir simulation model calibration/History matching to real Field data

Shale gas reservoir model has been set up with a volume of 3000 ft X 1500 ft X 300 ft, based on average reservoir data obtained from the study of Grieser et al. (2009). In this work, a field production dataset from Barnett Shale was used to perform history matching in order to validate hydraulic fracture model (Grieser, et al., 2009).

In this shale gas reservoir simulation model, the fracture half-lengths are different from each other and predictions of various values of fracture half length were provided by the fracture maps obtained by using geophones installed in offset wells (Grieser, et al., 2009; Wei Yu and Sephernoori, K, 2013a). Reservoir modeling including hydraulic fractures for this well is shown in Fig. 4.3. Fig. 4.4 presents the history matching results with considering gas desorption and geomechanics effects. It can be seen that a reasonable match between the numerical simulation results and the actual field data is obtained. History matching results showed that the shale gas reservoir simulation model is calibrated and given methodology for shale gas reservoir modeling can be used for shale gas production forecasting, prediction and optimization.

The shale gas reservoir information is shown in the table 4.1.

Table 1: Table 4.1: Basic Shale Gas Reservoir Information

Input Parameters	Values	Units
Initial reservoir pressure	3800	psi
Depth of the reservoir	7000	ft
Reservoir Temperature	180	°F
Initial Gas Saturation	0.7	fraction
Matrix Permeability (Average from history matching)	0.00001	md
Matrix Porosity (ϕ) (Average from history matching)	0.04	fraction
Shale Compressibility (c)	10^{-6}	psi-1
Viscosity of Gas (μ)	0.02	cp
Bottom-hole pressure (BHP)	1500	psi
Reservoir Model dimensions (Length X Width X Height)	3000x1500x300	ft x ft x ft
Production Time Period (Total Production Time)	10	years
Fracture height	300	ft
Horizontal wellbore length	2120	ft
Number of Grid Block in X direction	60	Grids
Number of Grid Block in Y direction	30	Grids
Number of Grid Block in Z direction	3	Grids
Direction of Minimum Horizontal Stress	X	direction
Phases	Gas	
Number of Multi-fracturing Stages	20	Stages
Langmuir Volume	96	scf/ton
Langmuir Pressure	650	psi
Fracture Spacing	100	ft
Fracture Conductivity of all fracturing Stages	1	md-ft
Bulk Density	2.58 (161.02)	g/cm^3 (lb/ft^3)

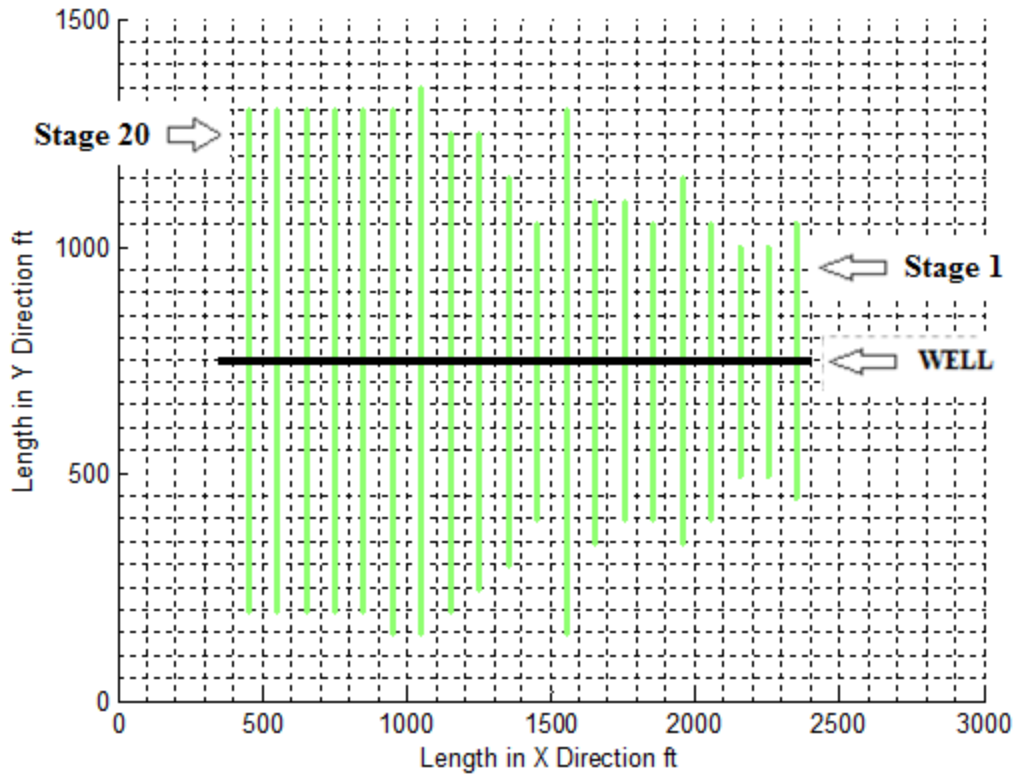


Figure 4.3: Top view of Shale gas reservoir model with hydraulic fractures of different lengths

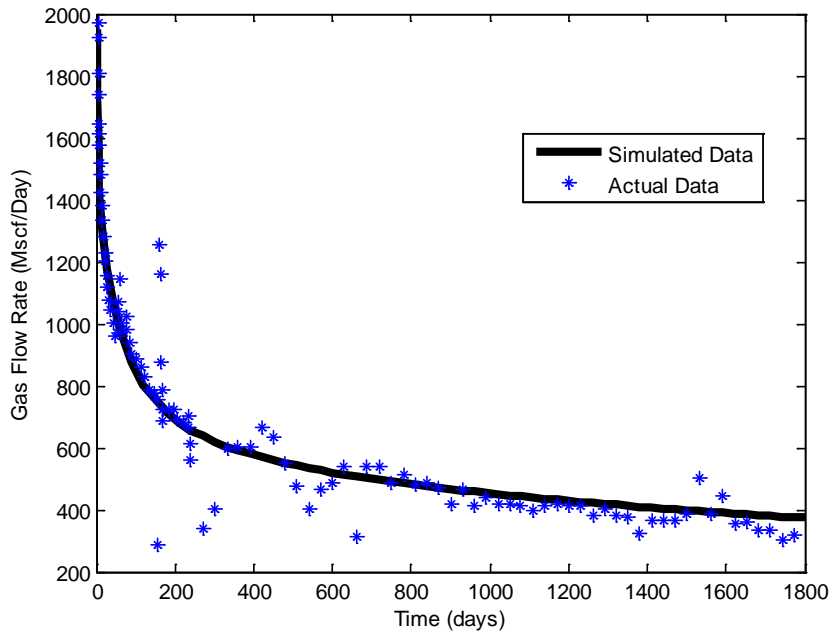


Figure 4.4: History Matched Results of Shale gas reservoir simulation model with Real Field Data

4.2 Economic Model, Objective and Cost Functions

In this work, the objective of the optimization in Shale gas reservoir is to increase the profit. Net present value is the key parameter to profit evaluations and quantification. In order to calculate the profit or net present value, revenues from gas and costs of horizontal well with multi stage hydraulic fracturing are calculated.

The general net present value mathematical relationship with horizontal wells and multi stage hydraulic fracturing is given in equation 4.4. This relationship can be used to evaluate profits in terms of Net present value for any number of wells and multi fracturing stages in shale gas reservoir.

$$NPV = \sum_{k=1}^{N_{ts}} \sum_{j=1}^{N_{wells}} \frac{(Q_{gas} \Delta t_k R_{gas} - Q_w \Delta t_k R_{water})}{(1+d)^{\frac{t_k}{365}}} - \left(FC + \sum_{j=1}^{N_{wells}} \left(C_{well_j} + \sum_{i=1}^{N_{fsj}} C_{fs_{ij}} \right) \right) \quad (4.4)$$

In the above equation N_{ts} is the total number of time steps, k is index of first time step to total number of time steps, N_{wells} is the total number of wells, j is the index of first well to total number of wells, N_{fsj} total number of fracturing stages in well j , i is the index of first fracturing stage to total number of fracturing stages of well j , Q_{gas} is the producing rate of gas at time step k , Δt_k is the time step at index k , R_{gas} is the price of the gas, Q_w is the producing rate of water at time step k , R_{water} is the cost of water disposal, d is the discount rate, FC is the fixed cost, C_{well_j} is the cost of well j and $C_{fs_{ij}}$ is the cost of fracturing stage i well j .

The first term of the above equation is representing discounted revenue generated from the gas production subtracted water production disposal cost and the second term is

related to the fixed cost of multistage hydraulic fracturing of N_{wells} , cost of N_{wells} and cost of N_{fs} multi fracture stages of N_{wells} .

In this work one well is considered in shale gas reservoir simulation modeling for maximization of Net present value and there is no water production so above relationship can be written as in the following way.

$$NPV = \sum_{k=1}^{N_{ts}} \frac{Q_{gas} \Delta t_k R_{gas}}{(1+d)^{\frac{t_k}{365}}} - \left(FC + \left(C_{well} + \sum_{i=1}^{N_{fs}} C_{fs_i} \right) \right) \quad (4.5)$$

The first term of the equation 4.5 is representing discounted revenue generated from the gas production and the second term is related to the fixed cost of multistage hydraulic fracturing of one well, cost of one well and cost of N_{fs} multi fracture stages of one well.

In order to calculate cost of horizontal well and multi stage hydraulic fracturing, there is a need of appropriate cost functions. These cost functions can be used to calculate the total cost and net present value or profit during the optimization process.

Cost of multi stage hydraulic fracturing depends on cost of fracturing fluid and proppant. Table 4.2 contains economic parameters related to Hydraulic Fracturing. (Mei Yang and Michael J. Economides, 2012). This table contains Mob/Demob and Pumping Charges, which are taken as fix cost, Proppant and Fracturing fluid cost. These hydraulic fracturing economic parameters are used to calculate cost functions related to multi stage hydraulic fracturing.

Table 4.2: Economic parameters related to Hydraulic Fracturing

Parameters	Value
Pumping Charges, \$ (Fix Cost)	100,000
Mob/Demob, \$ (Fix Cost)	70,000
Proppant (Brown Sand) cost, \$/lbm	0.159
Proppant (White Sand) cost, \$/lbm	0.182
Proppant (Ceramic) cost, \$/lbm	0.6
Fracturing Fluids (40 lb/1000gal X-linked gel) cost, \$/gal	0.37
Gas Price, \$/Mscf	4
Discount rate	0.1 (10 %)

For the calculation of cost of multistage hydraulic fracturing, the volume of each fracture stage is calculated. The fracture volume of each stage is used to calculate amount/volume of fracturing fluid and Mass of Proppant. Hydraulic fracture volume is calculated by using equation 4.6.

$$V_f = 2w_f x_f h_f \quad (4.6)$$

In above equation w_f is the width of hydraulic fracture stage, x_f is the half length of hydraulic fracture stage and h_f is the height of hydraulic fracture stage. Cost of fracturing fluid is calculated by the equation 4.8.

$$C_{ff} = 7.48052 \left(\frac{V_f}{\eta_f} \right) R_{ff} \quad (4.7)$$

In equation 4.7, V_f is the volume of hydraulic fracture stage, η_f is the efficiency of fracturing fluid, R_{ff} is the unit cost of fracturing fluid in dollar per unit gallon and C_{ff} is the total cost of fracturing fluid of single stage. Efficiency of fracturing fluid is defined as

volume of fracture created by volume of fracturing fluid and in this work it is taken as 0.5 (50 %).

$$\eta_f = \frac{V_f}{V_{ff}}$$

In order to estimate the cost of proppant the total mass of proppant is required. Mass of the Proppant can be related to the volume of the fracture by using appropriate relationship of fracture conductivity and concentration of Proppant. Figure 4.5 shows the relationship between fracture conductivity and Proppant concentration for ranges 1000 to 10000 md-ft. (Economides and Kenneth G. Nolte 1989)

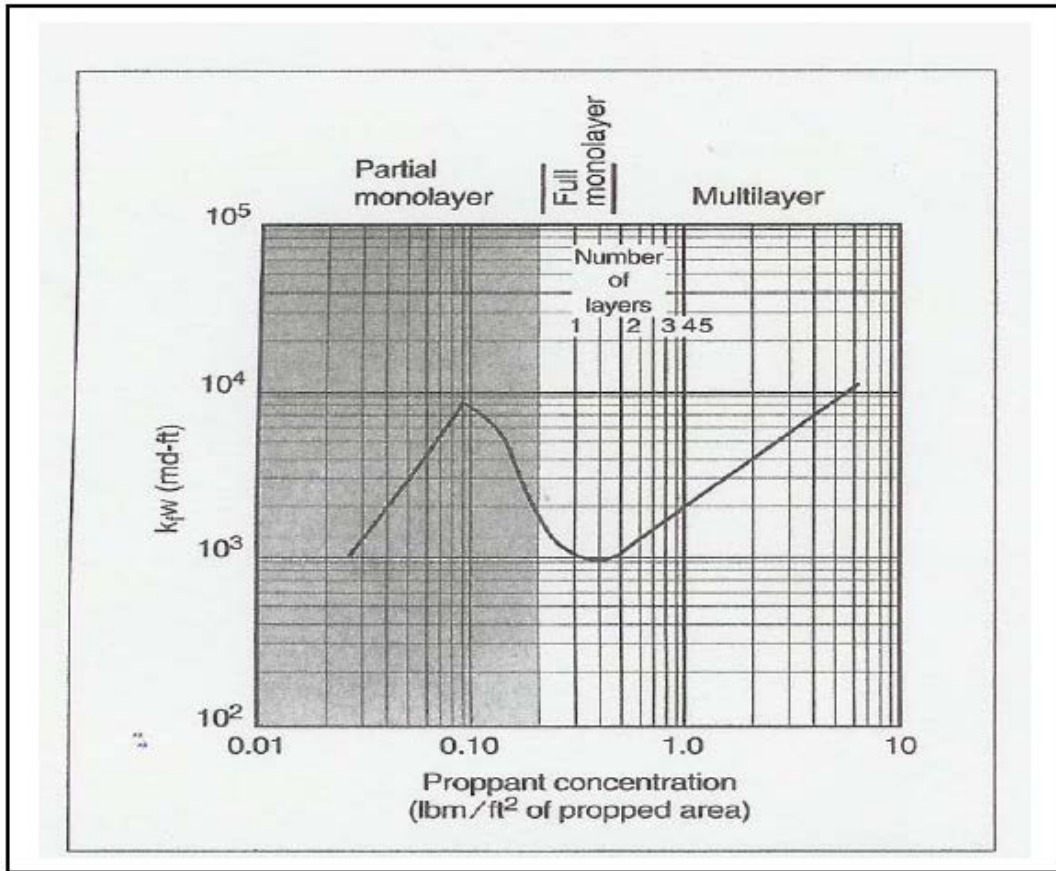


Figure 4.5: Relationship of Fracture conductivity (1000-10000 md-ft) to Proppant concentration

Figure 4.6 shows the relationship between fracture conductivity and Proppant concentration for ranges 1 to 100 md-ft (Junjing Zhang et al 2013). From these two figures it is clearly evident that the fracture conductivity increases with the increase in Proppant concentration. Cost functions for Mass of Proppant are developed based on the data in Figure 4.5 and Figure 4.6. It requires the mathematical relationship between Proppant concentration and Fracture Conductivity. Figure 4.7 and Figure 4.8 show these mathematical relationships for Fracture conductivity ranges between 1 to 1000 md-ft and 1000 to 10000 md-ft respectively.

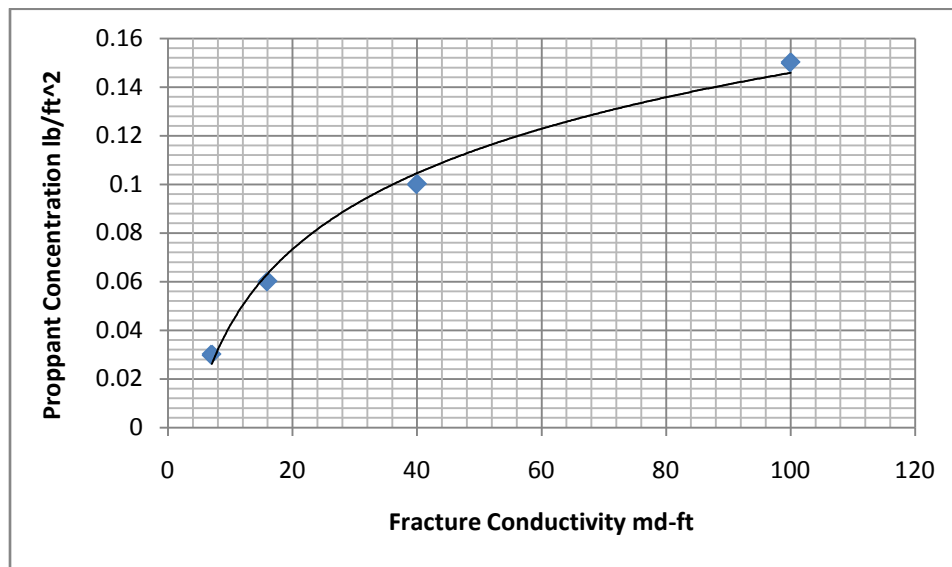


Figure 4.6: Relationship of Fracture conductivity (1-100 md-ft) to Proppant concentration

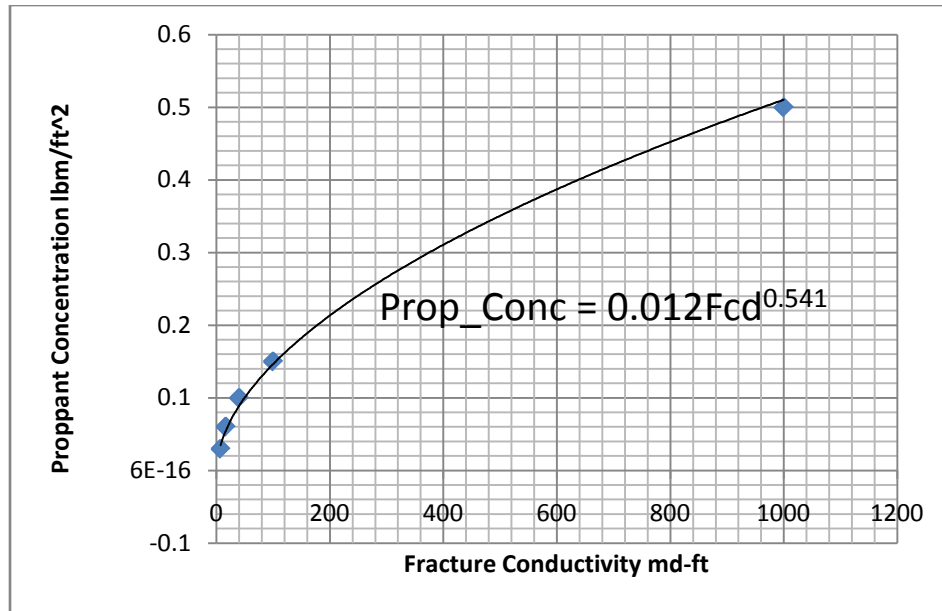


Figure 4.7: Mathematical Relationship of Fracture conductivity (0-1000 md-ft) to Proppant concentration

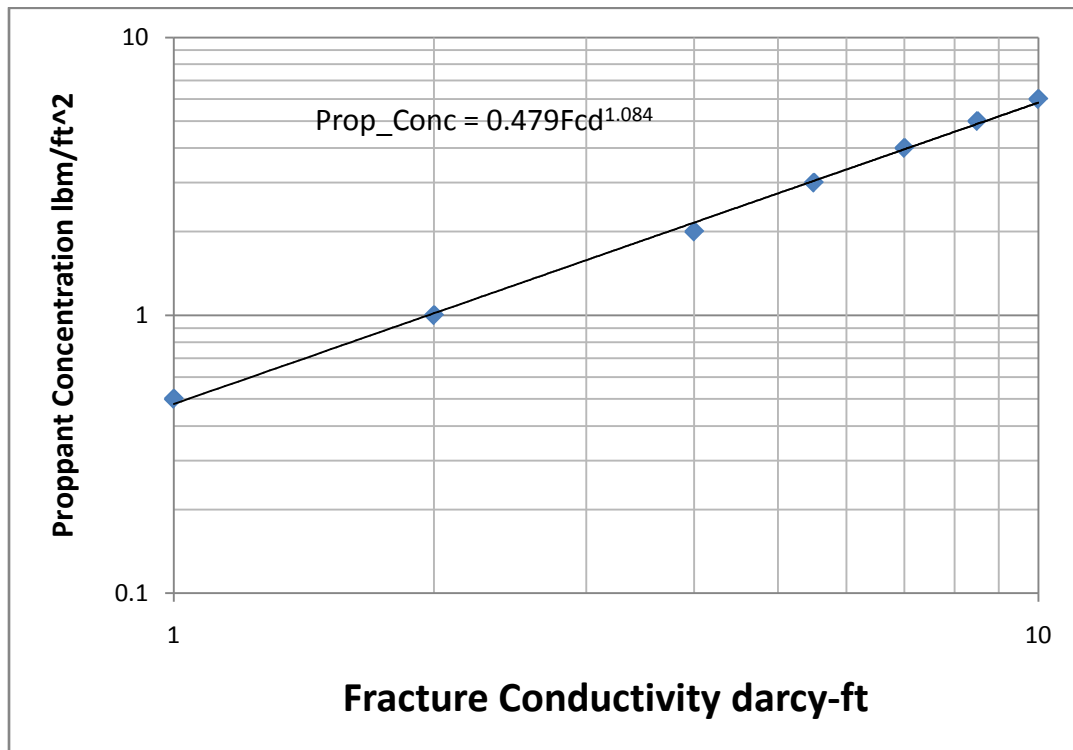


Figure 4.8: Mathematical Relationship of Fracture conductivity (1000-10000 md-ft) to Proppant concentration

$$C_p = \begin{cases} 0.012Fcd^{0.541} & 0 \leq Fcd < 1000md - ft \\ 0.479(Fcd / 1000)^{1.084} & 1000 \leq Fcd \leq 10000md - ft \end{cases} \quad (4.8)$$

The equation 4.8 shows the mathematical relationship between Proppant concentration ‘Cp’ and fracture conductivity ‘Fcd’. Mass of Proppant can be calculated by using Proppant concentration and hydraulic fracture dimensions. Mass of Proppant ‘Mp’ equation is given in following mathematical relationship. (Economides 1992)

$$M_p = C_p (2x_f h_f)$$

Cost of Proppant of single stage can be calculated using Mass of Proppant and unit price of Proppant ‘Rp’ by following relationship.

$$C_{prop} = M_p R_p$$

Total cost of single fracturing stage *i* is given in the following relationship.

$$C_{fs_i} = C_{prop_i} + C_{ffi}$$

Cost of Horizontal well ‘Cwell’ is dependent on length of horizontal well or horizontal lateral. The costs of different horizontal well length or horizontal lateral are given in Table 4.3. This table shows the economic parameters related to Horizontal Well (Wei Yu and Kamy Sepehrnoori, 2013b).

**Table 4.3: Economic parameters related to Horizontal Well
(Wei Yu and Kamy Sepehrnoori, 2013b)**

Horizontal Well Length (ft)	Cost (\$)
1,000	2,000,000
2,000	2,100,000
3,000	2,200,000
4,000	2,300,000

Figure 4.9 shows the relation between length of Horizontal well and its associated cost. This figure is generated by plotting the data from table 4.6. In figure 4.9, linear relation is observed between the lengths of horizontal well and cost of horizontal well. Therefore the cost function of horizontal well length ‘L_{well}’ is represented by straight line equation and given in following equation.

$$C_{well} = 100L_{well} + 19*10^5$$

Therefore the Net Present value relationship for single horizontal well can be written in the following way.

$$NPV = \sum_{k=1}^{N_{is}} \frac{Q_{gas} \Delta t_k R_{gas}}{(1+d)^{\frac{t_k}{365}}} - \left(FC + \left((100L_{well} + 19*10^5) + \sum_{i=1}^{N_{fs}} (C_{propi} + C_{ffi}) \right) \right)$$

$$NPV = \sum_{k=1}^{N_{is}} \frac{Q_{gas} \Delta t_k R_{gas}}{(1+d)^{\frac{t_k}{365}}} - \left(FC + \left((100L_{well} + 19*10^5) + \sum_{i=1}^{N_{fs}} (M_{pi} R_p + 7.48052 \left(\frac{V_{fi}}{\eta_f} \right) R_{ff}) \right) \right)$$

$$NPV = \sum_{k=1}^{N_{is}} \frac{Q_{gas} \Delta t_k R_{gas}}{(1+d)^{\frac{t_k}{365}}} - \left(FC + \left((100L_{well} + 19*10^5) + \sum_{i=1}^{N_{fs}} (C_{pi} (2x_{fi} h_f) R_p + 7.48052 \left(\frac{2w_f x_{fi} h_f}{\eta_f} \right) R_{ff}) \right) \right)$$

$$NPV = \sum_{k=1}^{N_{is}} \frac{Q_{gas} \Delta t_k R_{gas}}{(1+d)^{\frac{t_k}{365}}} - \left(FC + \left((100L_{well} + 19*10^5) + \sum_{i=1}^{N_{fs}} (0.012 Fcd_i^{0.541} (2x_{fi} h_f) R_p + 7.48052 \left(\frac{2w_f x_{fi} h_f}{\eta_f} \right) R_{ff}) \right) \right) \quad (4.9)$$

OR

$$NPV = \sum_{k=1}^{N_{is}} \frac{Q_{gas} \Delta t_k R_{gas}}{(1+d)^{\frac{t_k}{365}}} - \left(FC + \left((100L_{well} + 19*10^5) + \sum_{i=1}^{N_{fs}} \left(\left(\frac{Fcd_i}{1000} \right)^{1.084} (2x_{fi} h_f) R_p + 7.48052 \left(\frac{2w_f x_{fi} h_f}{\eta_f} \right) R_{ff} \right) \right) \right) \quad (4.10)$$

Equations 4.9 and 4.10 show the final Net Present Value relationship for any number of fracture stages in a single horizontal well of variable (unknown) length. The objective function in this work can be described based on the above formulation of Net Present

Value. Since Net present value is the function of number of fracture stages, fracture conductivity of each fracture stage, length of horizontal well and fracture half length of each fracture stage. The objective is to determine these parameters or combination of these parameters, which gives maximum Profit or Net present value. Mathematically this objective function can be represented in the following way.

$$\text{Objective Function} = \max \left(NPV \left(L_{\text{well}}, Nfs, Fcd_i, x_{fi} \right) \right)$$

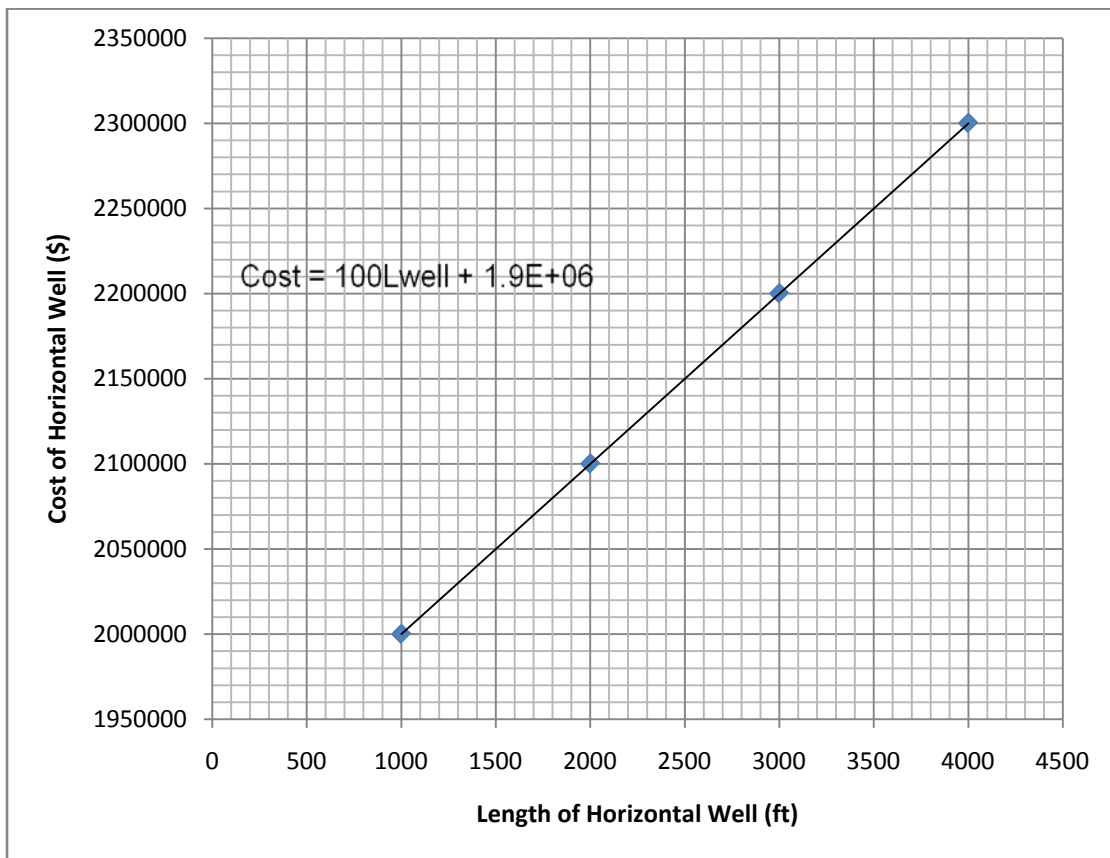


Figure 4.9: Relationship between length of horizontal well and cost of horizontal well

4.3 Optimization Methodology

Stochastic or Global optimization algorithm is coded in Matlab programming language. This algorithm is implemented from the Matlab environment. In this work Differential Evolution is selected as the stochastic or global optimization algorithm.

The optimization scheme is implemented by coupling of optimization algorithm from Matlab to the Shale Gas Simulation model from Commercial Simulator (Eclipse 300). A code from the Matlab calls commercial simulator in order to perform desired optimizations.

Three types of different optimization methodology cases are discussed and implemented in this work. These three cases are given below.

4.3.1 Case 1

In case 1 hydraulic fractures stages, hydraulic fractures spacing and horizontal well length are fixed. Number of fracture stages is also fixed due to the constant hydraulic fractures spacing and horizontal well length. In this case 20 number of fracture stages are taken, which is same as of calibrated (history matched to real field data) base case.

In this case each fracture stage length and conductivity are optimized simultaneously in order to get the optimal fracture length pattern and fracture conductivity pattern, which give maximum net present value or profit. The objective function for this case is given below.

$$\text{Objective Function} = \max \left(NPV \left(Fcd_i, x_{fi} \right) \right) \quad (4.11)$$

Differential Evolution randomly picked values of fracture length in the range of 50 to 1500 ft and fracture conductivity in the range of 1 to 2000 md-ft to each fracture stage. DE tried to maximize objective function using 150 iterations or 3000 function evaluations as stopping criteria (each iteration contains 20 function evaluations). Fracture length and conductivity of each stage are increased or decreased by the incorporating corresponding permeability value to Local Refined Grid of width 1 ft in global grid. For example, if 40 md-ft fracture conductivity is selected by the algorithm, the code incorporate 40 md permeability to 1 ft wide locally refined grid in global grid. Similarly if 500 ft fracture length is selected by the algorithm the code distribute the fracture length symmetrically around the well bore and calculates the number of global grids to obtain the 500 ft fracture length and place the hydraulic fracture by increasing the permeability of 1 ft wide local refined grids of calculated global grids.

The Flow chart of Differential Evolution algorithm for this case is given in figure 4.10.

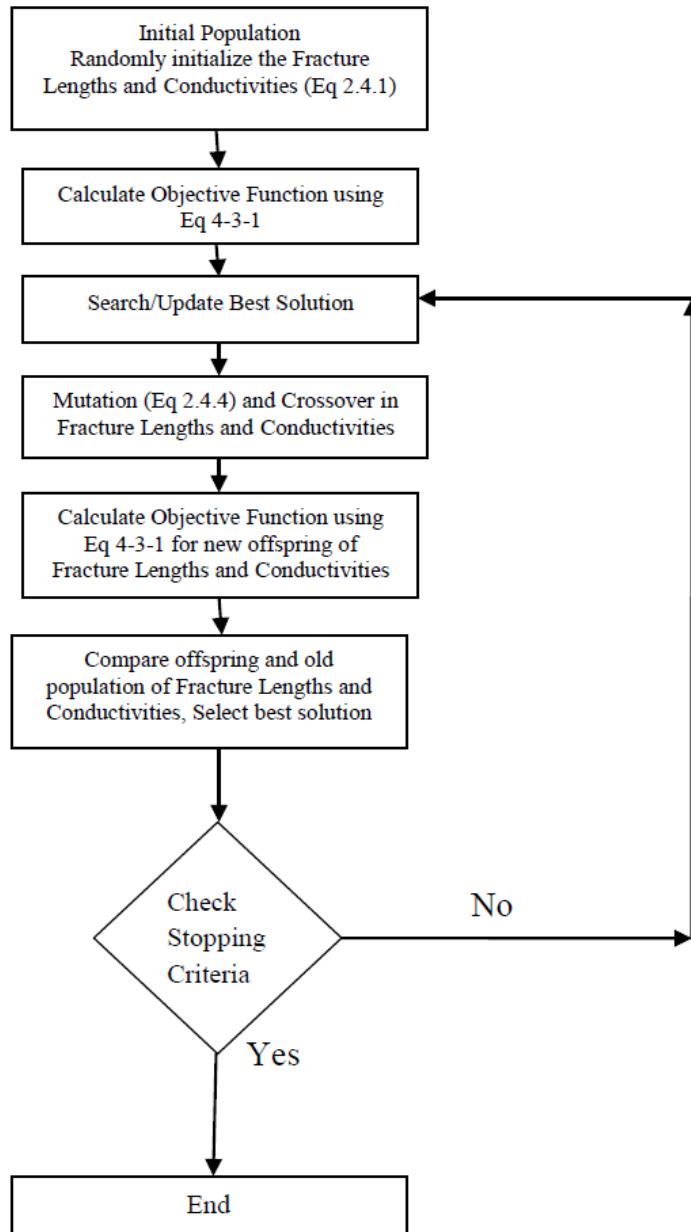


Figure 4.10: Flow Chart for Differential Evolution Algorithm for Case 1

4.3.2 Case 2

In case 2 horizontal well length is fixed. Number of fracture stages, fracture spacing between stages, fracture lengths and fracture conductivities are variables. In this case each fracture stage length, conductivity, spacing with other fracture stage are optimized simultaneously in order to get the optimal fracture length pattern, fracture conductivity pattern, number of fracture stages and fracture spacing, which give maximum net present value or profit. The objective function for this case is given below.

$$\text{Objective Function} = \max \left(NPV \left(N_{fs}, Fcd_i, x_{fi} \right) \right) \quad (4.12)$$

Differential Evolution randomly picked values of fracture spacing in the range of 50 to 400 ft to each fracture stage. Horizontal well length is 2000 ft for this case, which did not change during optimization process. In case 2 number of fracture stages was not directly taken as the optimization parameter, and instead of this code calculates total fractures spacing by summing up individual fracture spacing. If total fractures spacing is greater than fixed horizontal well length, the code eliminates one fracture stage and recalculate the total fracture spacing and this process continues unless total fracture spacing is less than or equal to fixed horizontal well length. Hence the final number of fracture stages is decided by the code after checking total fracture spacing with horizontal well length. For example the code takes initially maximum number of fracture stages, which are 40 stages in this case. After randomly picking of fracture spacing in the range of 50 to 400 ft of each stage the code calculates total fracture spacing. Consider the code picks spacings of individual fracture stage such that total spacing is around 3000 ft, which is greater than horizontal well length (2000 ft), the code eliminates the fracture stages from maximum 40 fracture stages unless total fracture spacing is equal to or less than horizontal well

length (2000 ft). In the end the final number of fracture stages reduced so that total fracture spacing is equal to or less than horizontal well length (2000 ft).

In other words number of fracture stages is decided by the code after checking whether desired number of fracture stages can be incorporated into the fixed horizontal well length under particular fracture spacings constraints. The advantage of this technique is the reduction in number of optimization parameters due to the dependence of number of fracture stages, individual fracture spacing and horizontal well length. DE tried to maximize objective function using 150 iterations or 3000 function evaluations as stopping criteria (each iteration contains 20 function evaluations). Fracture length and conductivity of each stage are increased or decreased by the same methodology as of case 1.

The Flow chart of Differential Evolution algorithm for this case is given in figure 4.11.

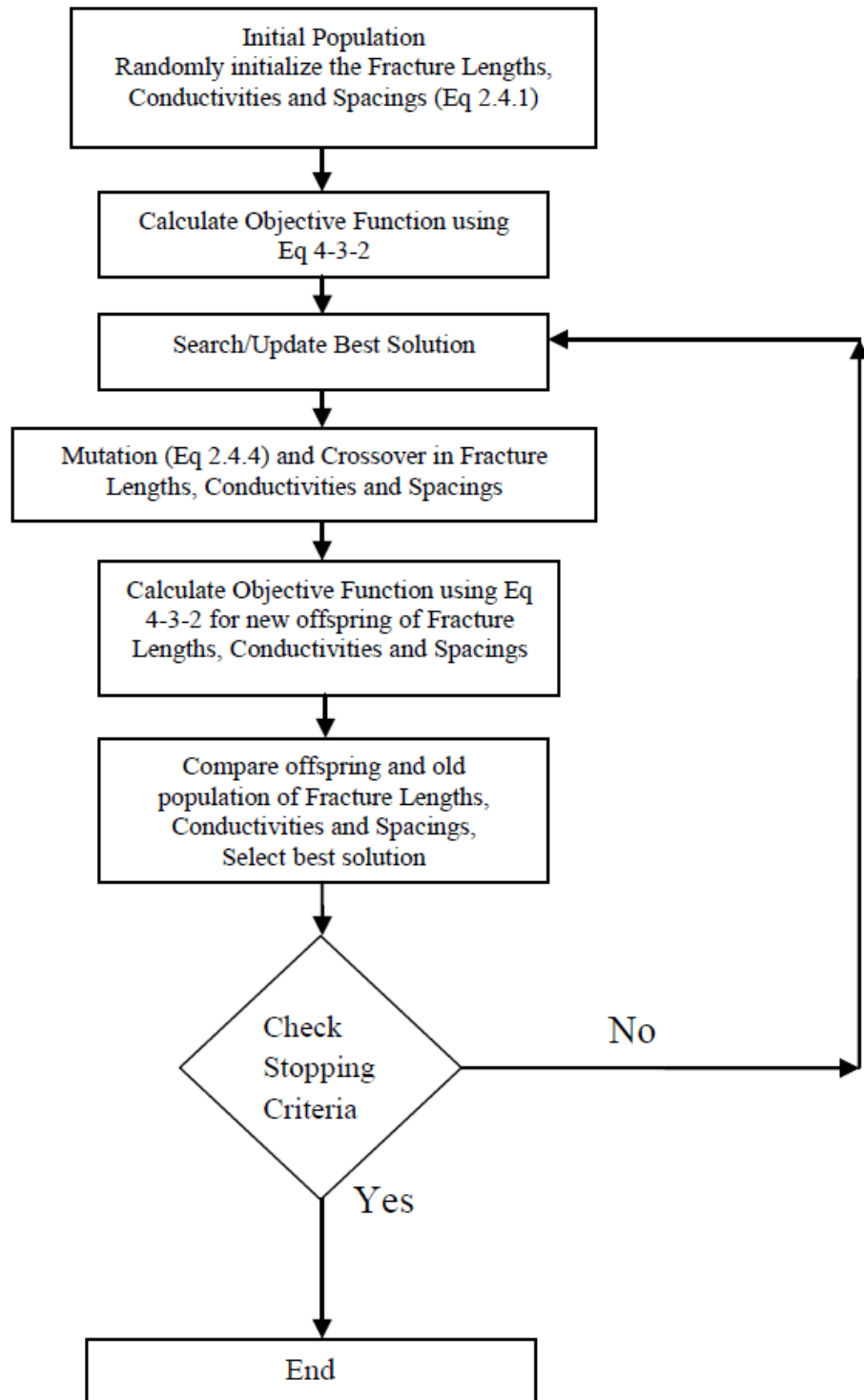


Figure 4.11: Flow Chart for Differential Evolution Algorithm for Case 2

4.3.3 Case 3

In case 3 horizontal well length, number of fracture stages, fracture spacing between stages, fracture lengths and fracture conductivities are variables. In this case each fracture stage length, conductivity, spacing with other fracture stage and horizontal well length are optimized simultaneously in order to get the optimal fracture length pattern, fracture conductivity pattern with number of fracture stages, fracture spacing and well length, which give maximum net present value or profit. The objective function for this case is given below.

$$\text{Objective Function} = \max \left(NPV \left(L_{well}, N_{fs}, Fcd_i, x_{fi} \right) \right) \quad (4.13)$$

Differential Evolution randomly picked values of horizontal well length between 1000-2500 ft. Fracture spacings, fracture conductivities and fracture lengths ranges are same as in previous cases 1 and 2. In case 3 number of fracture stages was not directly taken as the optimization parameter, and instead of this code calculates total fractures spacing by summing up individual fracture spacing i.e. in case 3 the optimization methodology for number of fracture stages selection is same as of case 2. Fracture length and conductivity of each stage are changed by the same methodology as of case 1. The only difference in case 3 is that, the horizontal well length is not fixed and it is also taken as the optimization parameter. For example the code takes initially the horizontal well length between 1000-2500 ft and maximum number of fracture stages, which are 50 stages in this case. After randomly picking of well length between 1000-2500 ft and fracture spacings in the range of 50 to 400 ft of each stage the code calculates total fracture spacing. Consider code picks 1500 ft of horizontal well length and spacings of individual fracture stage such that total spacing is around 2500 ft, which is greater than horizontal

well length (1500 ft), the code eliminates the fracture stages from maximum 50 fracture stages unless total fracture spacing is equal to or less than horizontal well length (1500 ft). In the end the final number of fracture stages reduced so that total fracture spacing is equal to or less than horizontal well length (1500 ft). DE tried to maximize objective function using 150 iterations or 3000 function evaluations as stopping criteria (each iteration contains 20 function evaluations).

The Flow chart of Differential Evolution algorithm for this case is given in figure 4.12.

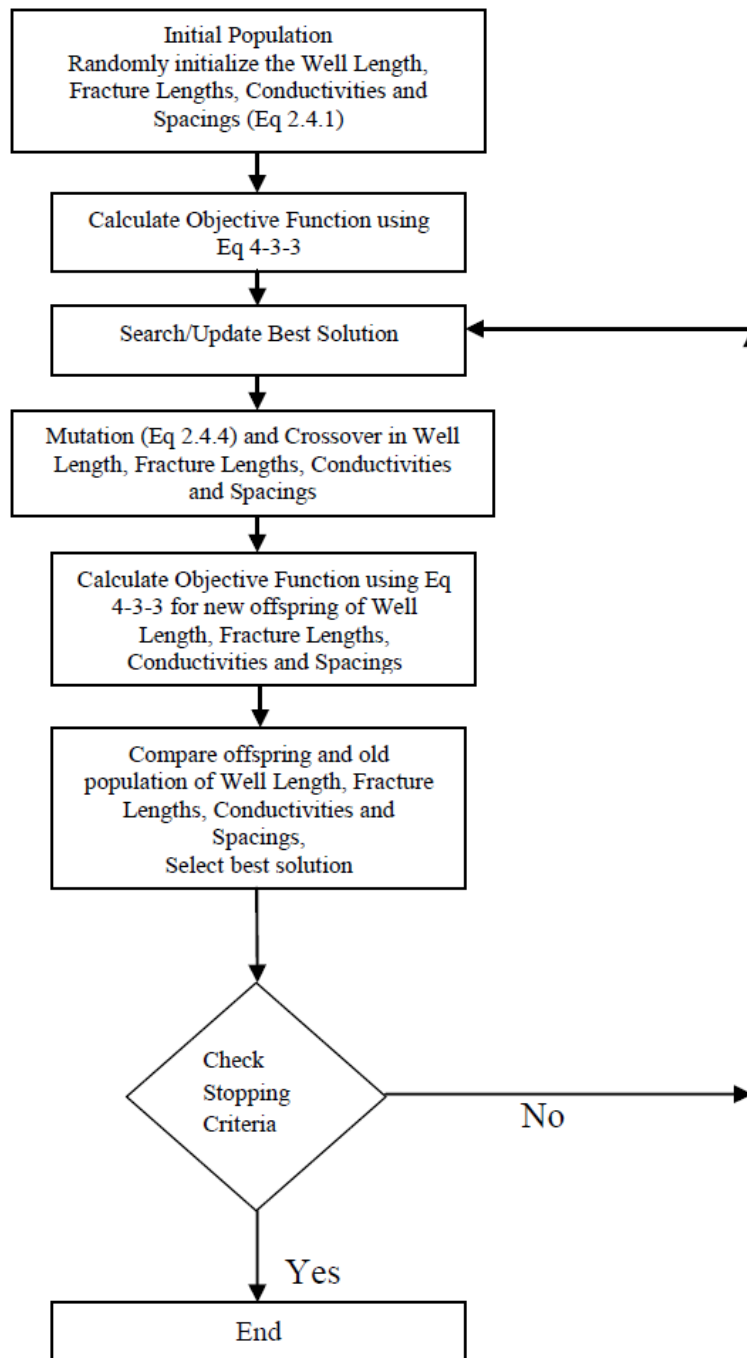


Figure 4.12: Flow Chart for Differential Evolution Algorithm for Case 3

Chapter 5 RESULTS AND DISCUSSIONS

There is a requirement of sensitivity study of hydraulic fracture parameters, which needs to be optimized, in order to select the ranges or search spaces of these parameters. Sensitivity study can give us the idea of what should be the ranges of parameters or search space of parameters during optimization process. The sensitivity study of five hydraulic fracture stages with respect to different fracture spacing and fracture conductivity is given below. The fracture lengths (800 ft) are also kept constant, in order to see only the effect of fracture conductivity and fracture spacing.

5.1 Sensitivity Study of Fracture Spacing and Fracture Conductivity

Figure 5.1a and figure 5.1b show the total cumulative gas production and NPV versus fracture spacing at equal fracture lengths of 800 ft and 5 fracturing stages for different fracture conductivities respectively.

From the figure 5.1a, it is clearly evident that as fracture spacing increases cumulative gas production also increases. It is due to the production interference between fracture stages. At 50 ft the production interference between fracture stages is high, which leads to low cumulative production. Similarly at 100 ft the production interference is relatively low, which lead to relatively high cumulatively production. There is a slight increase in the cumulative production at 150 ft, due to the very low production interference between fracture stages. Total cumulative gas production is the same after 150 ft i.e. from 200 ft to 400 ft, because no production interference was occurred at 200 ft to 400 ft between fracture stages. Figure 5.1a also shows the significant increase in total cumulative production with the increases in fracture conductivity from 1 to 5 md-ft. This is because

more fracture conductivity drains more gas from shale reservoir. In figure 5.1b, similar trends of NPV versus fracture spacing are observed as figure 5.1a, because due to increase in total cumulative gas production, NPV also increases. NPV is negative, because in the sensitivity study only five multi-fracture stages have been taken. For five fracture stages, NPV cannot be positive for all fracture conductivities and fracture spacings. Moreover the sensitivity study has been done for selection of search spaces for fracture conductivities and fracture spacings not for optimization purpose.

Figure 5.2a shows almost the same trend as figure 5.1a. In figure 5.2a fracture spacing trend is almost the same as figure 5.1a i.e. no production interference between fracture stages is observed after 150 ft. More increase in total cumulative gas production is observed in figure 5.2a as compared to figure 5.1a, due to the high fracture conductivity. In figure 5.2b, similar trends of NPV versus fracture spacing is observed as figure 5.2a, because due to increase in total cumulative gas production, NPV also increases.

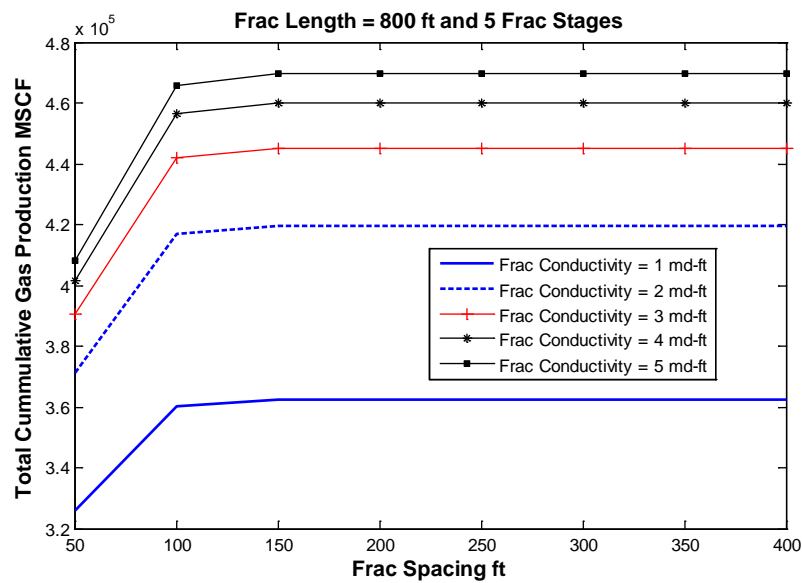


Figure 5.1a: Total Cumulative Gas Production versus Fracture Spacing at Fracture Conductivity 1 to 5 md-ft

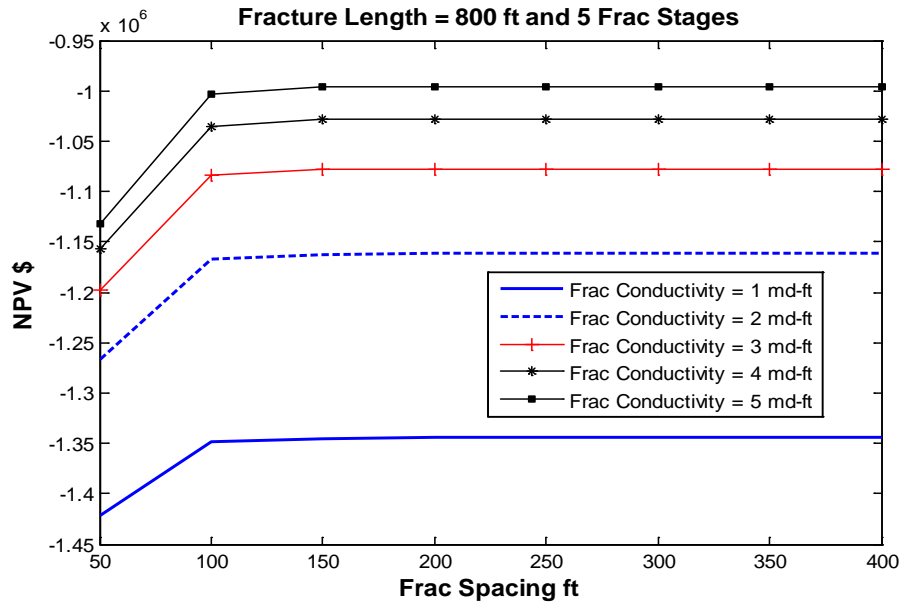


Figure 5.1b: NPV versus Fracture Spacing at Fracture Conductivity 1 to 5 md-ft

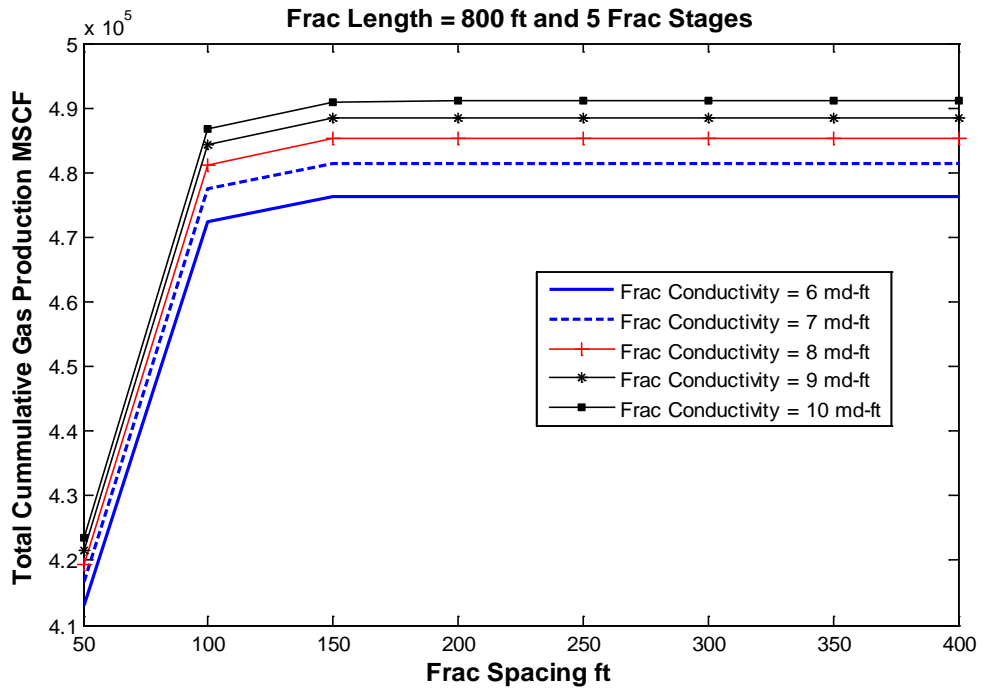


Figure 5.2a: Total Cumulative Gas Production versus Fracture Spacing at Fracture Conductivity 6 to 10 md-ft

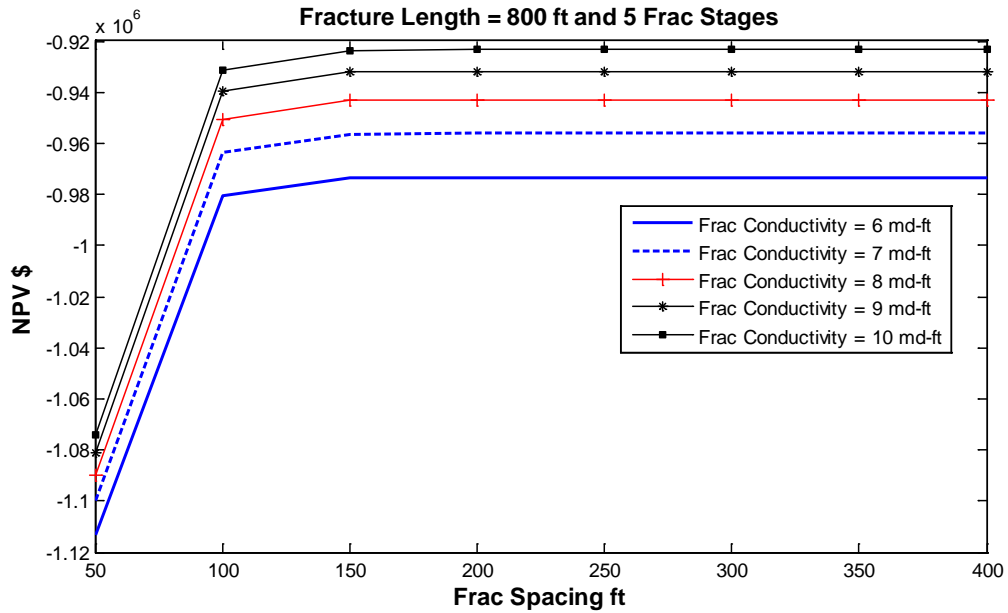


Figure 5.2b: NPV versus Fracture Spacing at Fracture Conductivity 6 to 10 md-ft

Figure 5.3a shows almost the same trend as figure 5.2a. In figure 5.3a fracture spacing trend is almost the same as figure 5.2a i.e. no production interference between fracture stages is observed after 150 ft. More increase in total cumulative gas production is observed in figure 5.3a as compared to figure 5.2a, due to the high fracture conductivity. Moreover in figure 5.3a the increase in total cumulative gas production with respect to fracture conductivity at the same fracture spacing is less as compared to figure 5.2a. In figure 5.3b, similar trends of NPV versus fracture spacing is observed as figure 5.3a, because due to increase in total cumulative gas production, NPV also increases.

Figure 5.4a shows almost the same trend as figure 5.3a due to the same reasons and physical phenomena. Figure 5.4b shows similar trends of NPV versus fracture spacing as observed in figure 5.4a. At fracture conductivity 200 md-ft, NPV is relatively lower than at other fracture conductivities, because rate of increase in cost related to 200 md-ft is higher than the rate of increase in revenue or total gas production.

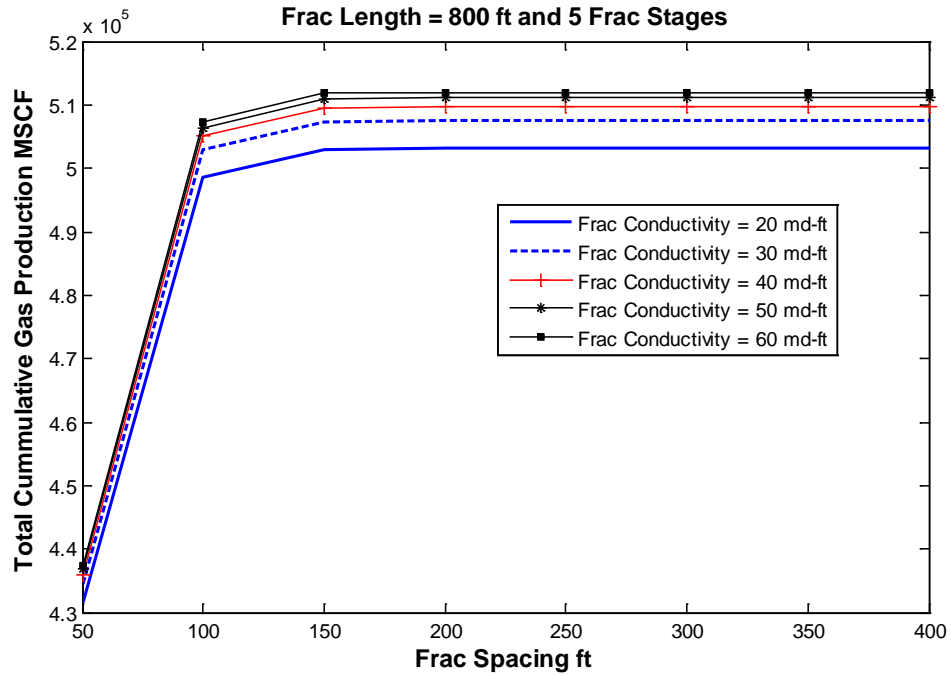


Figure 5.3a: Total Cumulative Gas Production versus Fracture Spacing at Fracture Conductivity 20 to 60 md-ft

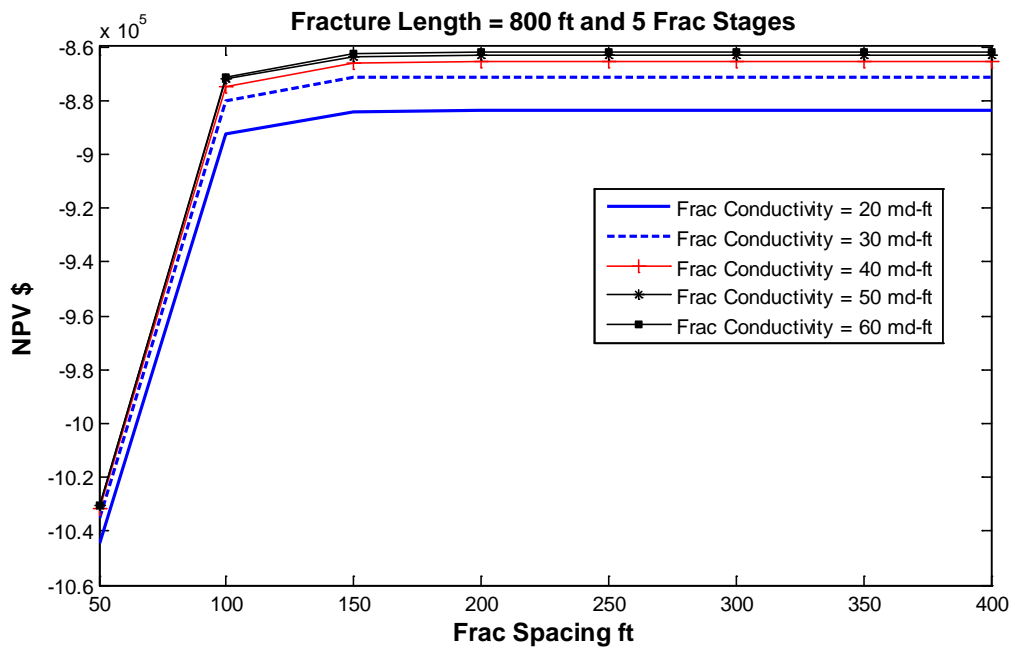


Figure 5.3b: NPV versus Fracture Spacing at Fracture Conductivity 20 to 60 md-ft

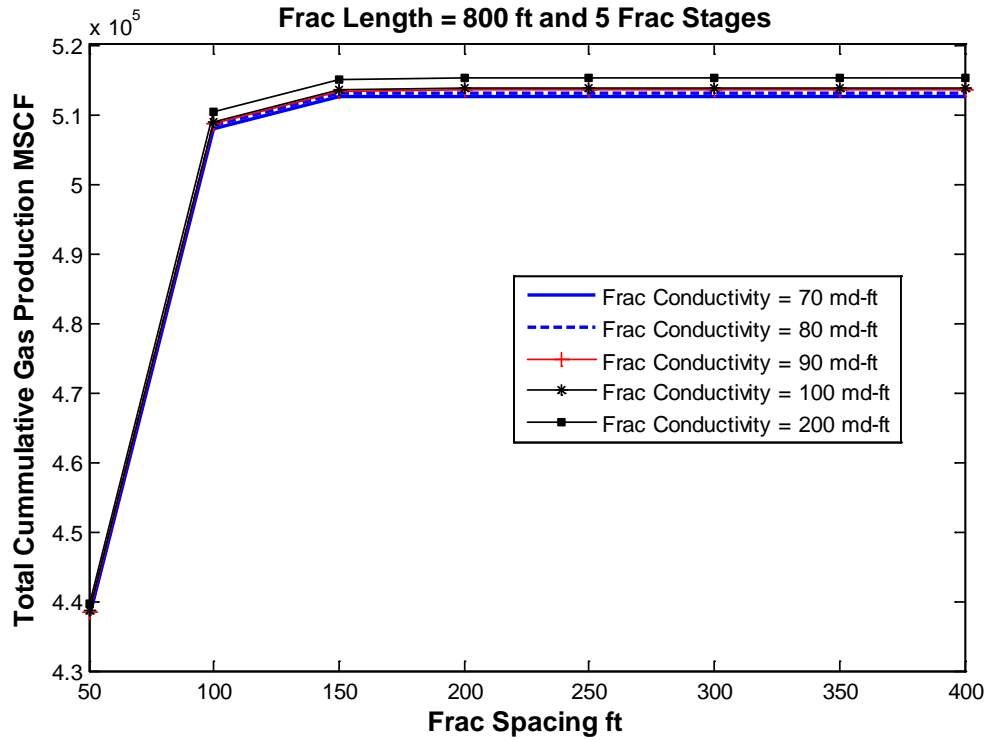


Figure 5.4a: Total Cumulative Gas Production versus Fracture Spacing at Fracture Conductivity 70 to 200 md-ft

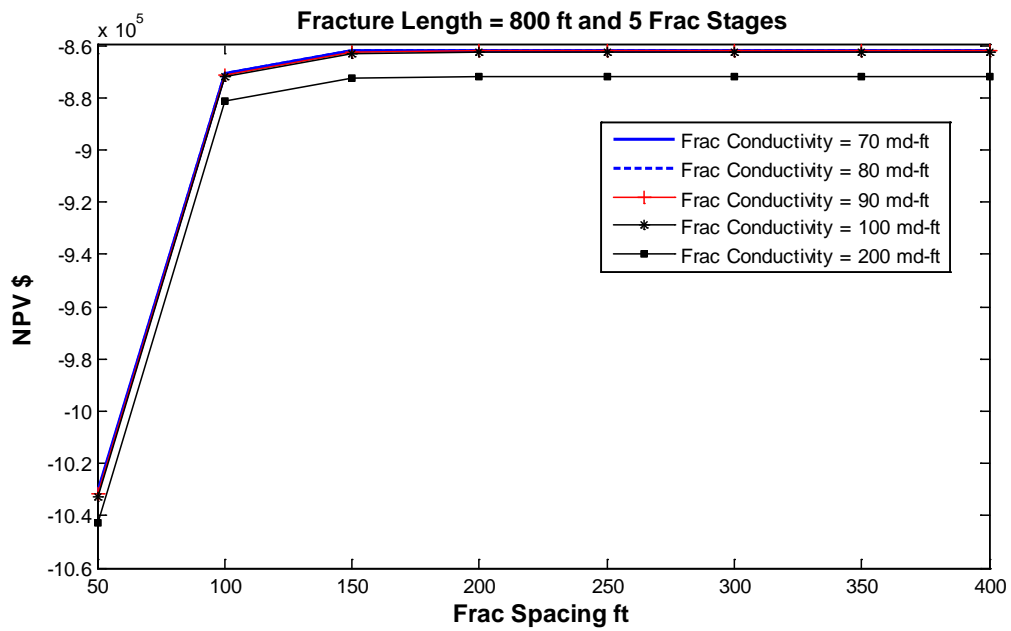


Figure 5.4b: NPV versus Fracture Spacing at Fracture Conductivity 70 to 200 md-ft

Figures 5.5a, 5.6a, 5.7a and 5.8a show almost the same trend as figure 5.4a related to change in total cumulative gas production with respect to fracture spacing. In figures 5.5a, 5.6a, 5.7a and 5.8a fracture spacing trends are almost the same as figure 5.4a i.e. no production interference between fractures stages are observed after 150 ft. Moreover in figure 5.5a, 5.6a, 5.7a and 5.8a the increase in total cumulative gas production with respect to fracture conductivity at the same fracture spacing is almost the same. It may be due to the fact that critical conductivity is achieved or near to fracture conductivity between 300 to 700 md-ft, 800 to 3000 md-ft, 4000 to 8000 md-ft or 9000 to 10000 md-ft at five fracture stages with equal fracture length of 800 ft.

Figures 5.5b, 5.6b, 5.7b and 5.8b show similar trends of NPV versus fracture spacing as observed in figures 5.5a, 5.6a, 5.7a and 5.8a. In Figures 5.5b, 5.6b, 5.7b and 5.8b, NPV is decreasing with the increase in fracture conductivities. It is due to the fact that rate of increase in gas production is low or negligible with respect to high fracture conductivities, as compared to the rate of increase in cost with respect to high fracture conductivities.

From these results it can be easily concluded that search space of fracture spacing during optimization should be between 50 and 200 ft at every two consecutive fracture stages, because after that the cumulative production and net present values remain the same at fracture conductivity between 1 and 10000 md-ft. For appropriate fracture conductivity search space determination, total cumulative production and NPV are plotted against fracture conductivity in semi-log plot at different fracture spacing in figures 5.9a, 5.9b 5.10a and 5.10b.

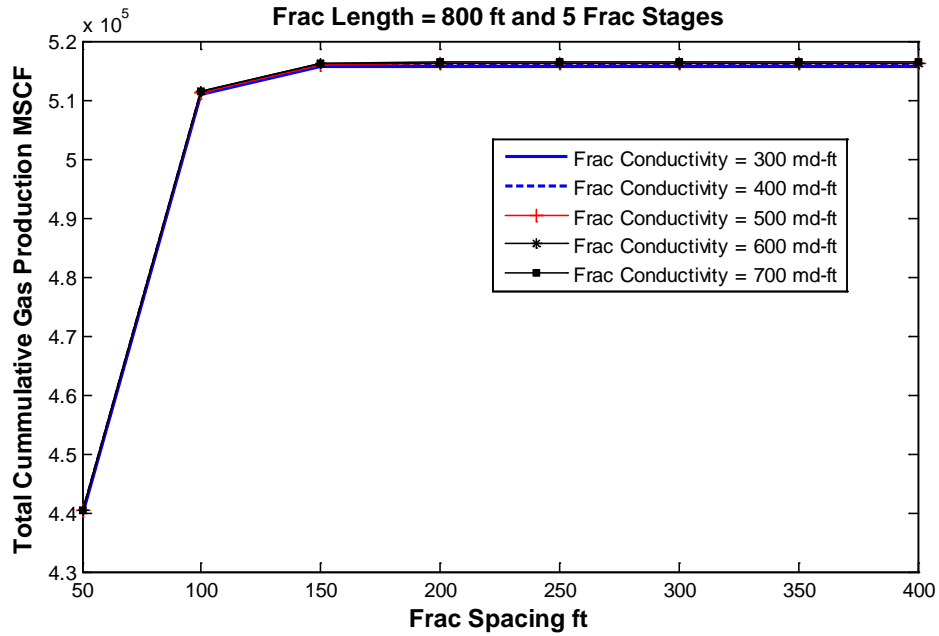


Figure 5.5a: Total Cumulative Gas Production versus Fracture Spacing at Fracture Conductivity 300 to 700 md-ft

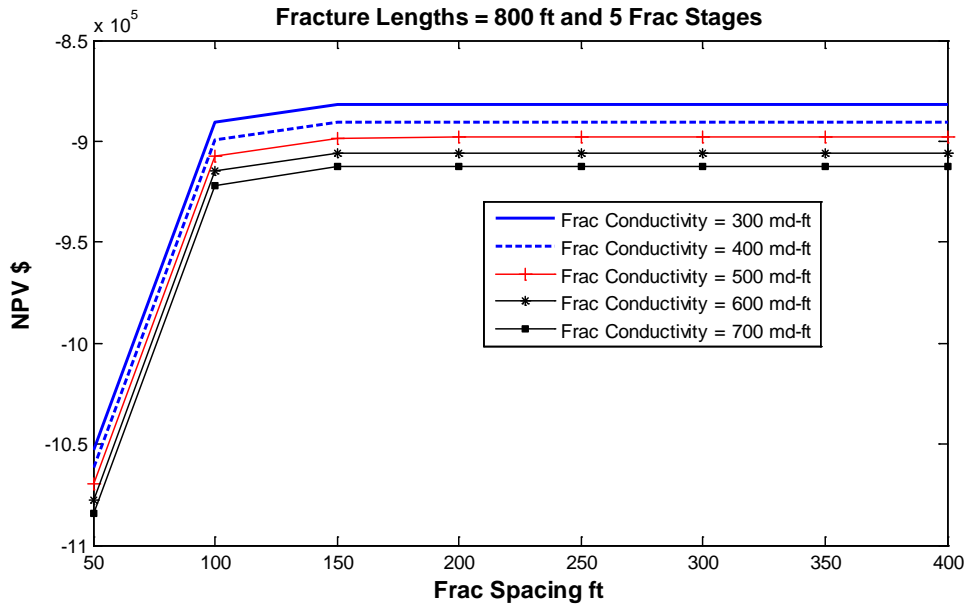


Figure 5.5b: NPV versus Fracture Spacing at Fracture Conductivity 300 to 700 md-ft

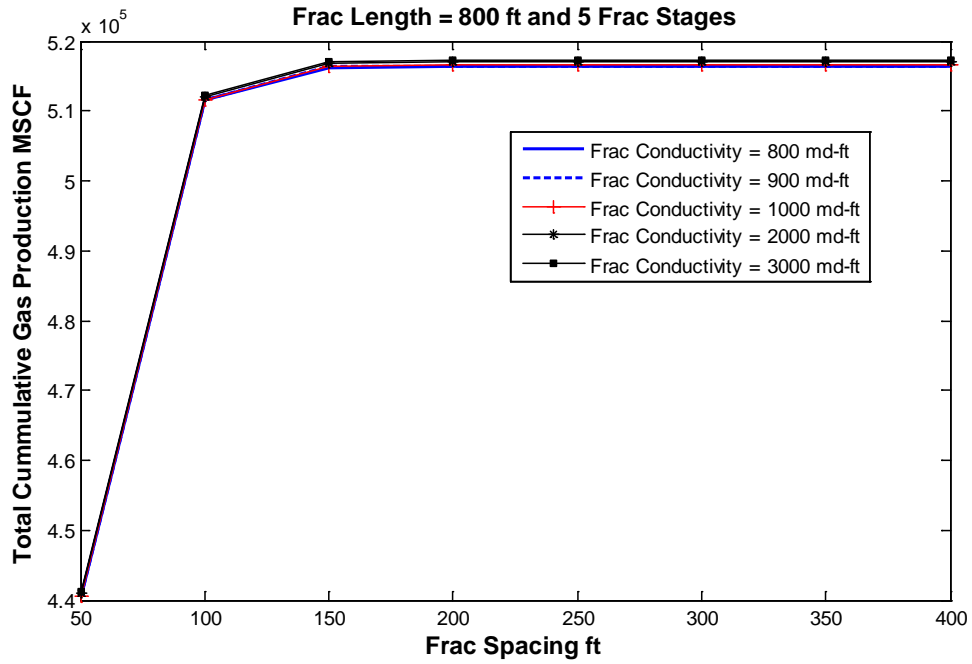


Figure 5.6a: Total Cumulative Gas Production versus Fracture Spacing at Fracture Conductivity 800 to 3000 md-ft

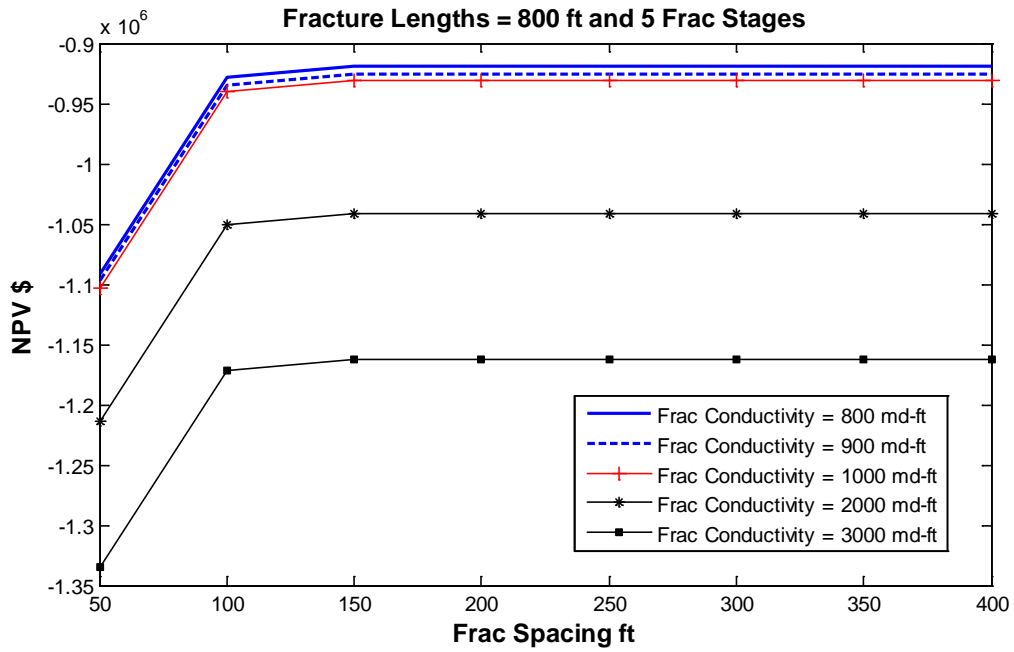


Figure 5.6b: NPV versus Fracture Spacing at Fracture Conductivity 800 to 3000 md-ft

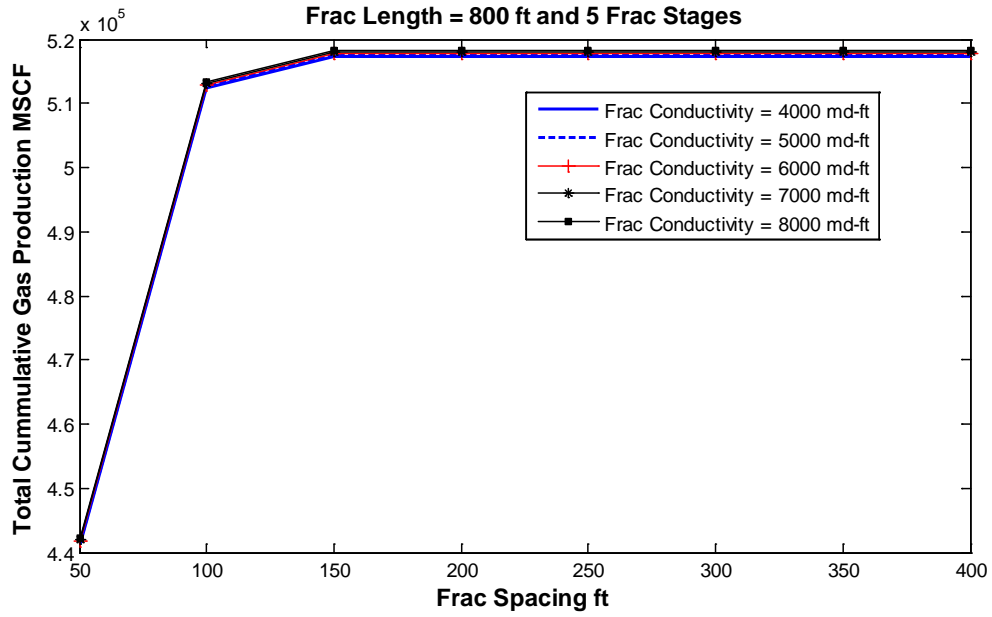


Figure 5.7a: Total Cumulative Gas Production versus Fracture Spacing at Fracture Conductivity 4000 to 8000 md-ft

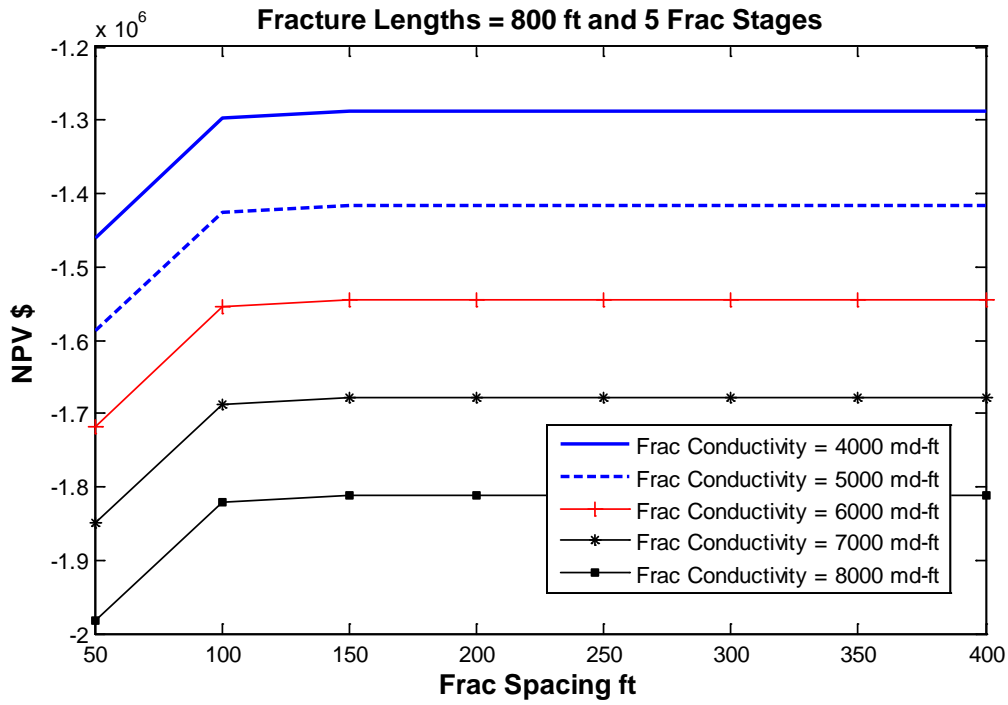


Figure 5.7b: NPV versus Fracture Spacing at Fracture Conductivity 4000 to 8000 md-ft

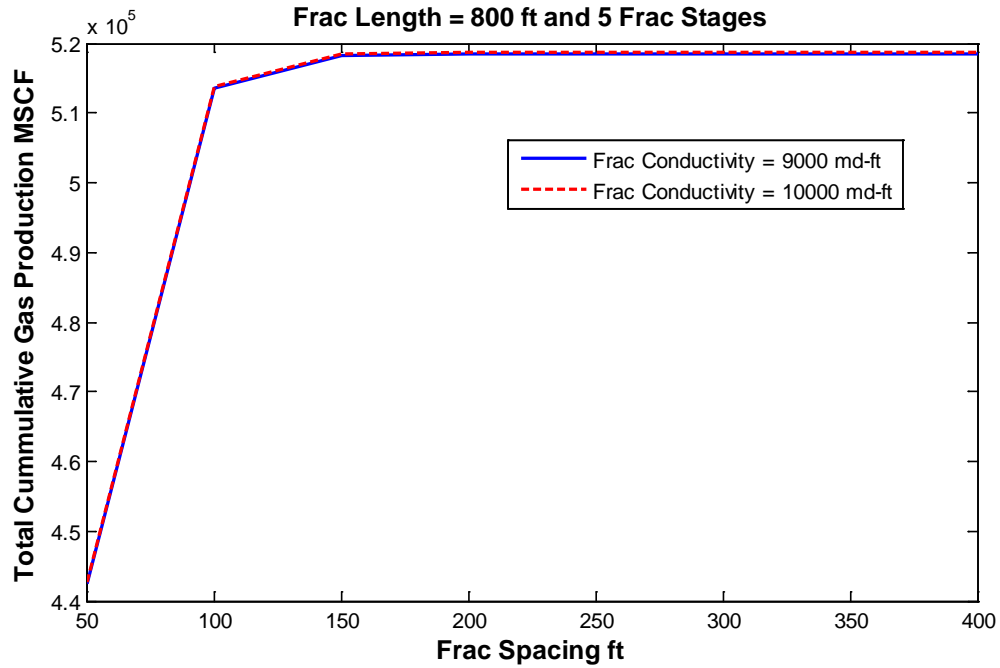


Figure 5.8a: Total Cumulative Gas Production versus Fracture Spacing at Fracture Conductivity 9000 to 10000 md-ft

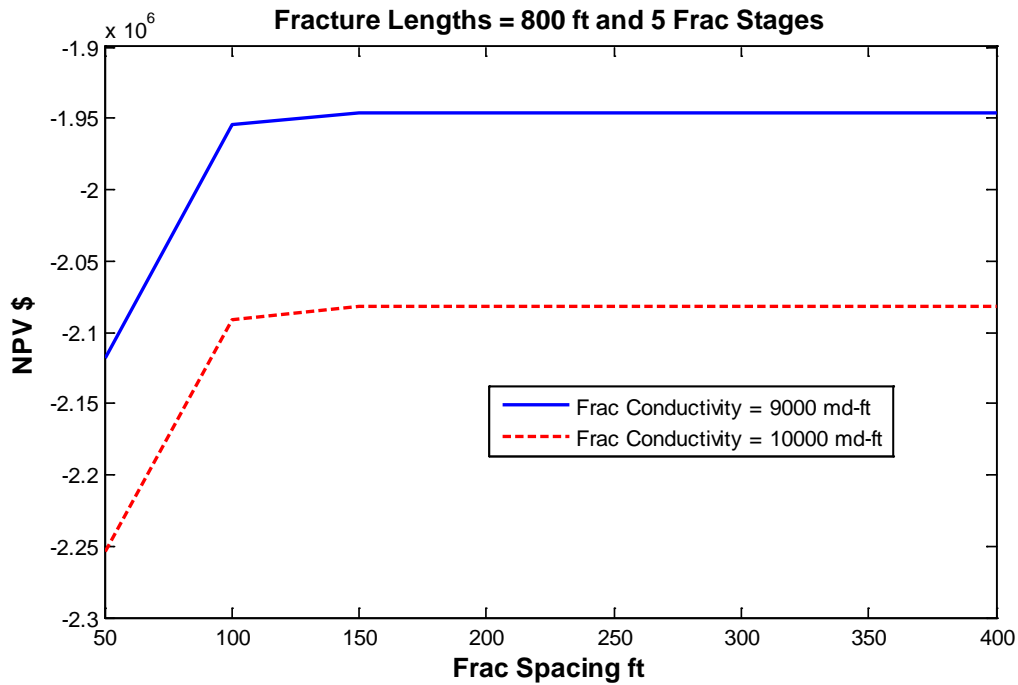


Figure 5.8b: NPV versus Fracture Spacing at Fracture Conductivity 9000 to 10000 md-ft

Figure 5.9a and Figure 5.10a show that as fracture conductivity increases, total cumulative gas production also increases. The increase in total cumulative gas production is high in the range of 1 to 100 md-ft fracture conductivity, after that there is a very little slight increase in total cumulative gas production in the range of fracture conductivity 200 to 2000 md-ft. No increase is observed between 2000 md-ft to 10000 md-ft. Figure 5.9a shows different total cumulative gas production plots versus fracture conductivity at different fracture spacing, it is due to the interference of gas production between fracture stages. In figure 5.9a total cumulative gas production plots are same at fracture spacing 150 ft and 200 ft, because there is no gas production interference after 150 ft fracture spacing. Figure 5.10a shows same total cumulative gas production versus fracture conductivity at fracture spacing 250 ft to 400 ft, because there is no gas production interference after 150 or 200 ft fracture spacing and total cumulative production remains same with respect to fracture spacing greater than 150 or 200 ft.

The trend of figure 5.9b and figure 5.10b are almost same as figure 5.9a and figure 5.10a around 1000 md-ft. After 1000 md-ft, NPV is decreasing with the increase in fracture conductivities significantly. It is due to fact that rate of increase in gas production is low or negligible with respect to high fracture conductivities, as compare to the rate of increase in cost with respect to high fracture conductivities.

It can be easily concluded from the sensitivity results in figures 5.9a, 5.9b, 5.10a and 5.10b that the search space of fracture conductivities during optimization should be between 1 and 2000 md-ft, because after that the cumulative production does not change with respect to fracture conductivities and significant decrease in NPV is observed after 2000 md-ft.

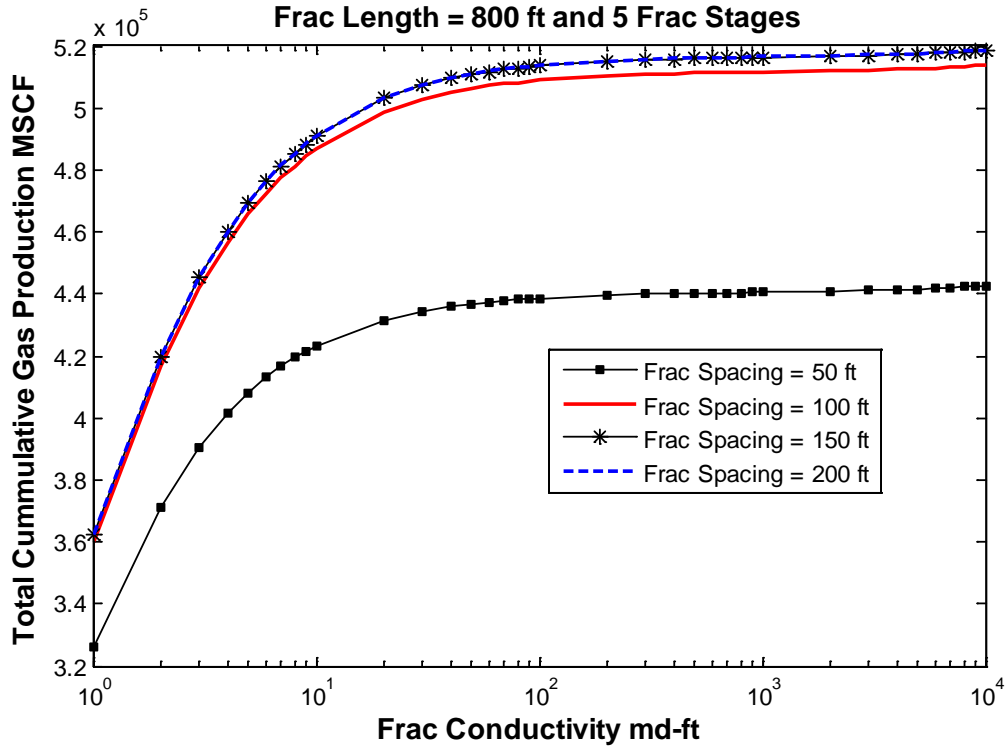


Figure 5.9a: Total Cumulative Gas Production versus Fracture Conductivity at Fracture Spacing 50 to 200 ft

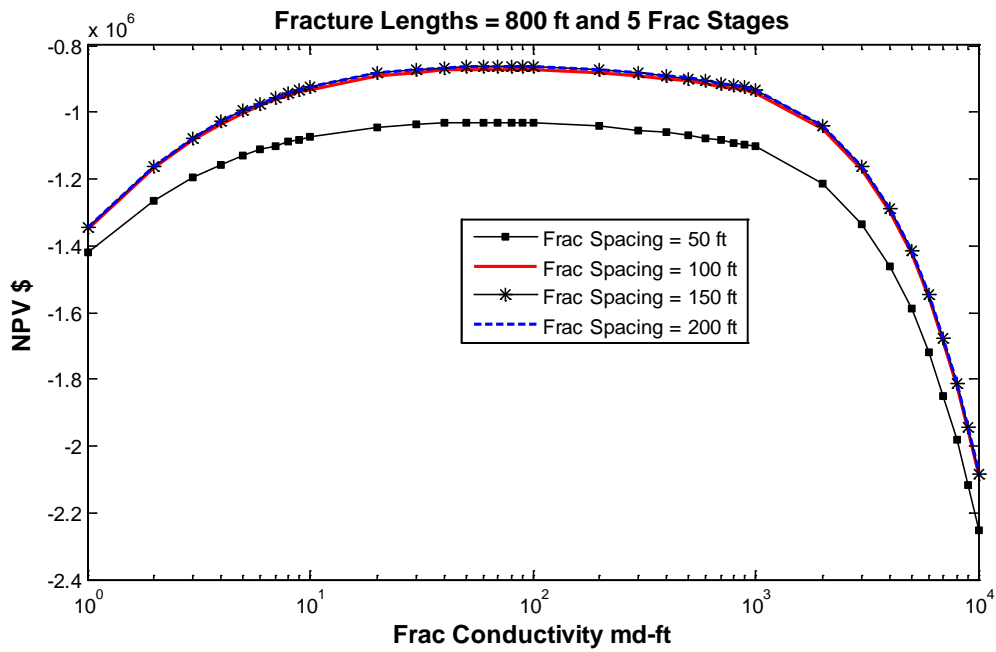


Figure 5.9b: NPV versus Fracture Conductivity at Fracture Spacing 50 to 200 ft

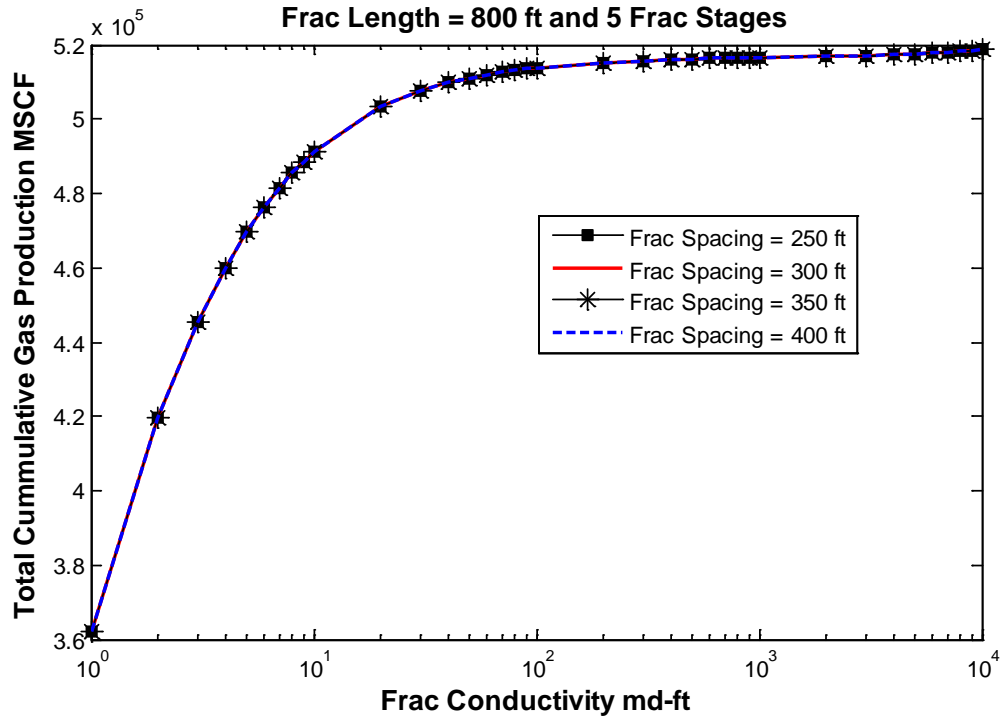


Figure 5.10a: Total Cumulative Gas Production versus Fracture Conductivity at Fracture Spacing 250 to 400 ft

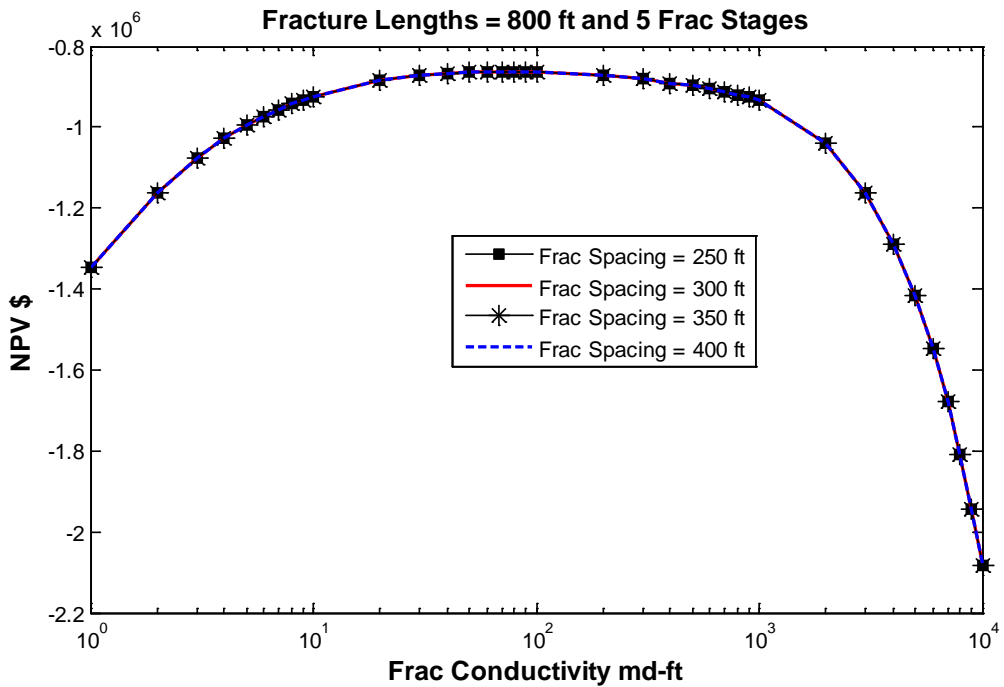


Figure 5.10b: NPV versus Fracture Conductivity at Fracture Spacing 250 to 400 ft

5.2 Case 1 - Optimization of Fracture Lengths and Fracture Conductivities

In case 1 hydraulic fractures stages, hydraulic fractures spacing and horizontal well length are fixed. Number of fracture stages is also fixed due to the constant hydraulic fractures spacing and horizontal well length, because this case contains 100 ft equal fracture spacing in horizontal well of 2000 ft, therefore twenty fracture stages are possible in this horizontal well. Therefore in this case 20 number of fracture stages are taken, which is same as of calibrated (history matched to real field data) base case.

In case 1 twenty fracture lengths and twenty fracture conductivities are optimized in order to find the optimum fracture lengths pattern with fracture conductivities patterns, which give maximum net present value (profit).

Figure 5.11 shows the maximum net present value with respect to realization number obtained after optimization of parameters in Case 1, Case 2 and Case 3. For Case 1 figure 5.11 shows that, realization number 1 gives the highest net present value (6.7 MM\$), realization 2 gives the second best net present value (6.47 MM\$), realization 3 gives the median net present value (6.32 MM\$), realization 4 gives the fourth best net present value (5.84 MM\$) and realization 5 gives the lowest net present value (5.35 MM\$).

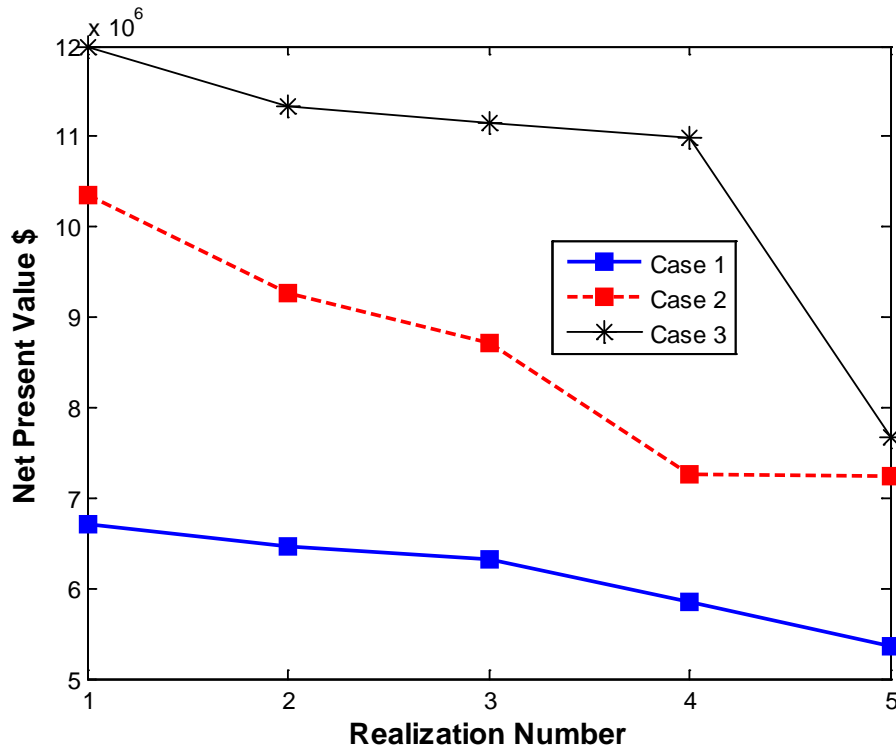


Figure 5.11: Comparison of Net Present Value versus Realization Number for all three cases

Figure 5.12 and figure 5.13 show the Optimal Fracture Lengths and Fracture Conductivities for Case 1, which give best result in terms of net present value. The fracture lengths of fracture stages 8, 14 and 15 are 1450, 1400 and 1450 ft respectively. All fracture stages except 8, 14 and 15 have full fracture lengths of 1500 ft. Fracture conductivities are high of corner fracture stage, which possibly drains more gas from outside of the horizontal well. The middle fracture stages from 7 to 10 contains low fracture conductivities, because they are surrounded by high conductivity fracture stages so this pattern can effectively drains maximum gas from multi-frac stages in horizontal well of length 2000 ft.

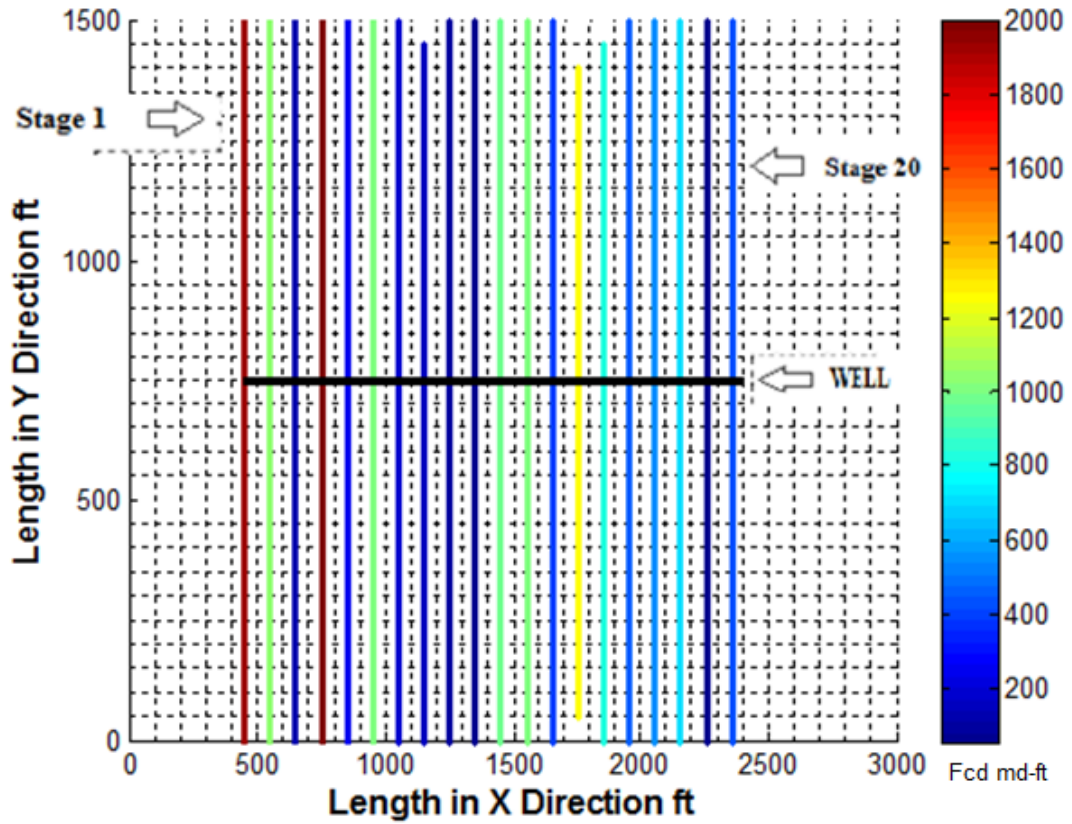


Figure 5.12: Optimal Fracture Lengths and Fracture Conductivities for Case 1 best NPV realization

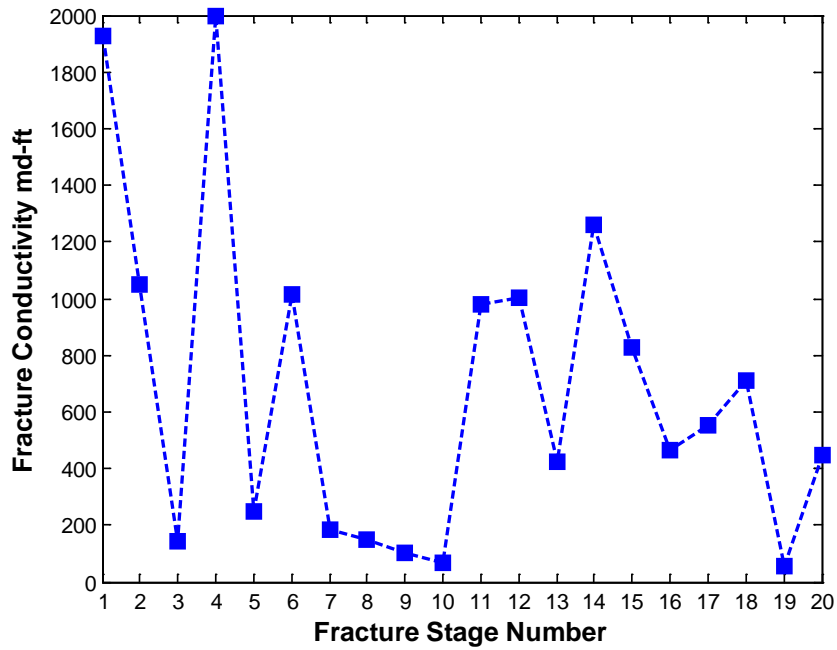


Figure 5.13: Optimal Fracture Conductivities for Case 1 best NPV realization

Figure 5.14 and figure 5.15 show the Optimal Fracture Lengths and Fracture Conductivities for Case 1, which give median net present value. The fracture lengths of fracture stages 5, 6, 8, 13, 15 and 17 are 1450, 1450, 1450, 50 and 1450 ft respectively. All fracture stages except 5, 6, 8, 13, 15 and 17 have full fracture lengths of 1500 ft. Fracture conductivities is in one high of corner fracture stages, which possibly drains more gas from outside of the horizontal well. Due to the suboptimal arrangements of fracture conductivities to fracture stages, the net present value of this realization is lower than best net present value realization.

Figure 5.16 and figure 5.17 show the Optimal Fracture Lengths and Fracture Conductivities for Case 1, which give lowest net present value. The fracture lengths pattern is looking good but may be suboptimal for this Case 1, moreover due to the suboptimal arrangements of fracture conductivities to fracture stages, the net present value of this realization is lower than all realizations.

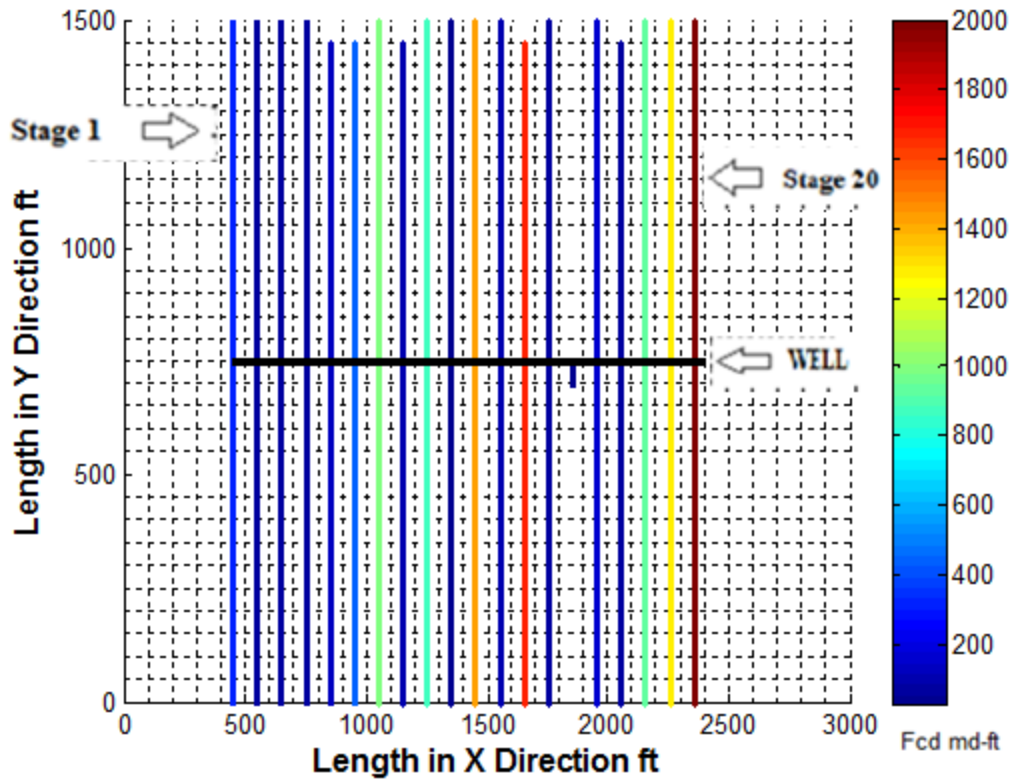


Figure 5.14: Optimal Fracture Lengths and Fracture Conductivities for Case 1 median NPV realization

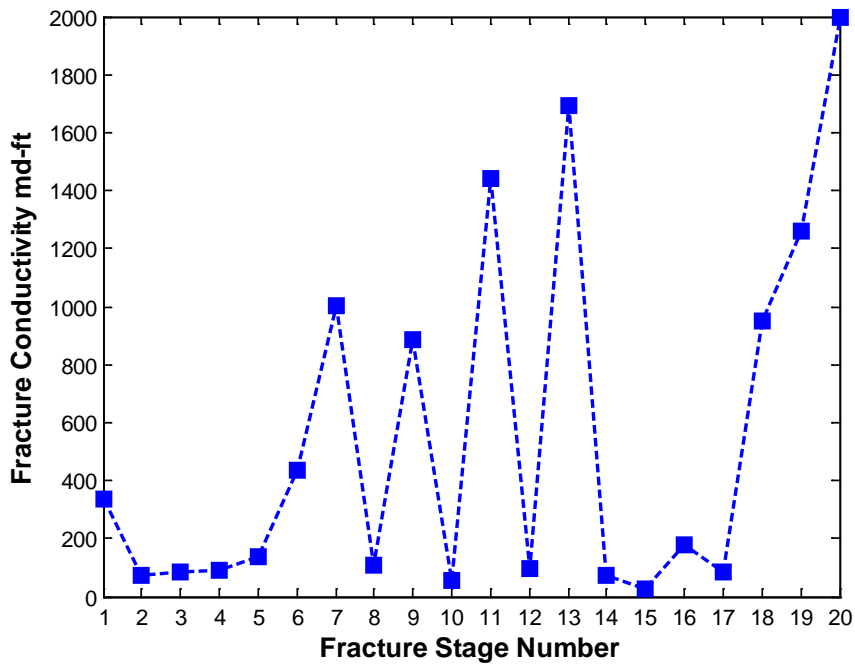


Figure 5.15: Optimal Fracture Conductivities for Case 1 median NPV realization

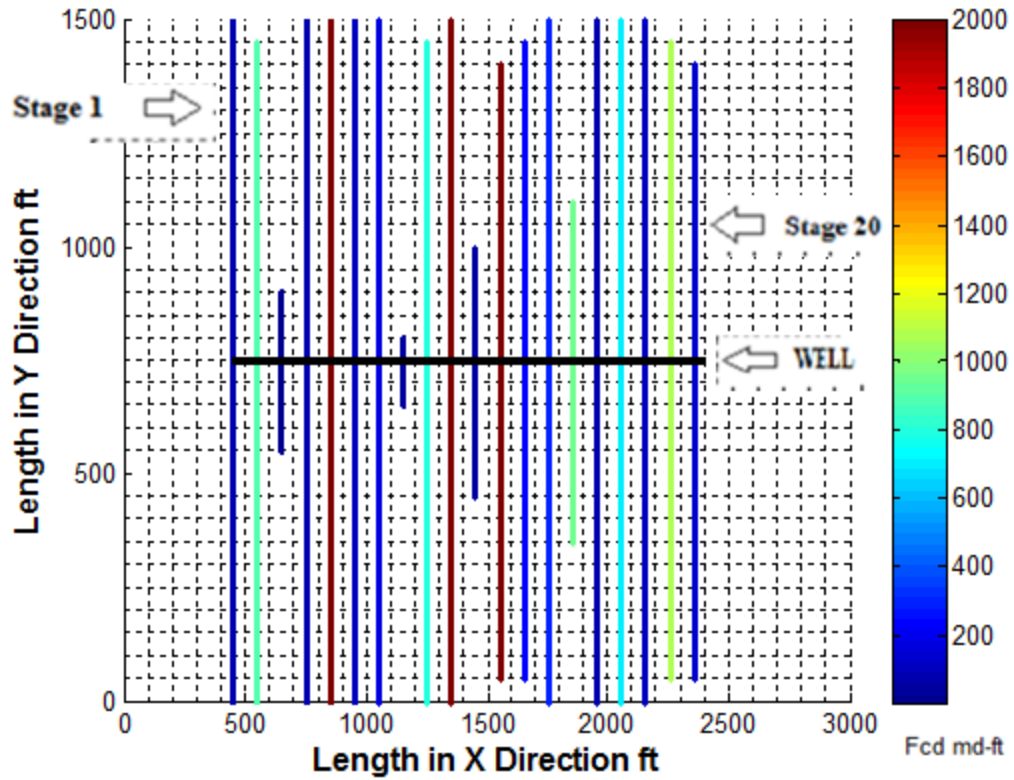


Figure 5.16: Optimal Fracture Lengths and Fracture Conductivities for Case 1 lowest NPV realization

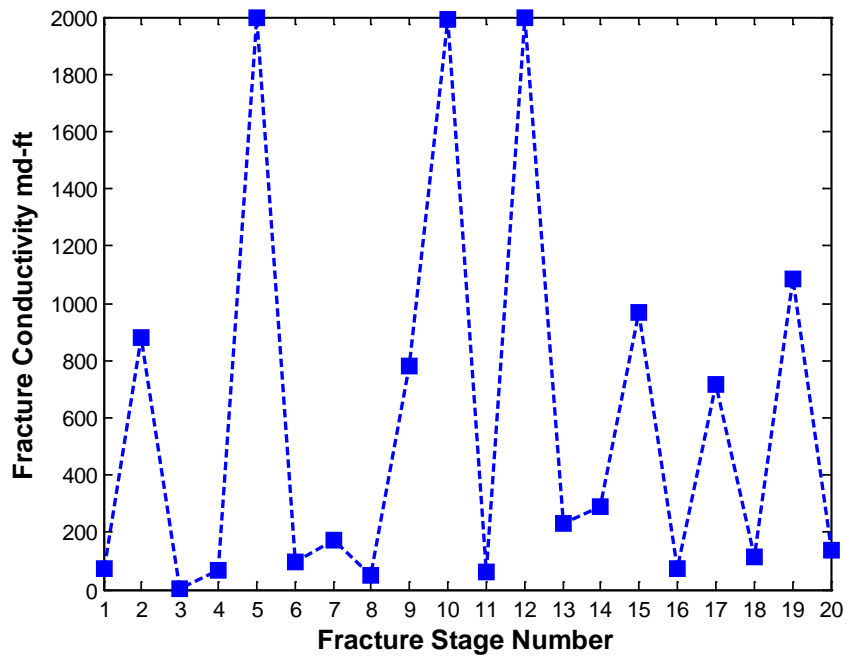


Figure 5.17: Optimal Fracture Conductivities for Case 1 lowest NPV realization

5.3 Case 2 - Optimization of Fracture Lengths, Conductivities, Spacings and Number of Stages

In Case 2 horizontal well length is fixed. Number of fracture stages, fracture spacing between stages, fracture lengths and fracture conductivities are variables. In this case each fracture stage length, conductivity, spacing with other fracture stage are optimized simultaneously in order to get the optimal fracture length pattern, fracture conductivity pattern, number of fracture stages and fracture spacing, which give maximum net present value or profit.

For Case 2 figure 5.11 shows that, realization number 1 gives the highest net present value (10.36 MM\$), realization 2, 3 and 4 give the second best net present value (9.26 MM\$), median net present value (8.72 MM\$) and fourth best net present value (7.27 MM\$) respectively and realization 5 gives the lowest net present value (7.24 MM\$).

Figure 5.18 and figure 5.19 show the Optimal Fracture Lengths, Fracture Conductivities, Number of fracture stages and Fracture spacing for Case 2, which give best result in terms of net present value. The optimal number of fracture stages in horizontal well length of 2000 ft is found to be 32 fracture stages. Full Fracture lengths are observed for corner fracture stages, which possibly drains more gas from outside of the horizontal well. Nice pattern of short, medium and long fracture lengths pattern for middle fracture stages are also observed in this realization of Case 2. Fracture conductivities are high of corner fracture stages, which possibly drain more gas from outside of the horizontal well. The middle fracture stages contain low, medium and high fracture conductivities pattern,

which can effectively drains more gas with low cost from multi-frac stages in horizontal well of length 2000 ft.

Figure 5.20 and figure 5.21 show the Optimal Fracture Lengths, Fracture Conductivities, Number of fracture stages and Fracture spacing for Case 2, which give median net present value. The optimal number of fracture stages in horizontal well length of 2000 ft is found to be 29 fracture stages for this median NPV realization of case 2. Nice pattern of short, medium and long fracture lengths pattern for middle fracture stages are also observed in this realization of Case 2. Full Fracture length is observed for one corner fracture stage but for other corner stage the fracture length is found to be 700 ft, which is due to the sub optimality in the solution of fracture length patterns. Fracture conductivities are relatively also low at corner fracture stages, which is due to the sub optimality in the solution of fracture conductivities for corner fracture stages. The middle fracture stages contain low, medium and high fracture conductivities pattern, which can effectively drains more gas with low cost from multi-frac stages in horizontal well of length 2000 ft. Due to the some suboptimal solutions of fracture lengths and conductivities to fracture stages, the net present value of this realization is lower than best net present value realization.

Figure 5.22 and figure 5.23 show the Optimal Fracture Lengths, Fracture Conductivities, Number of fracture stages and Fracture spacing for Case 2, which give lowest net present value. The optimal number of fracture stages in horizontal well length of 2000 ft is found to be 21 fracture stages for this lowest NPV realization of case 2. Full Fracture lengths are observed for all fracture stages, which is due to the sub optimality in the solution of fracture length patterns. Fracture conductivities are relatively also low at corner fracture

stages, which is due to the sub optimality in the solution of fracture conductivities for corner fracture stages. The middle fracture stages contain low, medium and high fracture conductivities pattern, which can effectively drains more gas with low cost from multi-frac stages in horizontal well of length 2000 ft. Due to the severe suboptimal solutions of fracture lengths to all fracture stages and conductivities to corner fracture stages, the net present value of this realization is lower than all realization.

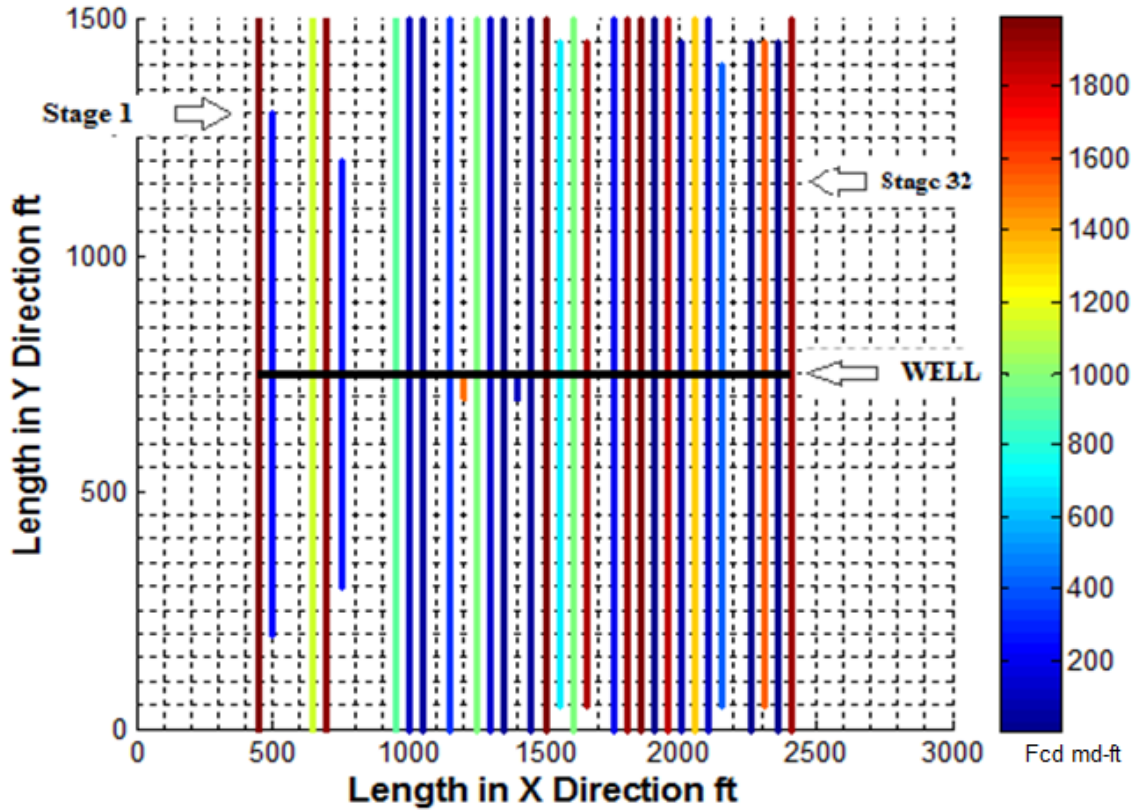


Figure 5.18: Optimal Fracture Lengths, Conductivities, Spacings and Number of Fracture Stages for Case 2 best NPV realization

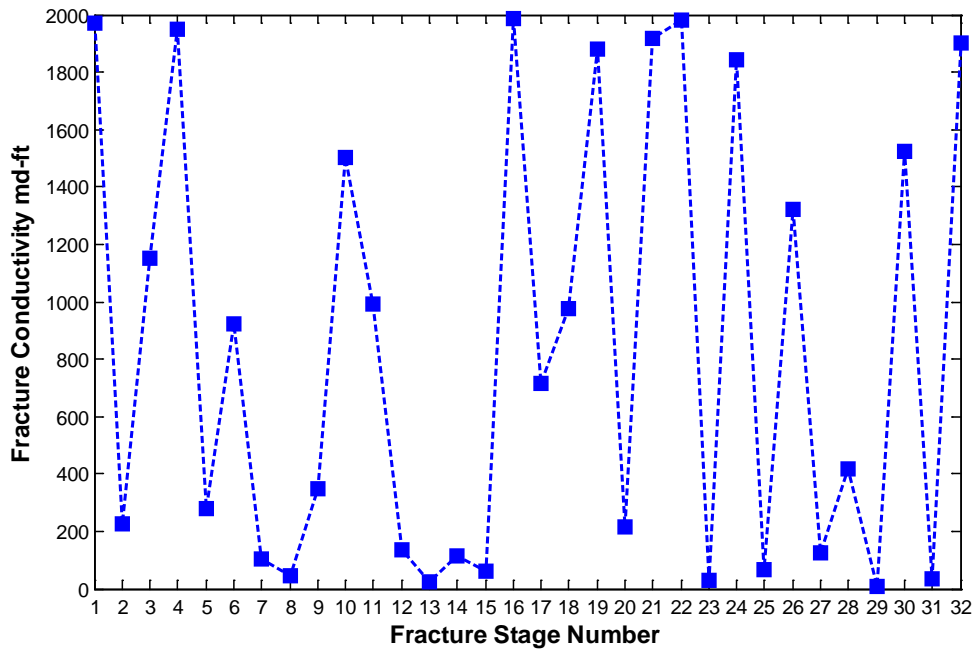


Figure 5.19: Optimal Fracture Conductivities for Case 2 best NPV realization

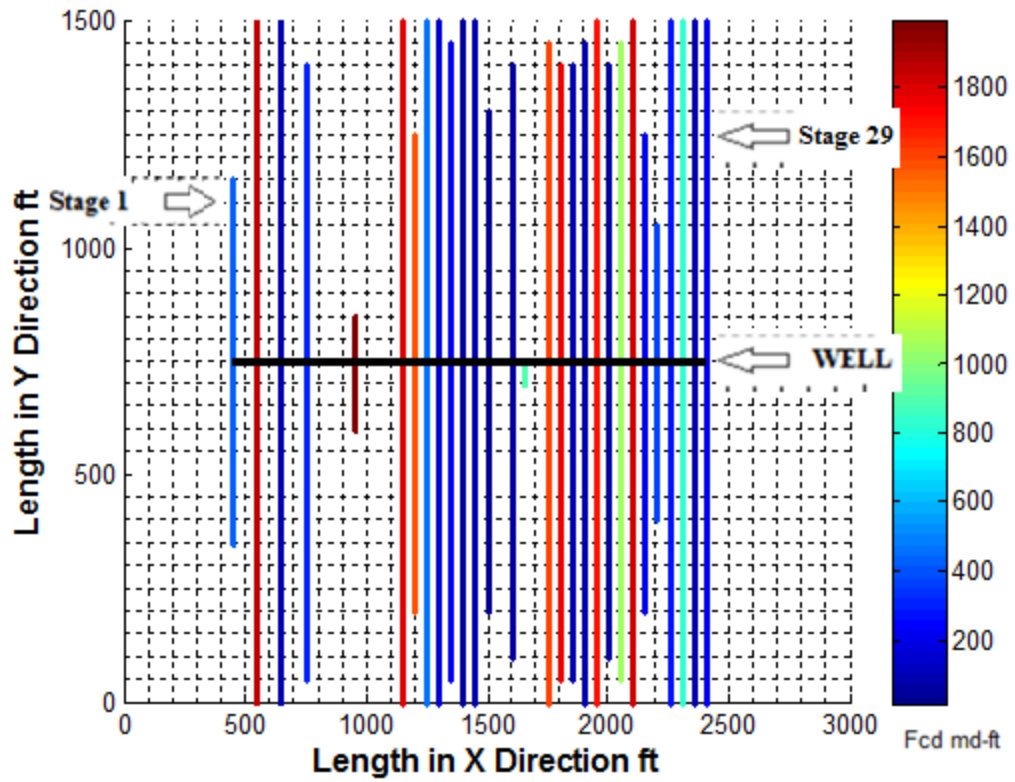


Figure 5.20: Optimal Fracture Lengths, Conductivities, Spacings and Number of Fracture Stages for Case 2 median NPV realization

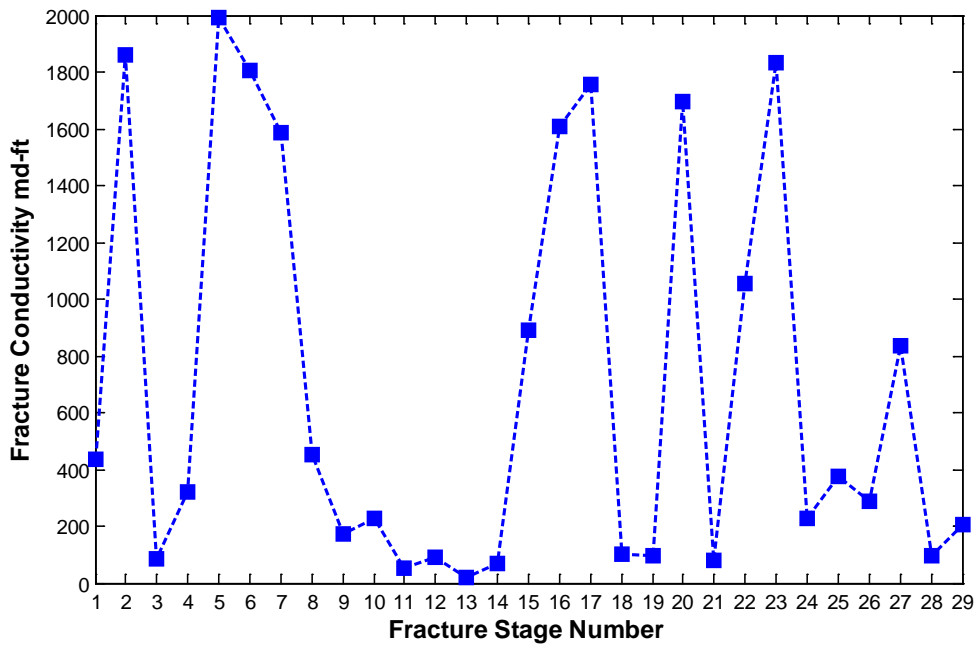


Figure 5.21: Optimal Fracture Conductivities for Case 2 median NPV realization

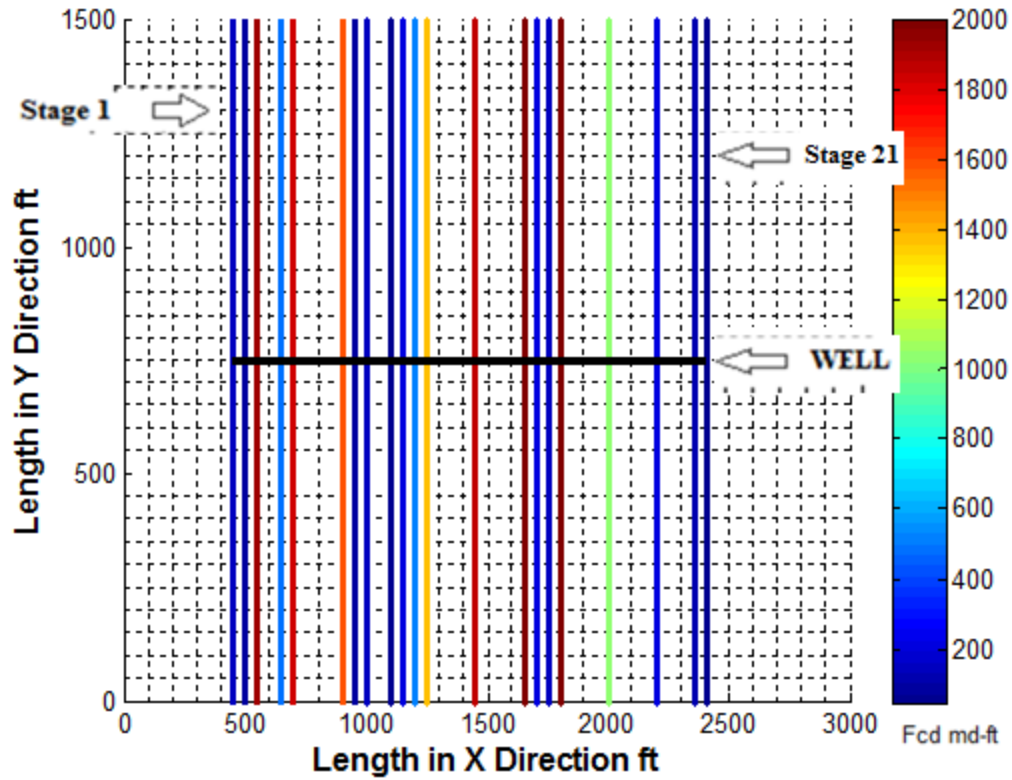


Figure 5.22: Optimal Fracture Lengths, Conductivities, Spacings and Number of Fracture Stages for Case 2 lowest NPV realization

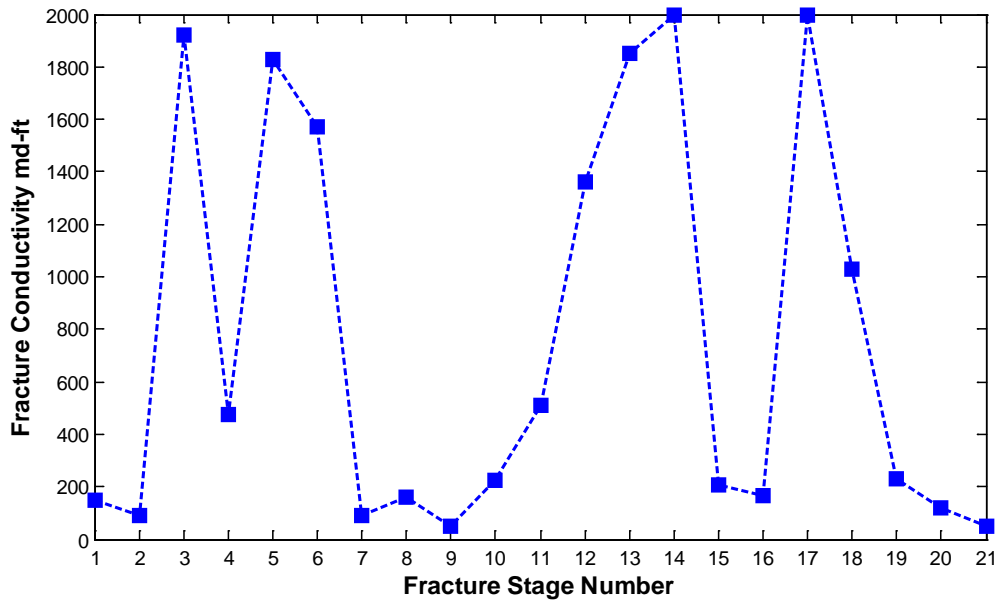


Figure 5.23: Optimal Fracture Conductivities for Case 2 lowest NPV realization

5.4 Case 3 - Optimization of Fracture Lengths, Conductivities, Spacings, Number of Fracture Stages and Well Length

In Case 3 horizontal well length, number of fracture stages, fracture spacing between stages, fracture lengths and fracture conductivities are variables. In this case each fracture stage length, conductivity, spacing with other fracture stage and horizontal well length are optimized simultaneously in order to get the optimal fracture length pattern, fracture conductivity pattern with number of fracture stages, fracture spacing and well length, which give maximum net present value or profit.

For Case 3 figure 5.11 shows that, realization number 1 give the highest net present value (11.98 MM\$), realization 2, 3, 4 and 5 give the second best net present value (11.33 MM\$), median net present value (11.15 MM\$), fourth best net present value (10.98 MM\$) and lowest net present value (7.66 MM\$) respectively.

Figure 5.24 and figure 5.25 show the Optimal Fracture Lengths, Fracture Conductivities, Number of fracture stages, Fracture spacing and Well Length for Case 3, which give best result in terms of net present value. The optimal number of fracture stages and optimal horizontal well length are found to be 36 fracture stages and 2350 ft respectively. Full Fracture length is observed for one corner fracture stage, which possibly drains more gas from outside of the horizontal well, but other corner does not contain full fracture length, it means optimality condition in solution is different for this case 3 as compare to case 2 and case 1. Nice pattern of short, medium and long fracture lengths pattern for middle fracture stages are also observed in this realization of Case 3. Fracture conductivity is high in one of the corner fracture stages, which possibly drain more gas from outside of

the horizontal well. But for other corner fracture stage the fracture conductivity is relatively low, which shows optimality condition in solution is different for this case 3 as compare to case 2 and case 1. The middle fracture stages contain low, medium and high fracture conductivities pattern, which can effectively drains more gas with low cost from multi-fracture stages in horizontal well of length 2350 ft.

Figure 5.26 and figure 5.27 show the Optimal Fracture Lengths, Fracture Conductivities, Number of fracture stages, Fracture spacing and Well Length for Case 3, which give median net present value. The optimal number of fracture stages and optimal horizontal well length are found to be 35 fracture stages and 2500 ft respectively for this median NPV realization of case 3. Nice pattern of short, medium and long fracture lengths pattern for middle fracture stages are also observed in this realization of Case 3. Full Fracture lengths are observed for corner fracture stages, which possibly drains more gas from outside of the horizontal well. Nice pattern of short, medium and long fracture lengths pattern for middle fracture stages are also observed in this realization of Case 3. Fracture conductivities are high of corner fracture stages, which possibly drain more gas from outside of the horizontal well. The middle fracture stages contain low, medium and high fracture conductivities pattern, which can effectively drains more gas with low cost from multi-frac stages in horizontal well of length 2500 ft. Some suboptimal solutions of fracture spacings between fracture stages (e.g. around 9th fracture stage the fracture spacing is very high) and horizontal well length of 2500 ft (maximum of search space for well length parameter) are also observed, due to these sub optimality the net present value of this realization is lower than best net present value realization for Case 3.

Figure 5.28 and figure 5.29 show the Optimal Fracture Lengths, Fracture Conductivities, Number of fracture stages, Fracture spacing and Well Length for Case 3, which give lowest net present value. The optimal number of fracture stages and optimal horizontal well length are found to be 21 fracture stages and 2500 ft respectively for this lowest NPV realization of case 3. Full Fracture lengths are observed for all fracture stages, which is due to the sub optimality in the solution of fracture length patterns. The middle fracture stages contain low, medium and high fracture conductivities pattern, which can effectively drains more gas with low cost from multi-frac stages in horizontal well of length 2500 ft. Suboptimal solutions of fracture spacings between fracture stages, Number of fracture stages and horizontal well length of 2500 ft (maximum of search space for well length parameter) are also observed. Due to these severe suboptimal solutions of fracture lengths to all fracture stages, fracture spacings between fracture stages, number of fracture stages and maximum horizontal well length, the net present value of this realization is lower than all realization of Case 3.

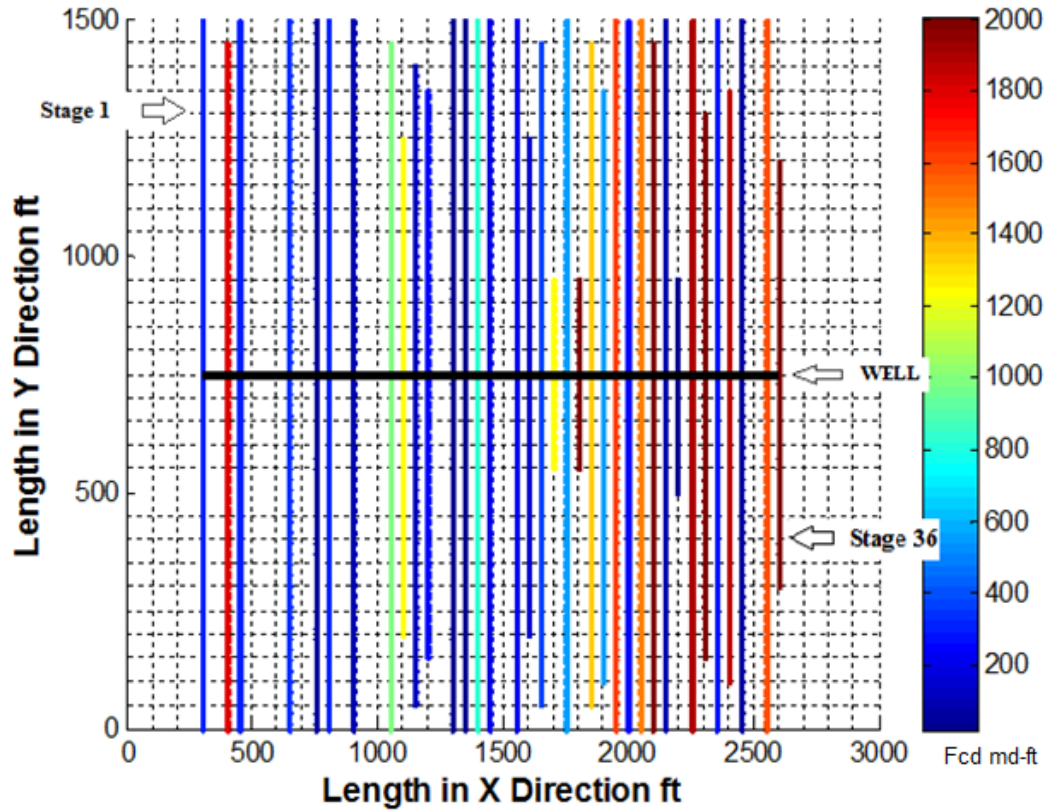


Figure 5.24: Optimal Fracture Lengths, Conductivities, Spacings, Number of Fracture Stages and Well Length for Case 3 best NPV realization

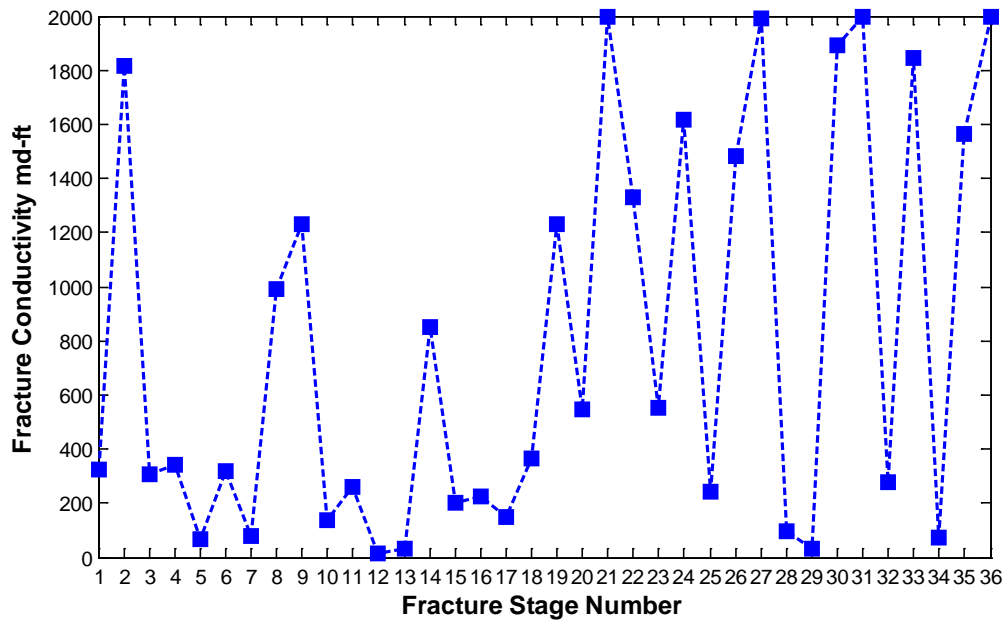


Figure 5.25: Optimal Fracture Conductivities for Case 3 best NPV realization

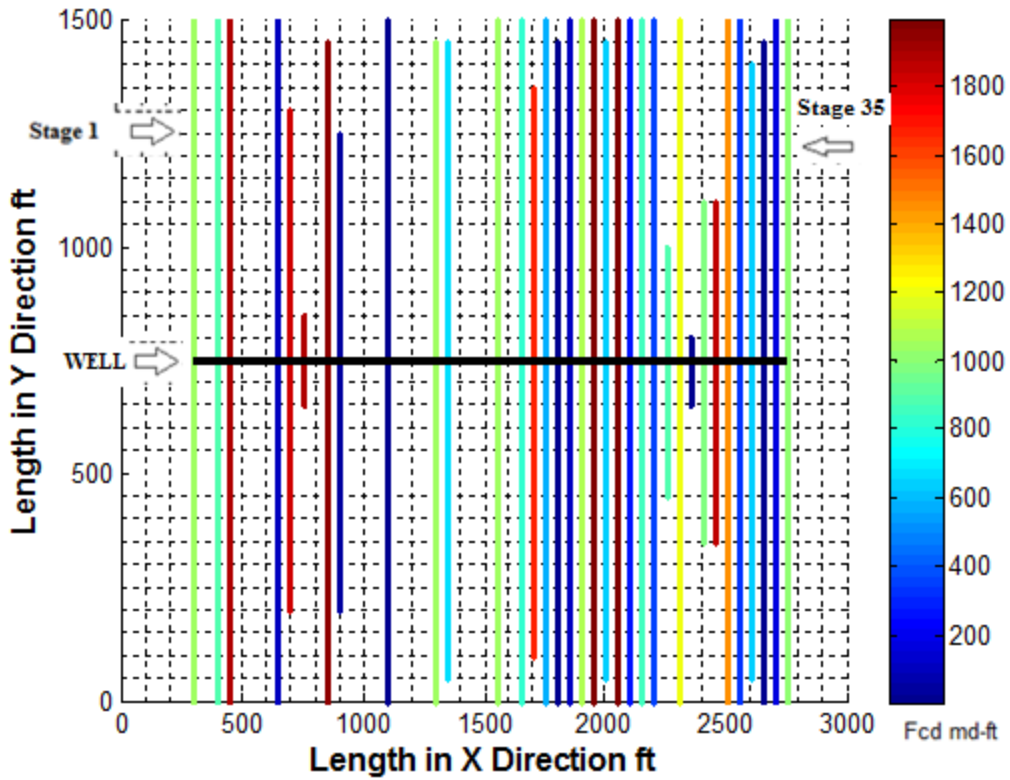


Figure 5.26: Optimal Fracture Lengths, Conductivities, Spacings, Number of Fracture Stages and Well Length for Case 3 median NPV realization

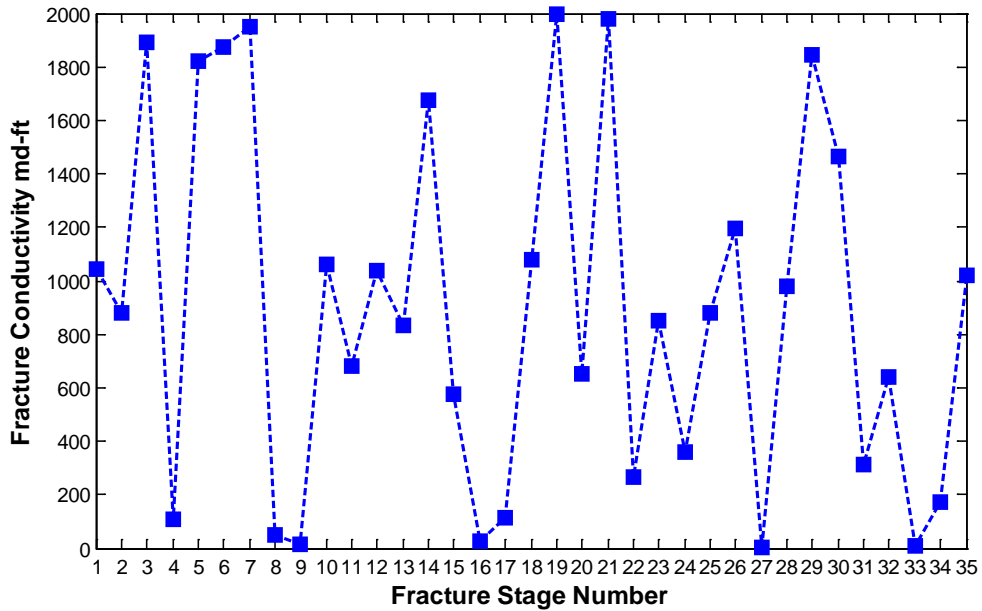


Figure 5.27: Optimal Fracture Conductivities for Case 3 median NPV realization

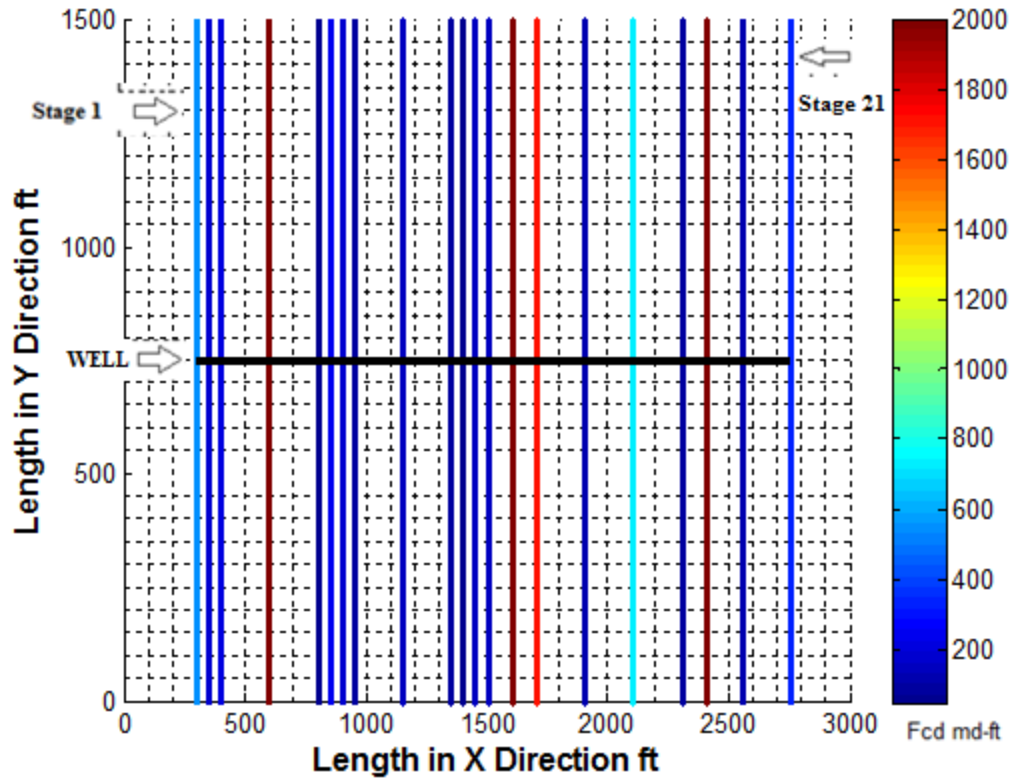


Figure 5.28: Optimal Fracture Lengths, Conductivities, Spacings, Number of Fracture Stages and Well Length for Case 3 lowest NPV realization

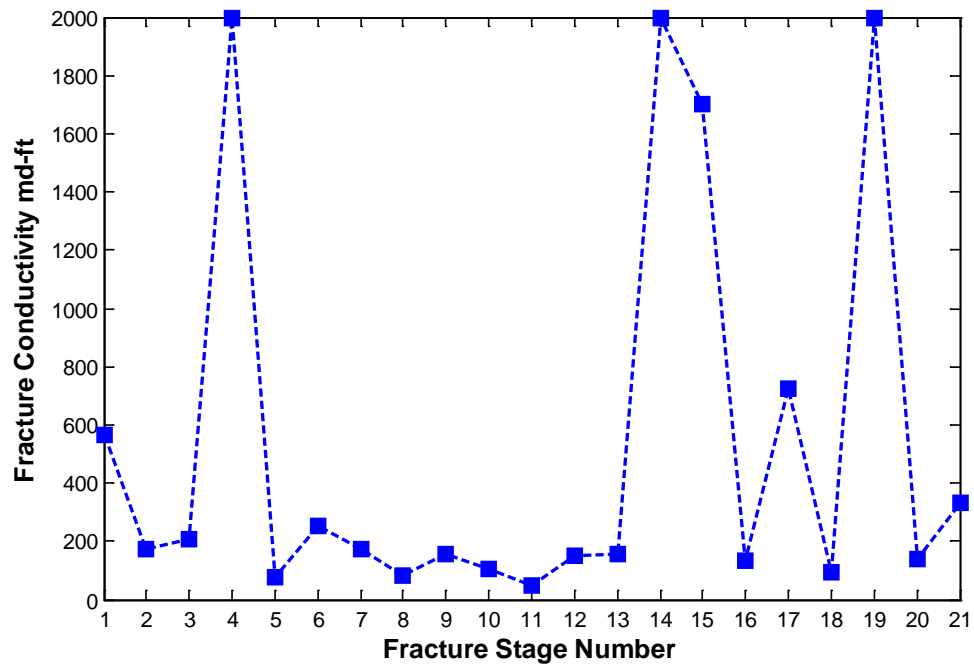


Figure 5.29: Optimal Fracture Conductivities for Case 3 lowest NPV realization

5.5 Comparison of Cases

Figure 5.30 shows the comparison of Net Present Value versus Iterations of Differential Evolution Algorithm for best solution of each case in terms of Net Present Value result. Each iteration consists of 20 function evaluations, so in total there are 3000 function evaluations during optimization process. Figure 5.30 shows that the initial net present value is almost the same for each case around 4 MM\$. The Net present value is increased from 4 MM\$ to 6.7 MM\$ after 150 iterations of DE, i.e. 67.5 % profit increase is observed after optimization of only Fracture Lengths and Fracture Conductivities (Case 1) from initial profit. The Net present value is increased from 4 MM\$ to 10.36 MM\$ after 150 iterations of DE, i.e. 159 % profit increase is observed after optimization of Fracture Lengths, Conductivities, Spacings and Number of Fracture Stages (Case 2) from initial net present value. The Net present value is increased from 4 MM\$ to 11.98 MM\$ after 150 iterations of DE, i.e. 199.5 % profit increase is observed after optimization of Well Length, Fracture Lengths, Conductivities, Spacings and Number of Fracture Stages (Case 3) from initial net present value. It is clearly evident from Figure 5.21 that, Case 3 performs better than Case 2, and Case 2 performs better than Case 1. It is due to the fact that number of Optimization Parameters in Case 3 > Case 2 > Case 1 and the chances of sub optimal solution in Case 1 > Case 2 > Case 3.

Figure 5.31 shows the comparison of Net Present Value versus Iterations of Differential Evolution Algorithm for median solution of each case in terms of Net Present Value result. Each iteration consists of 20 function evaluations, so in total there are 3000 function evaluations during optimization process. Figure 5.31 shows that the initial net present value is almost same for case 2 and case 3 around 3.9 MM\$ and different for case

1 around 3.2 MM\$. The Net present value is increased from 3.2 MM\$ to 6.32 MM\$ after 150 iterations of DE, i.e. 97.5 % profit increase is observed after optimization of only Fracture Lengths and Fracture Conductivities (Case 1) from initial net present value. The Net present value is increased from 3.9 MM\$ to 8.72 MM\$ after 150 iterations of DE, i.e. 123.6 % profit increase is observed after optimization of Fracture Lengths, Conductivities, Spacings and Number of Fracture Stages (Case 2) from initial profit. The Net present value is increased from 3.9 MM\$ to 11.15 MM\$ after 150 iterations of DE, i.e. 185.9 % profit increase is observed after optimization of Well Length, Fracture Lengths, Conductivities, Spacings and Number of Fracture Stages (Case 3) from initial profit. It is clearly evident from Figure 5.22 that, Case 3 performs better than Case 2, and Case 2 performs better than Case 1. It is due to the fact that number of Optimization Parameters in Case 3 > Case 2 > Case 1 and the chances of sub optimal solution in Case 1 > Case 2 > Case 3.

Figure 5.32 shows the comparison of Net Present Value versus Iterations of Differential Evolution Algorithm for worst solution of each case in terms of Net Present Value result. Each iteration consists of 20 function evaluations, so in total there are 3000 function evaluations during optimization process. Figure 5.32 shows that the initial net present values are 3 MM\$, 2.8 MM\$ and 4.1 MM\$ for Case 1, Case 2 and Case 3 respectively. The Net present value is increased from 3 MM\$ to 5.35 MM\$ after 150 iterations of DE, i.e. 78.3 % profit increase is observed after optimization of only Fracture Lengths and Fracture Conductivities (Case 1) from initial profit. The Net present value is increased from 2.8 MM\$ to 7.24 MM\$ after 150 iterations of DE, i.e. 158.6 % profit increase is observed after optimization of Fracture Lengths, Conductivities, Spacings and Number of

Fracture Stages (Case 2) initial net present value. The Net present value is increased from 4.1 MM\$ to 7.66 MM\$ after 150 iterations of DE, i.e. 86.83 % profit increase is observed after optimization of Well Length, Fracture Lengths, Conductivities, Spacings and Number of Fracture Stages (Case 3) from initial net present value. It is clearly evident from Figure 5.23 that, Case 3 performs better than Case 2, and Case 2 performs better than Case 1. It is due to the fact that number of Optimization Parameters in Case 3 > Case 2 > Case 1 and the chances of sub optimal solution in Case 1 > Case 2 > Case 3.

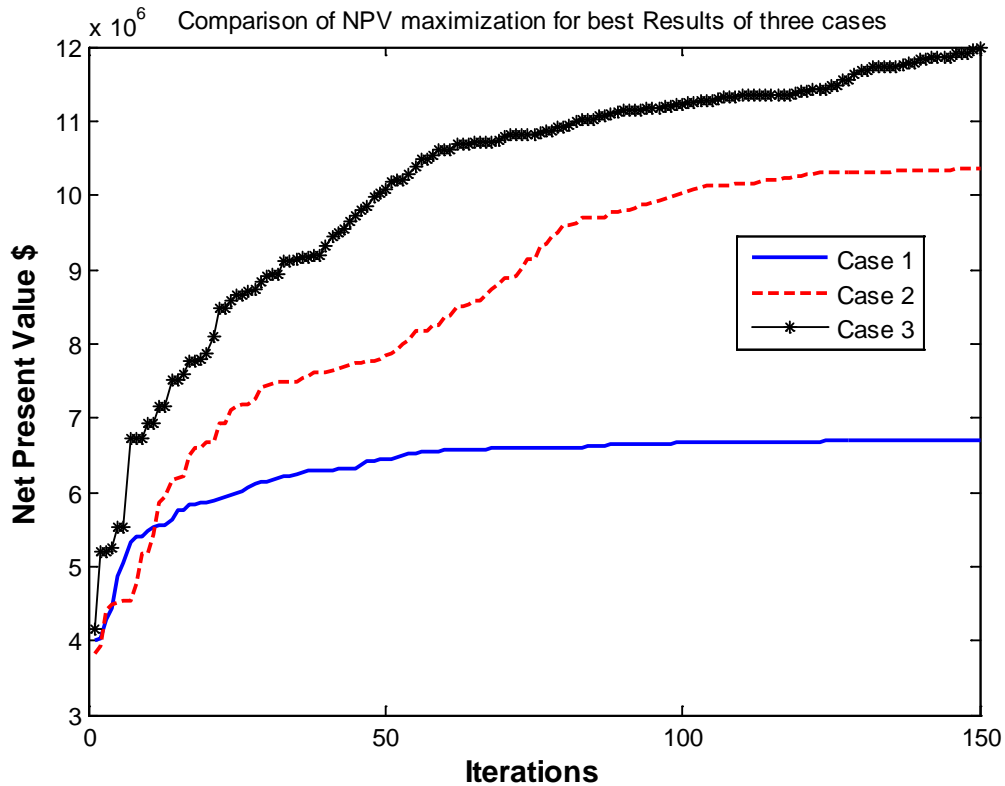


Figure 5.30: Comparison of three Cases best Net present value results versus Iterations of DE

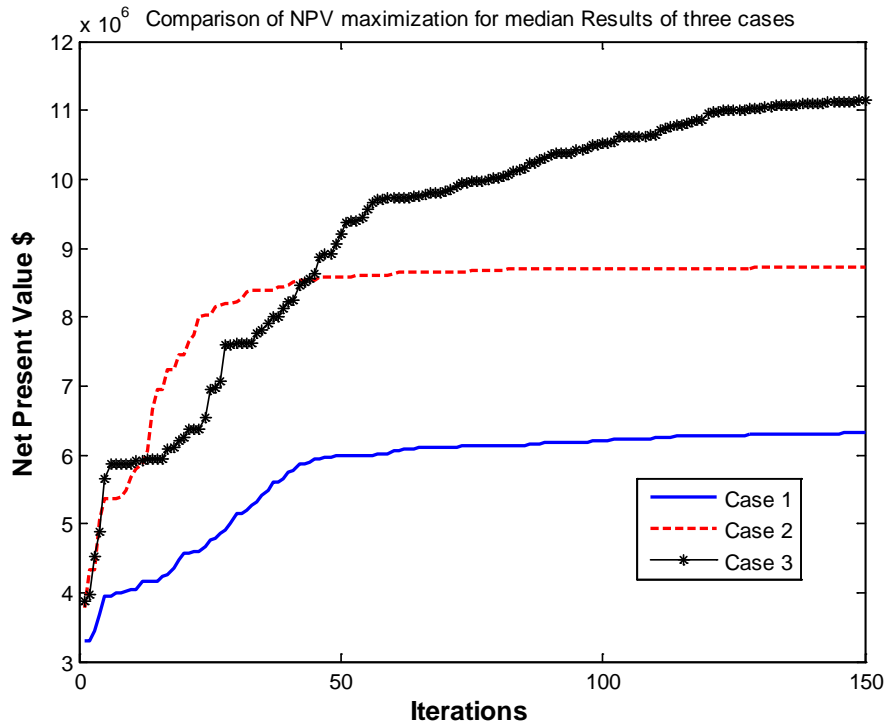


Figure 5.31: Comparison of three Cases median Net present value results versus Iterations of DE

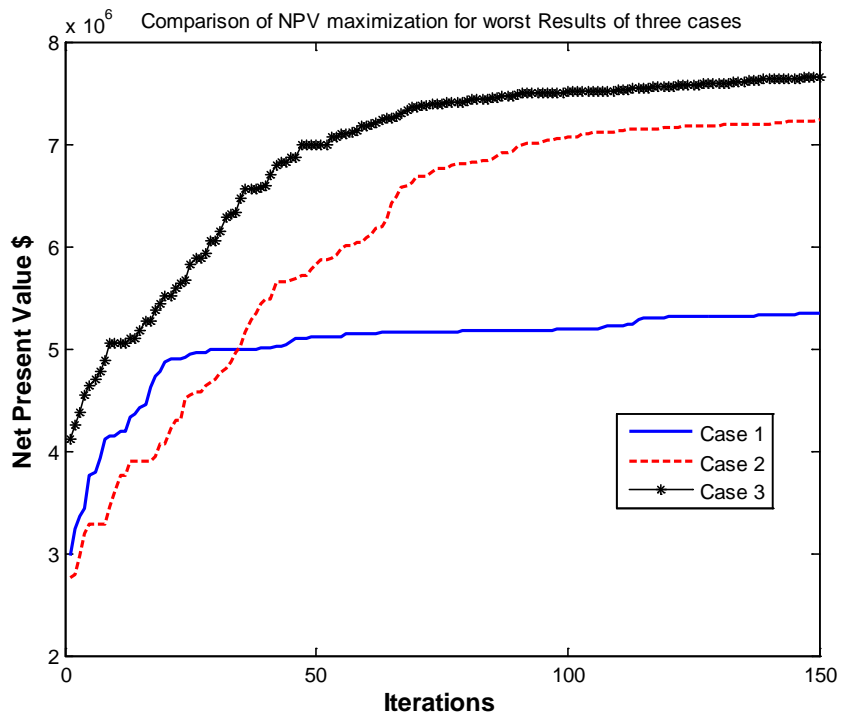


Figure 5.32: Comparison of three Cases worst Net present value results versus Iterations of DE

Figure 5.33 shows the comparison of cumulative gas production for three cases which give best results in terms of net present value after optimization. From this figure it is also clearly evident that the case 3 performs better than case 2 and case 1 in terms of cumulative gas production. Figure 5.34 shows the comparison of net present value of three cases with base case (calibrated/history matched case). This figure shows all three cases perform better than base case.

In order to check the versatility of solution from optimization algorithm, two more scenarios have been created for best NPV realization results. In first scenario fracture stages, which contain fracture conductivity less than 100 md-ft, have been eliminated. Similarly in second scenario fracture stages, which contain fracture conductivity less than 200 md-ft, have been eliminated. Figure 5.35 shows the comparison of cumulative gas production for case 1 of three scenarios. From this figure it is evident that the original optimal case 1 performs better than two scenarios of case 1 in terms of cumulative gas production. Figure 5.36 shows the comparison of cumulative gas production for case 2 of three scenarios. From this figure it is evident that the original optimal case 2 performs better than two scenarios of case 2 in terms of cumulative gas production.

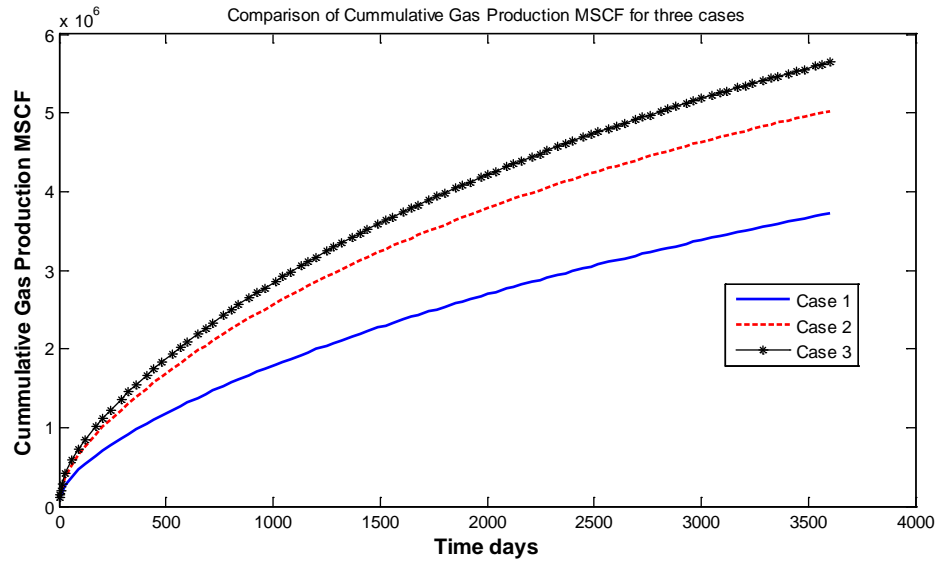


Figure 5.33: Comparison of three Cases of best realizations

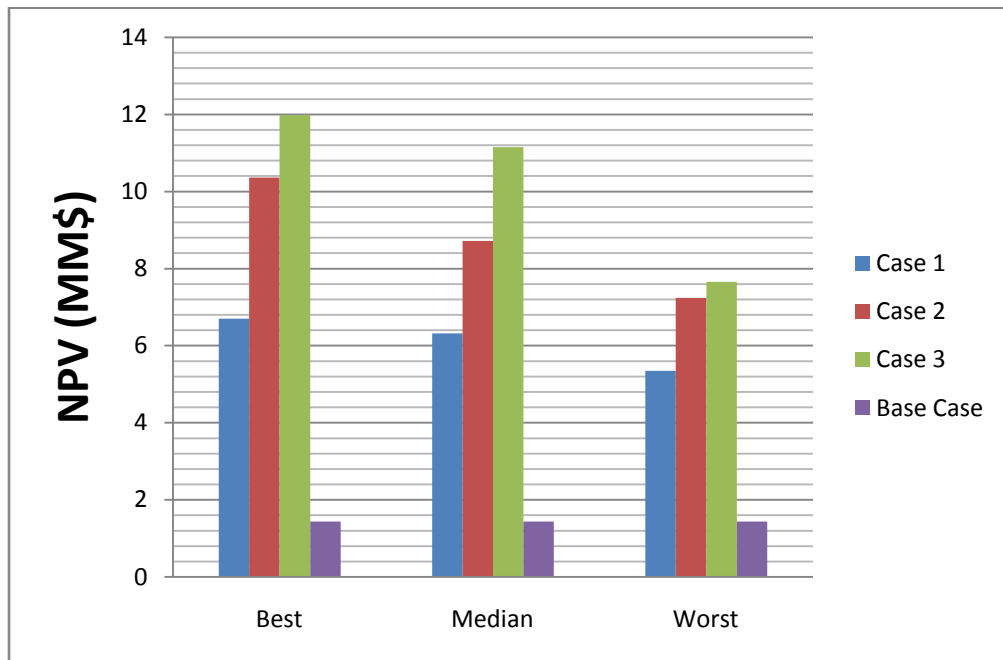


Figure 5.34: Comparison of three Cases with Base Case for best Net present value results

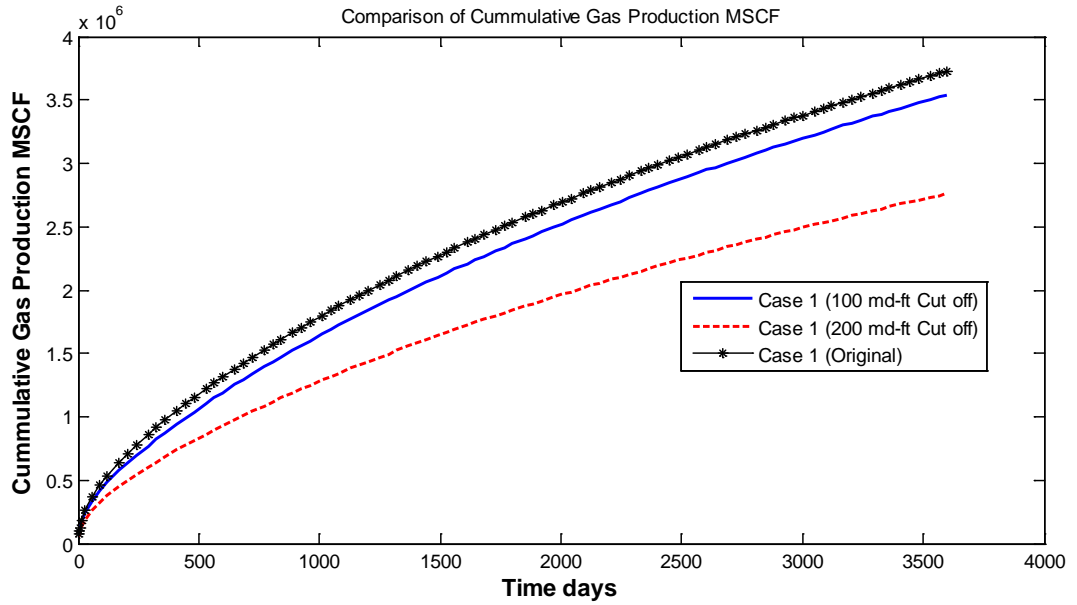


Figure 5.35: Comparison of Case 1 original optimal, 100 md-ft cut off, 200 md-ft cut off

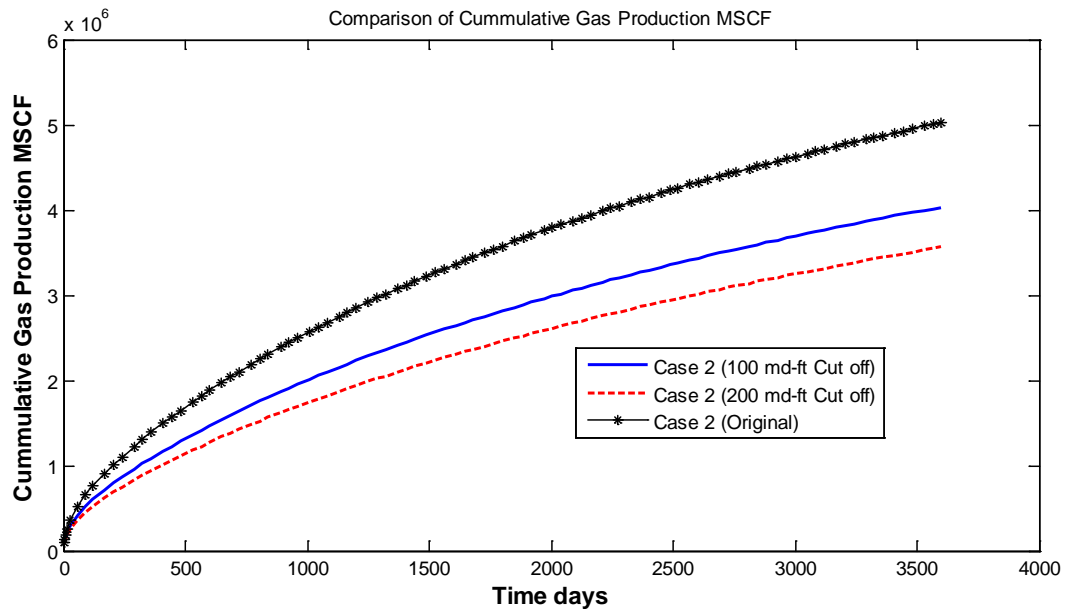


Figure 5.36: Comparison of Case 2 original optimal, 100 md-ft cut off, 200 md-ft cut off

Figure 5.37 shows the comparison of cumulative gas production for case 3 of three scenarios. From this figure it is evident that the original optimal case 3 performs better than two scenarios of case 3 in terms of cumulative gas production. Figure 5.38 shows the comparison of net present value for all cases with three scenarios. From this figure it

is evident that the original optimal cases perform better than two scenarios of cases in terms of net present value.

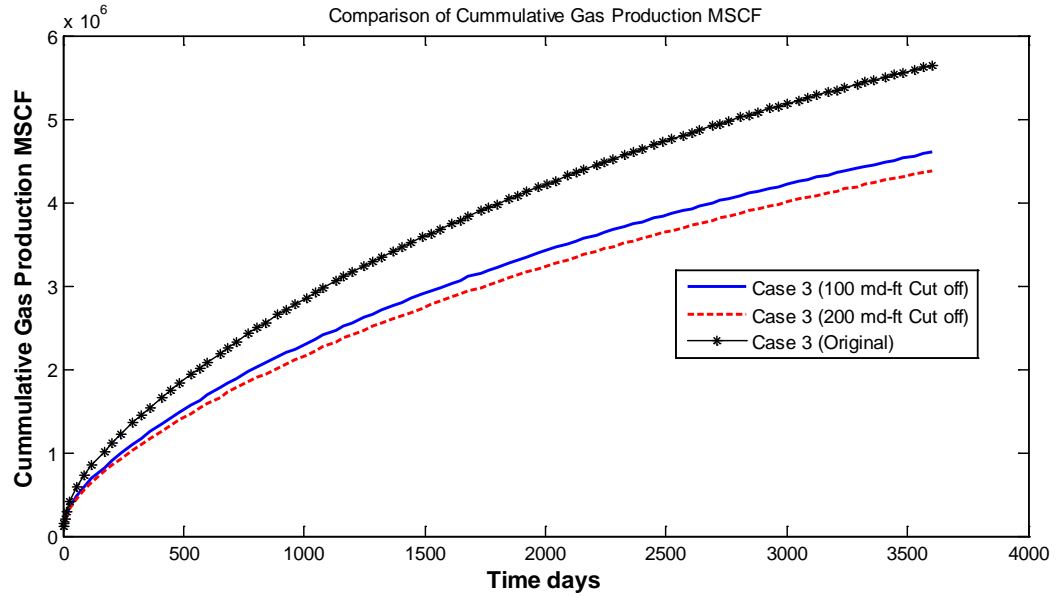


Figure 5.37: Comparison of Case 3 original optimal, 100 md-ft cut off, 200 md-ft cut off

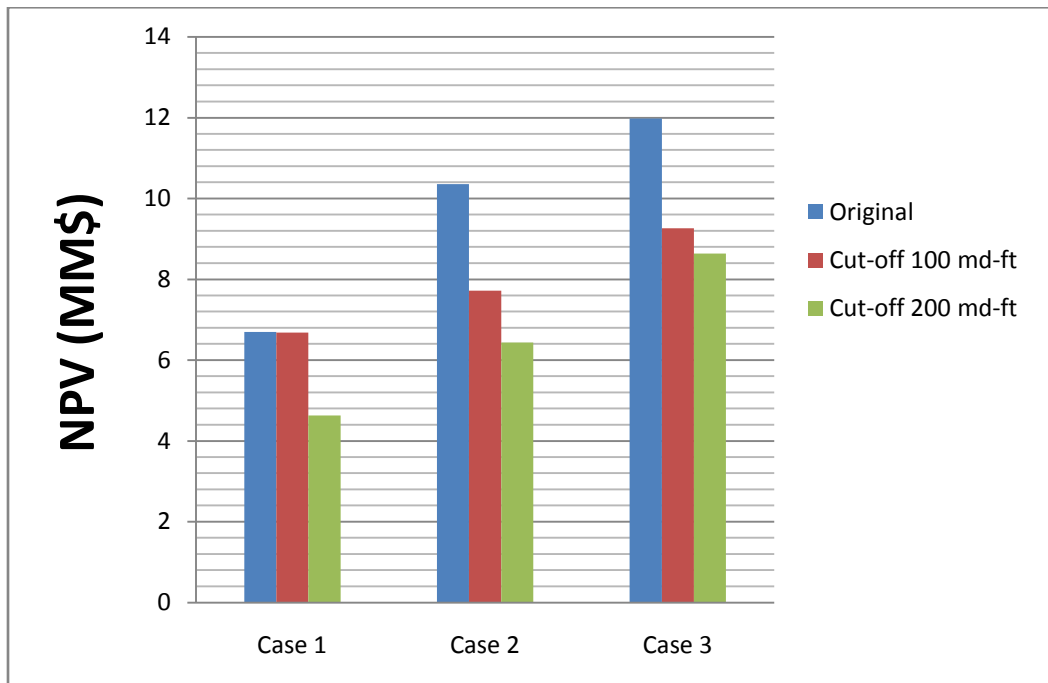


Figure 5.38: Comparison of Cases original optimal, 100 md-ft cut off, 200 md-ft cut off

Chapter 6 Conclusions and Recommendations

Planning optimum horizontal well with multi-fracturing stages in shale gas reservoirs is the challenging task. In this work shale gas reservoir model has been built by taking dual porosity model, Gas desorption effect using Langmuir isotherm, Stress sensitive fracture conductivity and Introducing local grid refinements into the model for modeling of hydraulic fractures in the simulation model. This shale gas simulation model has been calibrated or history matched with real field data.

In this work appropriate cost functions have been developed using published cost data and experimental data. These cost functions are useful for the realistic estimation related to horizontal well length and number of multi fracture stages. Based on these cost functions the net present value model has been developed for profit evaluations. The net present value model has been used for formulation of objective functions under different scenarios during stochastic optimization process.

In this work three optimization cases have been discussed and implemented in the calibrated shale gas model. Sensitivity Analysis is used to determine the search space of the parameters fracture spacing and fracture conductivity. Based on the results obtained after optimization for each case using Differential Evolution algorithm, it is evident that the stochastic optimization performed well in all cases. Comparison of results shows that Case 3 performs better than Case 2 for best, median and worst results. Similarly Case 2 performs better than Case 1 for best, median and worst results. It is due to the fact that number of Optimization Parameters in Case 3 > Case 2 > Case 1 and the chances of sub optimal solution in Case 1 > Case 2 > Case 3.

These optimization methodologies and framework can be applied to the heterogeneous shale gas reservoir as well. The need for these optimization methodologies and framework would be more in highly heterogeneous shale gas reservoir. The search space should be adjusted, when these optimization methodologies and framework applied to heterogeneous shale gas reservoir. Moreover as technology advances the cost of horizontal well, hydraulic fracturing fluid and Proppants may be different, so these costs should be adjusted according to current prices.

Optimal parameters and net present value results are strongly dependent on cost of horizontal well, hydraulic fracturing fluid and Proppants or cost functions, So if these cost and their functions are changed the optimization results would be changed. But these optimization methodologies and framework would remain the same. And they have capability to give particular optimal solution to particular cost of horizontal well, hydraulic fracturing fluid and Proppants or cost functions.

The outcomes of this research give Codes and Routines for Stochastic Optimization of Hydraulic Fracture and Horizontal Well Parameters in Shale Gas Simulation Models. Moreover it also gives the variation of the results on multiple realizations for different scenarios with analysis and insights of optimal solutions. Oil and gas industry can maximize Profits in terms of Net Present value from Shale Gas Reservoirs by using these computational algorithms, framework, analysis and insights of optimal solutions.

Nomenclature

C_{well} = Cost of well, \$

C_{fs} = Cost of fracturing stage, \$

C_{ff} = Total cost of fracturing fluid of single stage, \$

C_p = Proppant concentration, lb/ft²

C_{prop} = Cost of Proppant, \$

C_{well} = Cost of Horizontal well, \$

DE = Differential Evolution

d = Discount rate

FC = Fixed cost, \$

F_{cd} = Fracture conductivity, md-ft

G_s = Gas content, scf/ton

h_f = Height of the fracture, ft

i = Index of first fracturing stage to total number of fracturing stages

j = Index of first well to total number of wells

k = Index of first time step to total number of time steps

k_f = Fracture permeability, md

L_{well} = Horizontal well length, ft

$M = \text{Thousand } (10^3)$

$MM = \text{Million } (10^6)$

$M_p = \text{Mass of Proppant, lb}$

$NPV = \text{Net present value, \$}$

$N_{ts} = \text{Total number of time steps}$

$N_{wells} = \text{Total number of wells}$

$N_{fs} = \text{Total number of fracturing stages}$

$P_L = \text{Langmuir pressure, psi}$

$P = \text{Pressure, psi}$

$Q_{gas} = \text{Producing rate of gas, Mscf/day}$

$Q_w = \text{Producing rate of water, bbl/day}$

$R_{gas} = \text{Unit Price of the gas, \$/Mscf}$

$R_{water} = \text{Unit Cost of water disposal, \$/bbl}$

$R_{ff} = \text{Unit cost of fracturing fluid, \$/gallon}$

$R_p = \text{Unit price of Proppant, \$/lb}$

$\Delta t_k = \text{Time step at index k, days}$

$V_{ff} = \text{Volume of fracturing fluid, ft}^3$

$V_f = \text{Volume of hydraulic fracture, ft}^3$

V_L = Langmuir Volume, scf/ton

w_f = Width of hydraulic fracture stage, inch (ft)

x_f = Half length of hydraulic fracture stage, ft

η_f = Efficiency of fracturing fluid

ρ_B = Bulk density of shale, g/cm³ (lb/ft³)

v = Velocity, m/s (ft/s)

μ = Viscosity, cp

ρ = Phase density, g/cm³ (lb/ft³)

β = Non-Darcy Flow beta factor, ft⁻¹

Appendix: Shale Gas Simulation Model Parameters

Table A-1 contains all the variables that were used to construct the relative permeability and capillary pressure curves that will be used in Shale Gas Reservoir Simulation model. The values are taken from experimental work on very tight sandstones by Maas (2011). The relative permeability curves were constructed by applying the Corey functions for a gas/water system.

$$krw = krw(Sg_{\min}) \left(\frac{Sw - Swc}{Swmax - Swc - Sgmin} \right)^{Cw}$$

$$krw = krw(Sg_{\min}) \left(\frac{Swmax - Sw - Sgmin}{Swmax - Swi - Sgmin} \right)^{Cg}$$

The Van Genuchten relation was used to construct the capillary pressure curves.

$$Pc = Pentry \left(\left(\frac{Sw - Swc}{Swmax - Swc} \right)^{\frac{1}{\lambda}} - 1 \right)^{1-\lambda}$$

Table A-1: Variables used in the relative permeability and capillary pressure curves construction. Based on experimental values on very tight sandstones by Maas (2011)

Property	Units (Metric)	Value
Minimum water saturation	[-]	0.1
Critical water saturation	[-]	0.1
Minimum gas saturation	[-]	0.3
Relative water permeability at minimum gas saturation	[-]	0.3
Relative gas permeability at minimum water saturation	[-]	0.7
Maximum water saturation	[-]	1
Initial water saturation	[-]	0.1
Corey exponent for water	[-]	5
Corey exponent for gas	[-]	2
Entry Pressure Matrix	[Pa]	1x10 ⁶
Entry Pressure Fracture	[Pa]	0.5x10 ⁶
Sorting factor (λ) Matrix	[-]	0.5
Sorting factor (λ) Fracture	[-]	0.7

References

“Annual Energy Outlook Early Release, 2012”, US DOE, 2012.

A. A. Oyekunle, “Shale Oil and Gas Revolution: Implications on Energy Market Outlook and Politics”, presented at SPE Nigeria Annual International Conference and Exhibition, Lagos, Nigeria, 05–07 August 2014, SPE-172431-MS.

Aramahi B, Sundberg MI. Proppant embedment and conductivity of hydraulic fractures in shales. In: ARMA 12–291, presented at the 46th US rock mechanics/geomechanics symposium, Chicago, IL; June 24-27, 2012.

Anish Singh Chaudhary, Christine Ehlig-economides, Robert Wattenbarger, (November 2011). “Shale Oil Production Performance from a Stimulated Reservoir Volume”, SPE 147596, presented at the SPE Annual Technical Conference and Exhibition held in Denver, Colorado, USA, 30 October–2 November 2011.

Atefeh Jahandideh, Behnam Jafarpour, “Optimization of Hydraulic Fracturing Design under Spatially Variable Shale Fracability”, SPE-169521-MS, presented at the SPE Western North American and Rocky Mountain Joint Regional Meeting held in Denver, Colorado, USA, 16–18 April 2014.

B. Mille, J. Paneitz, M. Mullen, R. Meijs, M. Tunstall, and M. Garcia, “The successful application of a compartmental completion technique used to isolate multiple hydraulic-fracture treatments in horizontal bakken shale wells in North Dakota,” in Proceedings of the SPE Annual Technical Conference and Exhibition (ATCE '08), pp. 3992–4002, September 2008.

Cipolla CL, Lolon EP, Erdle JC, Rubin B, (August 2010), “Reservoir modeling in shale-gas reservoirs”. SPE Res Eval Eng 2010; 13(4):638–53.

Cipolla, C.L., Warpinski, N.R., Mayerhofer, M.J., Lolon, E.P., and Vincent, M.C. 2008a. The Relationship Between Fracture Complexity, Reservoir Properties, and Fracture Treatment Design. Paper SPE 115769 presented at the SPE Annual Technical Conference and Exhibition, Denver, 21–24 September. doi: 10.2118/115769-MS.

Cipolla, C.L., Lolon, E.P., and Dzubin, B. 2009b, “Evaluating Stimulation Effectiveness in Unconventional Gas Reservoirs” Paper SPE 124843, presented at the SPE Annual Technical Conference and Exhibition, New Orleans, 4–7 October. doi: 10.2118/124843-MS.

Cipolla, C.L., Lolon, E.P., Mayerhofer, M.J., and Warpinski, N.R. 2009c. “Fracture Design Considerations in Horizontal Wells Drilled in Unconventional Gas Reservoirs”, Paper SPE 119366, presented at the SPE Hydraulic Fracturing Technology Conference, The Woodlands, Texas, USA, 19–21 January. doi: 10.2118/119366-MS.

Cipolla, C et al. (November 2011). “New Algorithms and Integrated Workflow for Tight Gas and Shale Completions”, SPE 146872, Presented at the SPE Annual Technical Conference and Exhibition held in Denver, Colorado, USA, 30 October–2 November 2011.

C.J. Jin et al, Leopoldo Sierra, Mike Mayerhofer, “A Production Optimization Approach to Completion and Fracture Spacing Optimization for Unconventional Shale Oil Exploitation.” SPE 168813 / URTeC 1581809, presented at Unconventional Resources Technology Conference held in Denver, Colorado, USA, 12-14 August 2013.

Edgeman, J.R., and Walser, D.W.: “Comparison of Two Low-Permeability Horizontal Devonian Projects in the Permian Basin with Competing Completion Techniques”, paper SPE 84392, 2003.

Economides, Michael. J. and Kenneth G. Nolte, “Reservoir Stimulation”, Second Edition Copyright 1989, Schlumberger Educational Services, 5000 Gulf Freeway, Houston, Texas 77023.

Economides, Michael. J, “A practical companion to Reservoir Stimulation”, Copyright 1992, Elsevier Science Publishers, ISBN 0-444-89324-5.

Evans RD, Civan F. “Characterization of non-darcy multiphase flow in petroleum bearing formations”. Report, US DOE Contract No. DE-AC22-90BC14659, School of Petroleum and Geological Engineering, University of Oklahoma, 1994.

Grieser, B., Shelley, B., and Soliman, M. “Prediction Production Outcome from Multi-stage, Horizontal Barnett Completions.” Paper SPE 120271 presented at SPE Production and Operations Symposium, Oklahoma, OK, April 4–8, 2009.

Hansen, N. and Ostermeier, A. 2001. “Completely Derandomized Self-Adaptation in evolution strategies”, *Evol. Comput.* 9 (2): 159–195.

<http://dx.doi.org/10.1162/106365601750190398>.

Junjing Zhang, Anton Kamenov, D. Zhu, and A. D. Hill, “Laboratory Measurement of Hydraulic Fracture Conductivities in the Barnett Shale”, SPE 163839, Copyright 2013, Society of Petroleum Engineers, SPE Hydraulic Fracturing Technology Conference, Woodlands, Texas, USA, 4–6 February 2013.

Lan Ren, Jinzhou Zhao, and Yongquan Hu (June 2014), “Hydraulic Fracture Extending into Network in Shale: Reviewing Influence Factors and Their Mechanism”, *The Scientific World Journal* Volume Hindawi Publishing Corporation, Article ID 847107, 9 pages, <http://dx.doi.org/10.1155/2014/847107>.

Langmuir I. The Adsorption of gases on plane surfaces of glass, mica and platinum. *J Am Chem Soc* 1918; 40:1403–61.

L. E. East Jr., W. Grieser, B.W. McDaniel, B. Johnson, R. Jackson, and K. Fisher, “Successful application of hydrajert fracturing on horizontal wells completed in a thick shale reservoir,” in *Proceedings of the Society of Petroleum Engineers Eastern Regional Meeting (SPE '04)*, pp. 193–210, September 2004.

Luigi Saputelli, Carlos Lopez, Alejandro Chacon, Mohammed Soliman, “Design Optimization of Horizontal Wells with Multiple Hydraulic Fractures in the Bakken Shale”, SPE 167770, presentation at the SPE/EAGE European Unconventional Conference and Exhibition held in Vienna, Austria, 25–27 February 2014.

Lalehrokh, Farshad, and Jared Bouma, “Well Spacing Optimization in Eagle Ford”, SPE-171640-MS, presentation at the SPE/CSUR Unconventional Resources Conference - Canada held in Calgary, Alberta, Canada, 30 september – 2 october 2014.

Maas, J.G. 2011. Maas Special CORE Analysis, facts. Available at <http://www.jgmaas.com/scores/facts.html>.

Mayerhofer, M.J., Lolon, E.P., Youngblood, J.E., and Heinze, J.R. 2006. Integration of Microseismic Fracture Mapping Results With Numerical Fracture Network Production Modeling in the Barnett Shale. Paper SPE 102103 presented at the SPE Annual Technical Conference and Exhibition, San Antonio, Texas, USA, 24–27 September. doi:10.2118/102103-MS.

Mayerhofer, M.J., Lolon, E.P., Warpinski, N.R., Cipolla, C.L., Walser, D., and Rightmire, C.M. 2010. What Is Stimulated Reservoir Volume? *SPE Prod & Oper* 25 (1): 89–98. SPE-119890-PA. doi: 10.2118/119890-PA.

Michael J. Economides, Tony Martin (2007), “Modern Hydraulic Fracturing (Enhancing Natural Gas Production),” Published by: Energy Tribune Publishing Inc. 820 Gessner Rd.-Ste. 920, Houston, TX 77040.

Mei Yang and Michael J. Economides, “Natural Proppants for Hydraulic Fracture Production Optimization in Eagle Ford Shale”, presented at the 2012 SPE Western Regional Meeting held in Bakersfield, California, 21-23, March 2012, SPE 153811.

Mei Yang and Michael J. Economides, “Proppant Selection in Hydraulic Fracture optimization in Shale Plays”, presented at the 2012 SPE Eastern Regional Meeting held in Lexington, Kentucky, USA 3-5 October 2012.

Ming Gu, Pandurang Kulkarni, Mehdi Rafiee, and Endre Ivarrud (October 2014), “Understanding the Optimum Fracture Conductivity for Naturally Fractured.”, presented at the SPE/CSUR Unconventional Resources Conference - Canada held in Calgary, Alberta, Canada, 30 September –2 October 2014.

Mengal S.A., and Wattenbarger, R.A. “Accounting for Adsorbed Gas in Shale Gas Reservoirs.” Paper SPE 141085 presented at SPE Middle East Oil and Gas Show and Conference, Manama, Bahrain, September 25–28, 2011.

P. Saldungaray and T. Palisch. (Jan 2012), “Hydraulic Fracture Optimization in Unconventional Reservoirs”, SPE 151128.

P. Saldungaray and T. Palisch, (March 2013), “HYDRAULIC FRACTURE OPTIMIZATION IN UNCONVENTIONAL RESERVOIRS.” presented at the 11th Offshore Mediterranean Conference and Exhibition in Ravenna, Italy.

Rubin B. “Accurate simulation of non-darcy flow in stimulated fractured shale reservoirs” SPE 132093, presented at the SPE western regional meeting, Anaheim, CA; May 27-29, 2010.

R.S. Taylor, M.A. Glaser, J. Kim, B. Wilson, G. Nikiforuk, V. Noble, L. Rosenthal, R. Aguilera, O. Hoch,; K. Storozhenko, M. Soliman, N. Riviere, T. Palidwar, R. Romanson, "Optimization of Horizontal Wellbore and Fracture Spacing Using an Interactive Combination of Reservoir and Fracturing Simulation", CSUG/SPE 137416, presented at the Canadian Unconventional Resources & International Petroleum Conference held in Calgary, Alberta, Canada, 19–21 October 2010.

S. L. Montgomery, D. M. Jarvie, K. A. Bowker, and R. M. Pollastro, "Mississippian Barnett Shale, Fort Worth basin, north-central Texas: gas-shale play with multi-trillion cubic foot potential," AAPG Bulletin, vol. 89, no. 2, pp. 155–175, 2005.

Sam Holt, (2011): "Numerical Optimization of Hydraulic Fracture Stage Placement in a Gas Shale Reservoir". (MSc Thesis. TU Delft University, Netherlands).

Soliman. M.Y., Pongratz, R., Rylance, M., and Prather, D.: "Fracture Treatment Optimization for Horizontal Well Completions," paper SPE 102616, 2006.

Storn, R., Price, K. (1995) "Differential Evolution - A Simple and Efficient Adaptive Scheme for Global Optimization over Continuous Spaces", Technical Report for International Computer Science Institute, Berkeley, TR-95-012.

US Energy Information and Administration (2011) World Shale Gas Resources: An initial assessment by EIA.

Wang, F.P., and Reed, R.M., 2009, "Pore Networks and Fluid flow in Gas Shales", presented at 2009 SPE Annual Technical Conference and Exhibition, Oct 4-7, New Orleans, Louisiana, USA, SPE 124253.

Warpinski, N.R., Mayerhofer, M.J., Vincent, M.C., Cipolla, C.L. and Lonon, E.P. 2008. Stimulating Unconventional Reservoirs: Maximizing Network Growth While Optimizing Fracture Conductivity. Paper SPE 114173, presented at the SPE Unconventional Reservoirs Conference held in Keystone, Colorado, USA, 10-12 February.

Warpinski, N.R., Kramm, R.C., Heinze, J.R. and Waltman, C.K. 2005. Comparison of Single- and Dual- array Microseismic Mapping Techniques in the Barnett Shale. Paper SPE 95568 presented at the 2005 SPE Annual Technical Conference and Exhibition, Dallas, Texas, 9-12 October.

Wei Yu and Sephernoori, K., (2013a) “Numerical Evaluation of the Impact of Geomechanics on Well Performance in Shale Gas Reservoirs”, presented at the 47th US Rock Mechanics / Geomechanics Symposium held in San Francisco, CA, USA, 23-26 June 2013.

Wei Yu and Sephernoori, K., (2013b) “Optimization of Multiple Hydraulically Fractured Horizontal Wells in Unconventional Gas Reservoirs”, *Journal of Petroleum Engineering*, August 2013, Volume 2013, Article ID 151898, <http://dx.doi.org/10.1155/2013/151898>.

Wei Yu and Sepehrnoori, K. (2013c) “Simulation of Gas Desorption and Geomechanics Effects for Unconventional Gas Reservoirs.” *Fuel*, 116 (2014): 455–464.

Wei Yu and Sepehrnoori, K. (2013d) “Simulation of Proppant Distribution Effect on Well Performance in Shale Gas Reservoirs.” Paper SPE 167225 presented at SPE Unconventional Resources Conference–Canada, Calgary, Alberta, Canada, November 05-07, 2013.

Wei Yu, Z. Luo, F. Javadpour, A.Varavei, K. Sepehrnoori (2013e), “Sensitivity analysis of hydraulic fracture geometry in shale gas reservoirs”, *Journal of Petroleum Science and Engineering* 113 (2014), 1–7.

Wei Yu and Sepehrnoori, K. (2014a), “An Efficient Reservoir Simulation Approach to Design and Optimize Unconventional Gas Production”, Paper SPE 165343, Journal of Canadian Petroleum Technology.

Wei Yu and Sepehrnoori, K. (2014b), “Numerical Study of the Impact of Complex Fracture Patterns on Well Performance in Shale Gas Reservoirs”, Journal of Petroleum Science Research (JPSR) Volume 3 Issue 2, April 2014, doi: 10.14355/jpsr.2014.0302.05

Wei Yu and Sepehrnoori, K. (2014c), “Optimization of Well Spacing for Bakken Tight Oil Reservoirs”, URTeC: 1922108, presented at the Unconventional Resources Technology Conference held in Denver, Colorado, USA, 25-27 August 2014.

X Ma, Plaksina, T., & Gildin, E, "Optimization of Placement of Hydraulic Fracture Stages in Horizontal Wells Drilled in Shale Gas Reservoirs". Paper 168780-MS, presented at Unconventional Resources Technology Conference, Society of Petroleum Engineers, 12-14 August 2013a, Denver, Colorado.

X Ma, Plaksina, T., & Gildin, E, “Integrated Horizontal Well Placement and Hydraulic Fracture Stages Design Optimization in Unconventional Gas Reservoirs”, SPE 167246, presented at the SPE Unconventional Resources Conference-Canada held in Calgary, Alberta, Canada, 5–7 November 2013b.

X Zhang et al. (December 2009). “Sensitivity Studies of Horizontal Wells with Hydraulic Fractures in Shale Gas Reservoirs”, IPTC 13338, presented at the International Petroleum Technology Conference held in Doha, Qatar, 7–9 December 2009.

Zhenzhen Dong et al, (February 2014) “Probabilistic Assessment of World Recoverable Shale Gas Resources”, presented at the SPE/EAGE European Unconventional Conference and Exhibition held in Vienna, Austria, 25–27 February 2014, SPE 167768.

VITAE

- Name : Muzammil Hussain Rammay
- Nationality : Pakistan
- Date of Birth : 07/Sept/1988
- Email : hussain_petro@yahoo.com
- Address : Model Colony Malir, Karachi, Pakistan
- Academic Background : **Masters in Petroleum Engineering**
King Fahd University of Petroleum & Minerals
Dhahran, Saudi Arabia
BE in Petroleum Engineering
December, 2010
NED University of Engineering & Technology, Karachi
Pakistan
- Publications : 1. Muzammil Hussain Rammay & Abdulraheem, A. (2014, September 15), "Automated History Matching Using Combination of Adaptive Neuro Fuzzy System (ANFIS) and Differential Evolution Algorithm". Society of Petroleum Engineers, doi: 10.2118/172992-MS
2. Muzammil Hussain Rammay & Al-Nuaim, S. (2015, December 6). "Flow Regime Prediction Using Fuzzy Logic and Modification in Beggs and Brill Multiphase Correlation". International Petroleum Technology Conference. doi:10.2523/IPTC-18267-MS